doi:10.1038/nature16544

Table of Contents

SI 1: Chromosome 21 capture

All Neanderthal libraries used in the present study were prepared in previous studies (*1-3*) (see Table S1 for an overview). Libraries from El Sidrón and Vindija were generated using a double-stranded library preparation method (*4*). These libraries had been treated with uracil-DNA-glycosylase and *E.coli* endonuclease VIII to minimize the occurrence of damage-derived sequence errors (*5*). Libraries from the Altai Neanderthal were generated using a single-stranded protocol (*6*).

We used the probe set and the approach described in (*7*) to enrich these Neanderthal libraries for chromosome 21 sequences. This includes, briefly, (i) the synthesis of oligonucleotides targeting the unique sequence of chromosome 21 (29.8 Mbp) on arrays, (ii) their conversion into amplifiable probe libraries, (iii) the construction of single-stranded biotinylated DNA probes, (iv) the enrichment of the Neanderthal libraries through two rounds of in-solution hybridization capture, followed by (v) amplification and double-indexing (*4*) of the enriched Neanderthal libraries.

Sequencing of the enriched Neanderthal libraries was performed using 17 (El Sidrón) and eight (Vindija) lanes of the Genome Analyzer IIx (Illumina). Paired end sequencing was carried out for 2x 76 cycles, and additional 7-cycle sequencing reactions were performed to read the indexes in both adaptors (*4*). In addition to the methodology described in (*7*), we also produced single-stranded biotinylated RNA probes as described by Gnirke et al. (*8*) and used them to enrich chromosome 21 from the El Sidrón libraries. We did not detect differences in capture efficiency between these two approaches and thus merged all data for their combined analysis. The four libraries captured from the Altai Neanderthal were sequenced on one Illumina HiSeq 2500 lane.

Table S1. List of extracts and libraries used for the array capture of chromosome 21.

Bone	Library preparation described in	ID in previous study	ID after enrichment in present study
El Sidrón 1253	Castellano et al. 2014	L8201	L10840, L10936
El Sidrón 1253	Castellano et al. 2014	L8204	L10841, L10937
El Sidrón 1253	Castellano et al. 2014	L8205	L10842, L10938
El Sidrón 1253	Castellano et al. 2014	L8206	L10843, L10939
El Sidrón 1253	Castellano et al. 2014	L8207	L10844, L10940
El Sidrón 1253	Castellano et al. 2014	L8208	L10845, L10941
El Sidrón 1253	Castellano et al. 2014	L8209	L10846, L10942
El Sidrón 1253	Castellano et al. 2014	L8210	L10847, L10943
El Sidrón 1253	Castellano et al. 2014	L8211	L10848, L10944
El Sidrón 1253	Castellano et al. 2014	L8212	L10849, L10945
El Sidrón 1253	Castellano et al. 2014	L8213	L10850, L10946
El Sidrón 1253	Castellano et al. 2014	L8214	L10851, L10947
El Sidrón 1253	Castellano et al. 2014	L8215	L10852, L10948
El Sidrón 1253	Castellano et al. 2014	L8216	L10853, L10949
El Sidrón 1253	Castellano et al. 2014	L8219	L10854, L10950
El Sidrón 1253	Castellano et al. 2014	L8220	L10855, L10951
El Sidrón 1253	Castellano et al. 2014	L8221	L10856, L10952
El Sidrón 1253	Castellano et al. 2014	L8222	L10857, L10953
El Sidrón 1253	Castellano et al. 2014	L8223	L10858, L10954
El Sidrón 1253	Castellano et al. 2014	L8224	L10859, L10955
El Sidrón 1253	Castellano et al. 2014	L8229	L10860, L10956
El Sidrón 1253	Castellano et al. 2014	L8234	L10861, L10957
El Sidrón 1253	Castellano et al. 2014	L8237	L10862, L10958
El Sidrón 1253	Castellano et al. 2014	L8238	L10863, L10959
El Sidrón 1253	Castellano et al. 2014	L8239	L10864, L10960
El Sidrón 1253	Castellano et al. 2014	L8241	L10865, L10961
El Sidrón 1253	Castellano et al. 2014	L8242	L10866, L10962
El Sidrón 1253	Castellano et al. 2014	L8243	L10867, L10963
El Sidrón 1253	Castellano et al. 2014	L8244	L10868, L10964
El Sidrón 1253	Castellano et al. 2014	L8245	L10869, L10965
El Sidrón 1253	Castellano et al. 2014	L8246	L10870, L10966
El Sidrón 1253	Castellano et al. 2014	L8247	L10871, L10967
El Sidrón 1253	Castellano et al. 2014	L8249	L10832, L10928
El Sidrón 1253	Castellano et al. 2014	L8250	L10833, L10929
El Sidrón 1253	Castellano et al. 2014	L8251	L10834, L10930
El Sidrón 1253	Castellano et al. 2014	L8252	L10835, L10931
El Sidrón 1253	Castellano et al. 2014	L8253	L10836, L10932
El Sidrón 1253	Castellano et al. 2014	L8254	L10837, L10933
El Sidrón 1253	Castellano et al. 2014	L8255	L10838, L10873,

			L10874, L10934, L10969
El Sidrón 1253	Castellano et al. 2014	L8256	L10839, L10935
El Sidrón 1253	Burbano et al. 2010	L638	L10875, L10971
El Sidrón 1253	Burbano et al. 2010	L639	L10876, L10972
El Sidrón 1253	Burbano et al. 2010	L640	L10877, L10973
El Sidrón 1253	Burbano et al. 2010	L641	L10878, L10974
Vindija 33.15	Castellano et al. 2014	L7849	L7801
Vindija 33.15	Castellano et al. 2014	L7850	L7802
Vindija 33.15	Castellano et al. 2014	L7851	L7803
Vindija 33.15	Castellano et al. 2014	L7852	L7804
Vindija 33.15	Castellano et al. 2014	L7853	L7805
Vindija 33.15	Castellano et al. 2014	L7855	L7807
Vindija 33.15	Castellano et al. 2014	L7856	L7808
Vindija 33.15	Castellano et al. 2014	L7857	L7809
Vindija 33.15	Castellano et al. 2014	L7858	L7810, L7823
Vindija 33.15	Castellano et al. 2014	L7859	L7811
Vindija 33.15	Castellano et al. 2014	L7860	L7812
Vindija 33.15	Castellano et al. 2014	L7861	L7813, L7824
Vindija 33.15	Castellano et al. 2014	L7862	L7814
Vindija 33.15	Castellano et al. 2014	L7863	L7815
Vindija 33.15	Castellano et al. 2014	L7864	L7816
Vindija 33.15	Castellano et al. 2014	L7865	L7817
Vindija 33.15	Castellano et al. 2014	L7866	L7818
Vindija 33.15	Castellano et al. 2014	L7868	L7820
Vindija 33.15	Castellano et al. 2014	L7869	L7821
Altai Neanderthal	Prüfer et al. 2014	L9198	A6600
Altai Neanderthal	Prüfer et al. 2014	L9199	A6601
Altai Neanderthal	Prüfer et al. 2014	L9302	A6602
Altai Neanderthal	Prüfer et al. 2014	L9303	A6603

SI 2. Processing and mapping

Base calling and raw sequence processing

We processed the raw sequencing data as previously described (*1*). Bases were called using Ibis (*9*) from the BCL and CIF intensity files from the Illumina Genome Analyzer RTA 1.9 software. The so-obtained raw reads were filtered for the presence of the correct library index sequences, allowing for one substitution and/or the skipping of the first base in each index (*10*). Minimum base quality score of 10 was required in both index reads. Overlapping paired-end reads were merged into single sequences and a consensus sequence was obtained for the overlapping bases (*11*). Reads with more than five bases with base quality scores below 15 were rejected. One Illumina HiSeq lane was analyzed for the Altai Neanderthal capture of chromosome 21, and processed the same way.

Mapping

Only merged sequences were used for mapping with BWA (*12*) 0.5.8a to two reference sequences: the human genome (GRCh37/1000 Genomes release) and the revised Cambridge Reference Sequence (rCRS) of the human mitochondrial genome (NC_012920.1) using parameters (-l 16500 -n 0.01 -o 2). Using BWA's samse command, alignments were converted to SAM format, and then via samtools (*13*) 0.1.18 to coordinate-sorted BAM files. The output files were filtered by removing non-aligned reads as well as reads shorter than 35 bp. Furthermore, BAM NM/MD fields were recalculated using samtools calmd, and reads with an edit distance of more than 20% of their sequence length were removed. This step was included to correct for non-A,C,G,T bases in the reference genomes being replaced by random bases when generating the BWA alignment index. Duplicate reads within each library were collapsed into a consensus sequence (*11*).

Mitigation of cytosine deamination

Although the vast majority of uracils was removed with UDG during library preparation, some deamination-induced errors remain. Sequences from the double-stranded libraries exhibit an elevation of C to T substitutions at their 5' end as well as an excess of G to A substitutions at their 3' end (Figure S1A and S1B). To mitigate this problem, we lowered the base quality to 2 for any 'T' nucleotide occurring within the first four bases or 'A' nucleotide within the last four positions. Sequences generated from libraries produced with the single-stranded method exhibit elevated frequencies of C to T substitutions mainly in the first and last two bases (*6*) (Figure S1C). We reduced the base quality of any 'T' of the first and last two bases of sequences from the Altai Neanderthal. These approaches resulted in heterozygous genotypes in Neanderthals (see Supplementary information 3) with comparable C to T and G to A substitution frequencies to present-day humans (Figure S2).

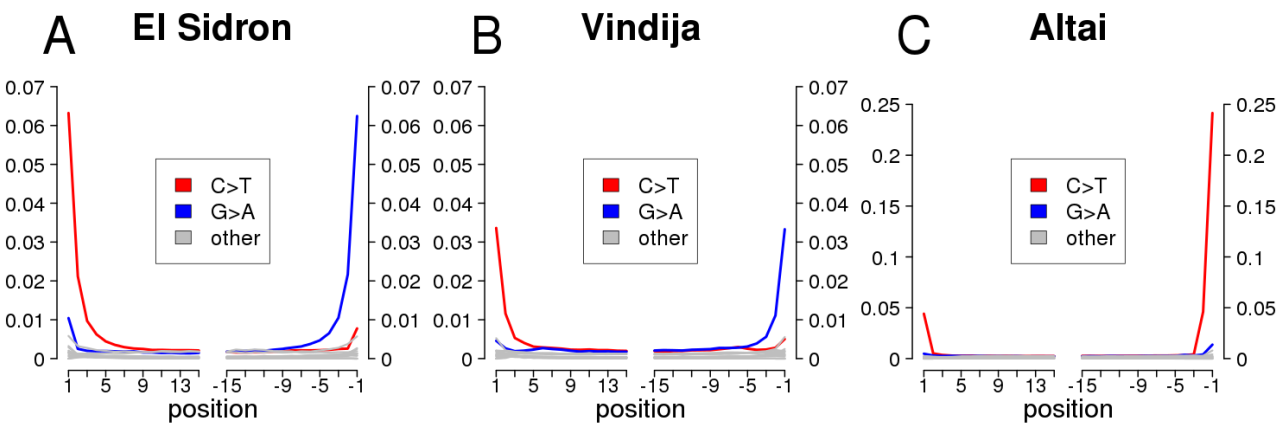

Figure S1. C to T and G to A substitution frequencies relative to the human reference sequence at the 5' and 3' ends as a proportion of Neanderthal sequences before deamination mitigation in: A) El Sidrón, B) Vindija and C) Altai (captured libraries). Note that panel C is on a different scale.

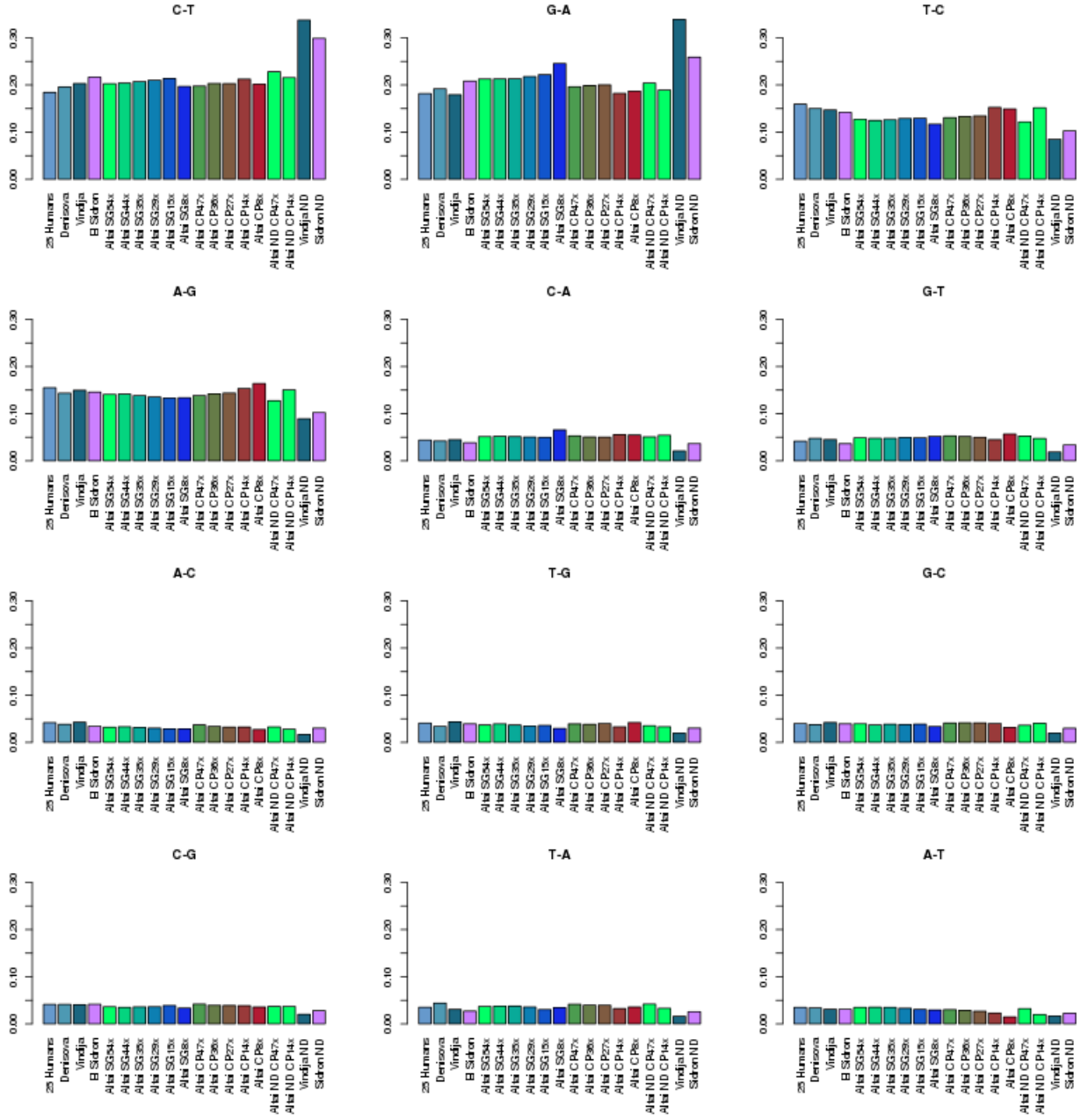

Figure S2. Frequency of nucleotide substitutions (ancestral to derived alleles) at heterozygous genotype calls after filtering, as a proportion of the heterozygous sites in each individual. 'ND' = Neanderthal samples before deamination mitigation. 'SG' = shotgun sequenced, 'CP' = sequencing after capture.

SI 3. Filtering and variation discovery

Genotype calling

We called genotypes separately for the El Sidrón, Vindija and Altai chromosome 21 using the GATK UnifiedGenotyper (*14*) 1.3-25-g32cdef9. Genotypes for the captured and shotgun sequenced chromosomes 21 from the Altai Neanderthal were also called separately. Both single nucleotide variants (SNVs) and insertions and deletions (InDels) were called. We performed a second call on all SNV sites where at least one non-reference allele was found, replacing the reference for the alternative allele in the reference genome and re-running GATK UnifiedGenotyper for those sites with the modified reference (*15*).

Variant annotation and variation discovery

Variant Call Format (VCF) files were annotated with supplementary information, using the extended VCF pipeline described previously in SOM 6 of Meyer *et al*. (*15*). We previously produced variation calls as described above for a Denisovan and 25 modern human high-coverage genomes (*3, 15*) from Africa (Mandenka, Mbuti, San, Yoruba and Dinka), Europe (French and Sardinian), Asia (Han and Dai), Oceania (Papuan, Australian), and America (Karitiana and Mixe). We performed the majority of the analyses on subsets of these individuals.

Filtering

We assessed genotype calls for each individual based on their annotation in a combined VCF file. A site was considered for analysis when it passed the following filters (*1*): 1) the site is part of the 29,833,522 bp in regions that were targeted by capture baits, and a GATK call was made; 2) the genotype quality (GQ) is at least 20, or 10 in El Sidrón; 3) a mapability score in the Duke 20mer uniqueness score (Map20) of 1; 4) the fraction of mapped reads with Mapping Quality (MQ) of zero is less than 10%; 5) coverage is within the central 95% of the chromosome-wide coverage (Table S2); 6) the site is not flagged as a systematic error (*16*); 7) the site is not flagged as LowQuality; 8) the site has Human-Chimpanzee ancestry information; 9) the Human-Chimpanzee ancestral allele matches either the human reference allele or the alternative allele at heterozygous sites; 10) Human and Chimpanzee appear no more than once in the EPO alignment block (*17, 18*). In Tables S3 and S4, we list the number of sites not passing each of the filters. In Table S5, we list the number of sites passing all filters and thus analyzed.

Coverage distribution

The average coverage for El Sidrón and Vindija chromosome 21 after removal of duplicate sequences and before filtering is 12.3-fold and 33-fold, respectively. The coverage distributions before filtering are shown in Figure S3A and B. After filtering, the average coverage increases to 14.1-fold in El Sidrón and 35.9-fold in Vindija (Figure S3C and D). The increase in coverage is a result of a lower coverage cutoff of six for the capture data, which removes more bases at low coverage than at high coverage. The average coverage of the captured Altai Neanderthal chromosome 21 is 38.7-fold before filtering, and 46.9-fold after filtering. To investigate whether differences in sequence coverage affect downstream analyses, we randomly down-

sampled the captured Altai chromosome 21 to a range of coverages from 7.7-fold to 44.3-fold using the downsampleSam function in Picard (http://picard.sourceforge.net/) (Table S2). The average coverage for the Altai Neanderthal is 53.7-fold, with bins 29-109 encompassing the central 95% of the data. We down-sampled the shotgun sequenced Altai Neanderthal to a similar range of coverages, and applied the same filters. We also computed the lower and higher coverage bins encompassing the central 95% of the data for the present-day human chromosomes 21 used in this work (Table S2).

Table S2: Central 95% coverage cutoffs (with a minimum of 6 reads) for the chromosome 21 analyzed. The cutoffs include the given values. The downsampling factor is the percentage of reads that were randomly selected.

Individual	Population	Lower cutoff	Higher cutoff	Downsampling (%)
Altai shotgun 53.7-fold	Neanderthal	29	109	(100)
Altai shotgun 44.3-fold	Neanderthal	24	102	88
Altai shotgun 34.5-fold	Neanderthal	18	78	67
Altai shotgun 28.5-fold	Neanderthal	13	58	50
Altai shotgun 15.1-fold	Neanderthal	6	31	26
Altai shotgun 7.7-fold	Neanderthal	6	15	12
Altai capture 46.9-fold	Neanderthal	6	94	(100)
Altai capture 35.7-fold	Neanderthal	6	73	76
Altai capture 26.7-fold	Neanderthal	6	60	60
Altai capture 14-fold	Neanderthal	6	31	30
Altai capture 8.1-fold	Neanderthal	6	12	10
El Sidrón	Neanderthal	6	33	
Vindija	Neanderthal	6	92	
Denisova	Denisovan	14	59	
WONM	Australian	21	78	
BURE	Australian	22	84	
HGDP01307	Dai	10	52	
HGDP01308	Dai	19	70	
DNK02	Dinka	13	59	
DNK07	Dinka	19	74	
HGDP00521	French	12	52	
HGDP00533	French	21	83	
HGDP00778	Han	12	54	
HGDP00775	Han	18	70	
HGDP00998	Karitiana	11	50	
HGDP01015	Karitiana	18	71	
HGDP01284	Mandenka	10	50	
HGDP01286	Mandenka	18	72	
HGDP0456	Mbuti	10	52	
HGDP00982	Mbuti	18	80	
MIXE0007	Mixe	19	71	
HGDP00542	Papuan	11	47	
HGDP00546	Papuan	21	79	
HGDP01029	San	15	66	
HGDP01036	San	19	68	
HGDP00665	Sardinian	11	47	
HGDP01076	Sardinian	19	72	
HGDP00927	Yoruba	14	58	
HGDP00936	Yoruba	19	66	

Table S3: Number of sites filtered out by each of the general filters in chromosome 21. Sites can be filtered out by more than one filter.

Category	No. of sites
Systematic Errors	1,545
Systematic Errors HCB	51
Map20 < 1	6,251,594
Sites with more than two alleles including ancestral allele	357,915
Ancestral allele not known	2,099,490

Table S4: Number of sites filtered out per individual and per filter. Sites can be filtered out by more than one filter.

	Low coverage	High coverage	GQ	MQ0>10%	LowQual tagged
Altai shotgun 53.7-fold	703,901	759,952	838,766	2,119,394	12,797
Altai shotgun 44.3-fold	564,389	685,219	844,794	2,116,832	14,177
Altai shotgun 34.5-fold	617,064	684,183	933,082	2,115,019	19,559
Altai shotgun 28.5-fold	652,735	692,924	1,125,865	2,114,693	34,682
Altai shotgun 15.1-fold	744,465	688,638	1,423,976	2,124,494	198,611
Altai shotgun 7.7-fold	11,921,527	722,094	6,000,320	2,063,018	236,477
Altai capture 46.9-fold	2,434,743	859,264	3,866,935	2,005,037	60,954
Altai capture 35.7-fold	3,129,342	829,227	4,723,314	1,989,624	73,335
Altai capture 26.7-fold	3,799,552	810,980	5,550,172	1,974,210	84,915
Altai capture 14-fold	7,400,217	788,620	6,297,251	1,911,225	146,000
Altai capture 8.1-fold	20,745,906	701,494	15,759,260	1,692,670	140,222
El Sidrón	8,574,149	822,073	7,101,380	1,851,857	80,404
Vindija	3,096,340	762,739	4,770,147	1,798,188	41,588
Denisova	697,976	787,789	1,166,763	2,147,895	25,804
WONM	757,627	776,961	710,571	1,156,885	10,225
BURE	730,661	773,169	755,794	1,146,833	10,278
HGDP01307	590,394	776,109	941,625	1,213,899	21,420
HGDP01308	774,107	767,399	747,317	1,149,885	11,406
DNK02	734,762	770,138	830,684	1,215,387	19,644
DNK07	764,452	759,842	742,079	1,167,046	12,976
HGDP00521	645,262	775,136	841,279	1,216,672	20,228
HGDP00533	743,639	768,113	666,474	1,120,923	9,989
HGDP00778	636,180	783,950	845,814	1,214,540	19,014
HGDP00775	736,544	762,954	752,205	1,155,608	12,214
HGDP00998	632,655	787,368	905,587	1,210,749	20,921
HGDP01015	746,055	767,824	702,025	1,121,471	10,445
HGDP01284	616,254	787,372	994,182	1,226,676	25,012
HGDP01286	705,273	772,625	708,499	1,136,961	11,963
HGDP0456	690,795	771,912	987,438	1,220,147	24,572
HGDP00982	714,714	763,675	674,456	1,141,177	11,622
MIXE0007	778,564	757,767	784,603	1,126,192	10,895
HGDP00542	671,826	827,378	921,381	1,201,760	21,177
HGDP00546	785,978	774,779	714,646	1,125,732	10,415
HGDP01029	727,471	772,290	792,195	1,256,378	20,049

HGDP01036	686,662	791,319	698,286	1,158,723	12,326
HGDP00665	724,993	802,039	919,571	1,206,078	22,476
HGDP01076	655,845	765,284	674,187	1,106,427	10,310
HGDP00927	644,841	790,328	835,101	1,243,393	18,469
HGDP00936	697,414	810,926	775,960	1,155,822	11,726

Table S5: Number of sites passing all filters in each individual, and average coverage.

Individual	Sites that pass all filters	Average coverage after filtering
Altai shotgun 53.7-fold	23,023,770	53.7
Altai shotgun 44.3-fold	23,123,749	44.4
Altai shotgun 34.5-fold	23,057,102	34.5
Altai shotgun 28.5-fold	22,930,992	28.5
Altai shotgun 15.1-fold	22,638,467	15.1
Altai shotgun 7.7-fold	13,478,957	7.7
Altai capture 46.9-fold	21,198,924	46.9
Altai capture 35.7-fold	20,608,493	35.7
Altai capture 26.7-fold	20,018,913	26.7
Altai capture 14-fold	17,751,364	13.9
Altai capture 8.1-fold	7,317,371	8.1
El Sidrón	17,014,623	14.1
Vindija	20,582,399	35.9
Denisova	22,945,618	31.1
WONM	23,042,590	41.7
BURE	23,070,934	42.4
HGDP01307	23,114,030	25.1
HGDP01308	23,091,608	37.1
DNK02	23,049,034	28.5
DNK07	23,105,579	35.8
HGDP00521	23,093,108	26.9
HGDP00533	23,078,540	42.2
HGDP00778	23,110,295	27.8
HGDP00775	23,093,756	35.4
HGDP00998	23,094,694	26.1
HGDP01015	23,069,804	35.2
HGDP01284	23,131,860	24.6
HGDP01286	23,111,109	36.9
HGDP0456	23,050,591	24.4
HGDP00982	23,105,976	36.7
MIXE0007	23,116,604	36.8
HGDP00542	23,021,525	26.1
HGDP00546	23,042,939	42.5
HGDP01029	23,080,869	33.1
HGDP01036	23,098,488	38.4
HGDP00665	23,018,781	24.9
HGDP01076	23,148,783	38.1
HGDP00927	23,122,644	32.2
HGDP00936	23,105,770	38.7

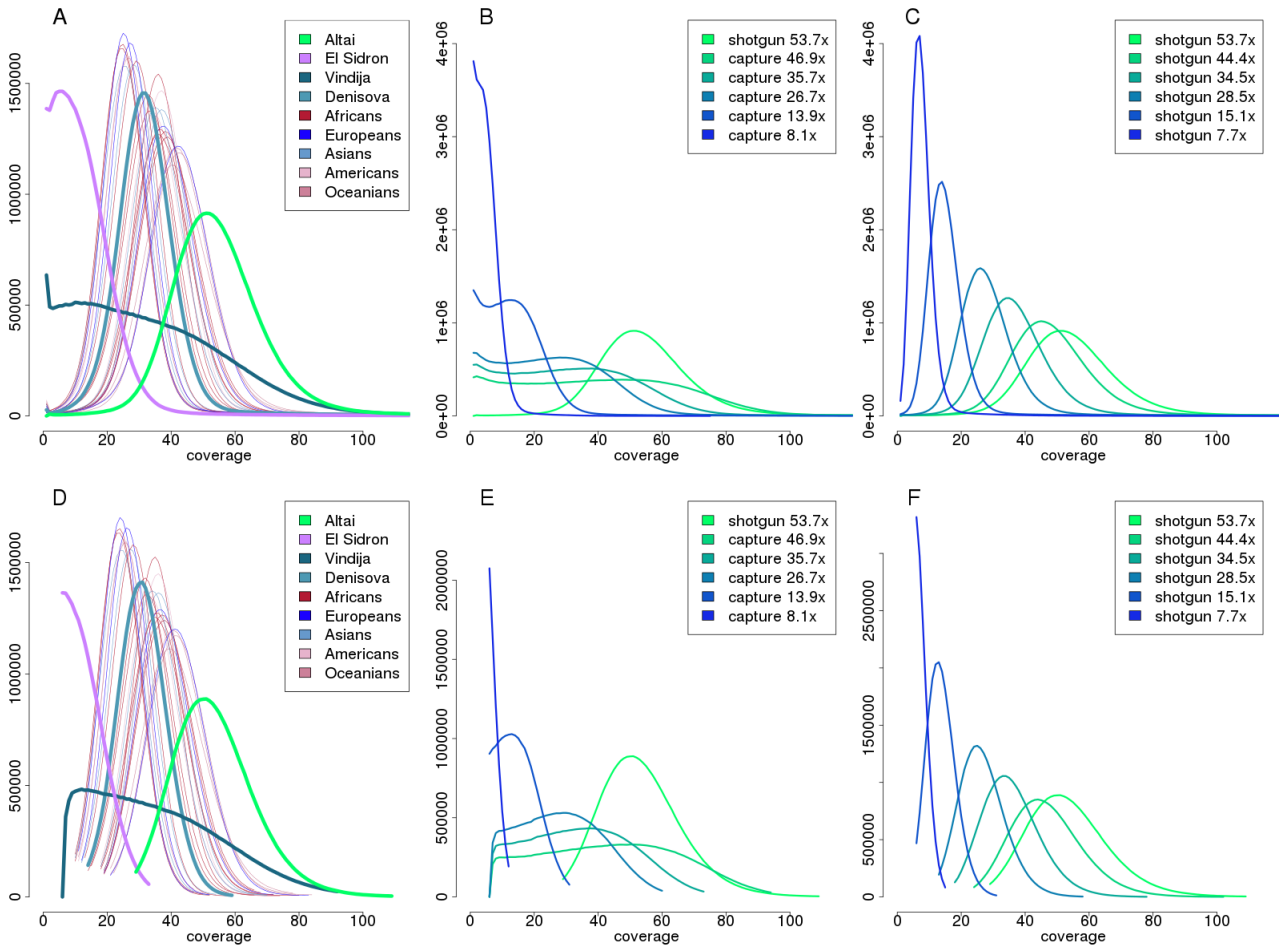

Figure S3. Coverage distributions: A) Neanderthals, Denisovans and 25 humans *before* filtering; B) Capture of Altai *before* filtering at different coverages; C) Shotgun sequencing of Altai *before* filtering at different coverages; D) Neanderthals, Denisovans and 25 humans *after* filtering; E) Capture of Altai *after* filtering at different coverages; F) Shotgun sequencing of Altai *after* filtering at different coverages.

SI 4. Contamination estimates and capture bias

Contamination estimates

As reported previously (*3*, *6*), the mitochondrial DNA contamination from present-day human sequences in the Altai Neanderthal and Denisovan libraries was estimated at 0.78% (CI: 0.75–0.82%) and 0.35% (CI: 0.33–0.36%), respectively. This estimate was calculated using sequences mapping to the mitochondrial genome and positions at which those differ from sequences in a worldwide panel of 311 present-day human mitochondria (*19*). Using the same method, present-day human contamination has been estimated at 0.40% (CI: 0.38–0.42%) for El Sidrón and 1.08% (CI: 1.05–1.08%) for the Vindija Neanderthal libraries. See Table S8 in (*1*) for details.

The nuclear DNA contamination from present-day humans in the same libraries of the Altai Neanderthal and Denisovan was reported at 0.80% (CI: 0.79–0.83%) and 0.22% (CI: 0.22–0.23%), respectively. These estimates were calculated using a maximum likelihood approach that co-estimates the contamination and sequence error in the autosomes, as described in (*6*). Using the same method, we estimate that present-day human contamination is 0.000023% (CI: 0–0.49%) for El Sidrón and 1.12% (CI: 0.95–1.30%) for Vindija Neanderthal libraries from chromosome 21. For comparison, we also estimated the contamination in the chromosome 21 of the Altai Neanderthal and Denisovan, which is 0.93% (CI: 0.79–1.08%) and 0.15% (CI: 0.09–0.23%), respectively. We conclude that present-day human contamination in the four archaic individuals is around 1%.

Note that these methods estimate the proportion of contaminated sequence fragments, but genotype calling (as described in Supplementary information 3) requires high sequence coverage at each site and, hence, the proportion of contaminated genotypes is likely to be smaller than 1%. That is, multiple contaminated DNA fragments are needed for a contaminated genotype to be called. In addition, present-day human contamination cannot explain the patterns of divergence and heterozygosity observed in the Altai Neanderthal genome (Supplementary information 9).

Reference allele frequencies

Sequence divergence between the Neanderthal sequences and the sequence of the human reference genome (GRCh37/hg19) used for probe design may lead to an underrepresentation of sequences with differences to the reference genome during capture. This problem is exacerbated by the uneven coverage distribution of capture compared to shotgun data (Figure S3), which results in a larger proportion of sites at low coverage. These may lead to the discovery of fewer heterozygous genotypes in the captured Neanderthals.

A previous study using present-day DNA has reported a shift of mean allele frequencies towards the reference allele from 0.5 to 0.54 at high-quality heterozygous sites as a result of bias in the capture (*20*). We find a mean reference allele frequency of 0.55 and 0.54 in the heterozygous sites of El Sidrón and Vindija chromosome 21, respectively (Figure S4). This suggests that array capture results in a similar reference

allele bias in Neanderthals and present-day humans. Note that deamination-induced sequence errors, unless corrected, create non-reference alleles and result in spurious heterozygous calls. Because most sequences have the reference allele in these positions, heterozygous calls due to deamination have higher reference allele frequencies (Figure S4). Interestingly, the reference allele frequency is 0.52 for the same chromosome from the Altai and Denisovan shotgun genomes, indicating a slight bias from other factors (*e.g.* mapping to the reference human genome), while it is 0.5 for the present-day humans (Figure S4). The array-captured Altai Neanderthal also shows a slightly higher mean reference allele frequency (0.54-0.55; depending on the sequence coverage). We also explored the distribution of reference to alternative ratios in the Neanderthal chromosomes. The variance of reference allele frequencies is larger in the captured compared to the shotgun-sequenced chromosomes. These observations are in agreement with previous observations in the exomes of present-day humans (*20*) and Neanderthals (*1*).

Another strategy to quantify the bias introduced by capture is to compare the reference allele frequency in sites called as heterozygous in the shotgun data as well as in the capture experiment. The mean increase in reference allele frequency is 3.7% at 46.9-fold coverage (Figure S5), and slightly lowering with lower coverages to 2.3% at 14-fold coverage, while the standard deviation increases with lower coverage (from 0.16 to 0.22). This suggests that capture bias leads to a small shift in average reference allele frequency, with lower coverage leading to a wider distribution of this shift. However, the proportion of sites with a shift of at least 50% in allele frequency is only around 5% even at a low coverage of 14-fold. Only at a coverage of 8.1-fold, this increases to more than 10% of heterozygous sites. This suggests that while many sites are subject to capture bias, the extent of that bias is small. Thus, the decrease in the call of heterozygous genotypes in capture data should be relatively small (see below).

Overlap of heterozygous sites

Sites that were called as homozygous in the capture data, but as heterozygous in the shotgun data in the Altai Neanderthal were not included in the above comparison. These sites are informative with regard to the effects of capture bias on the discovery of high-quality heterozygous sites, which are usually found at moderate to high sequence coverage. The fraction of heterozygous sites in the shotgun Altai Neanderthal that were called as homozygous in the capture of the same sample ranges from 3.76% (14-fold coverage) to 5.16% (46.9-fold coverage) (Table S6). To untangle the above effect of capture bias from the uneven coverage distribution in the capture data, we focused on heterozygous calls in the shotgun Altai Neanderthal that were not called at all in the capture from the same sample. These sites typically have low coverage. The fraction of heterozygous calls that were not called in the capture data ranges from 22.31% at high coverage (46.9-fold) to 45.38% at low coverage (14-fold), while only at a very low coverage (8.1-fold) the majority of sites will not be called (Table S6). We observe 14.81%-21.52% of sites that are heterozygous in the capture data are not called in the high-coverage shotgun data. However, the lower coverage cutoff for the shotgun sequencing is high (29-fold), and when we filter the genotype calls only for sites that affect all samples and for high coverage, we recover a larger fraction of heterozygous sites. 72.2% of sites that are heterozygous in

the capture data, but did not pass the filters at 53.7-fold coverage are called as heterozygous under these conditions. At lower coverage (15.1-fold), this drops to 48.4%, due to the fact that sites with very low coverage are likely to miss the other allele.

The effect of capture bias on high-quality genotype calls in both types of data is small compared to the effect of the distribution of coverage in capture data. As a result, the heterozygosity in the chromosome 21 of the Altai Neanderthal is similar between the shotgun (53.7-fold coverage) and capture data (46.9-fold, 35.7-fold and 26.7-fold coverages) (see Supplementary Information 6). At lower average coverage (14-fold), the heterozygosity suffers from the missed heterozygous genotypes that do not pass our quality filters. We miss sites under all conditions as a result of filtering, but further analyses (see Supplementary Information 6 and 7) suggest that under each condition the sites that pass our filters are representative.

Table S6. Number and percentage of heterozygous genotypes called in the Altai shotgun data that are called as homozygous or not called in the Altai capture data at different sequence coverage.

	Called as homozygous	Not passing filters	Average coverage of sites not passing filters
Altai shotgun vs. capture			
53.7-fold shotgun vs. 46.9-fold capture	157 (5.2%)	671 (22.3%)	14.5-fold
53.7-fold shotgun vs. 35.7-fold capture	140 (4.7%)	811 (27%)	10.4-fold
53.7-fold shotgun vs. 26.7-fold capture	129 (4.3%)	920 (30.6%)	8.3-fold
53.7-fold shotgun vs. 14-fold capture	115 (3.8%)	1365 (45.4%)	4.5-fold
53.7-fold shotgun vs. 8.1-fold capture	39 (1.3%)	2567 (85.3%)	2.5-fold
Altai capture vs. shotgun			
46.9-fold capture vs. 53.7-fold shotgun	155 (5.6%)	408 (14.9%)	22.8-fold
46.9-fold capture vs. 44.3-fold shotgun	157 (5.7%)	386 (14.1%)	20-fold
46.9-fold capture vs. 34.5-fold shotgun	149 (5.4%)	407 (14.8%)	15.9-fold
46.9-fold capture vs. 28.5-fold shotgun	134 (4.9%)	436 (15.9%)	12.7-fold
46.9-fold capture vs. 15.1-fold shotgun	161 (5.9%)	592 (21.6%)	6.9-fold
46.9-fold capture vs. 7.7-fold shotgun	96 (3.5%)	1793 (65.3%)	4.1-fold
Altai capture vs. shotgun (weak filters)			
46.9-fold capture vs. 53.7-fold shotgun	264 (9.6%)	16 (0.6%)	
46.9-fold capture vs. 44.3-fold shotgun	265 (9.7%)	15 (0.5%)	
46.9-fold capture vs. 34.5-fold shotgun	293 (10.7%)	17 (0.6%)	
46.9-fold capture vs. 28.5-fold shotgun	338 (12.3%)	18 (0.7%)	
46.9-fold capture vs. 15.1-fold shotgun	448 (16.3%)	36 (1.3%)	
46.9-fold capture vs. 7.7-fold shotgun	808 (29.4%)	110 (4%)	

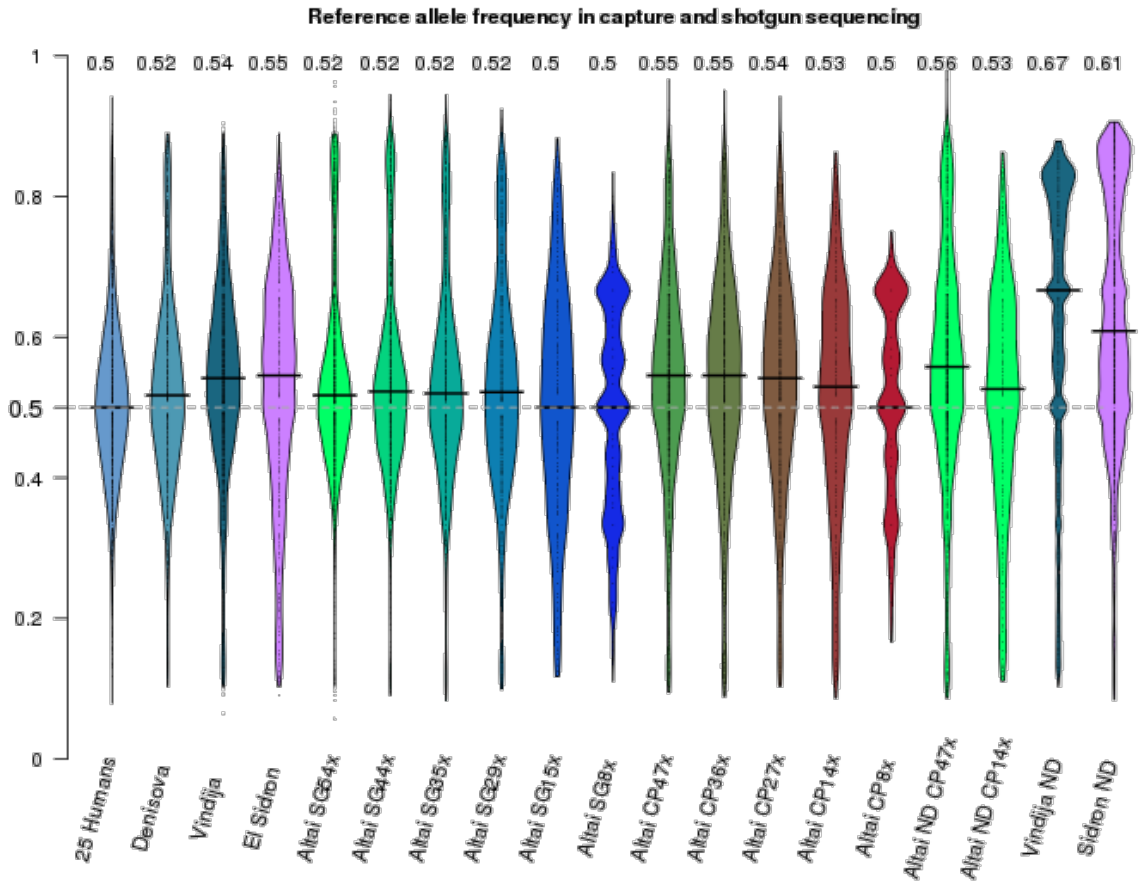

Figure S4. Reference allele frequency distributions. ND = samples without deamination correction (Supplementary Information 3). Median values are shown above the distributions.

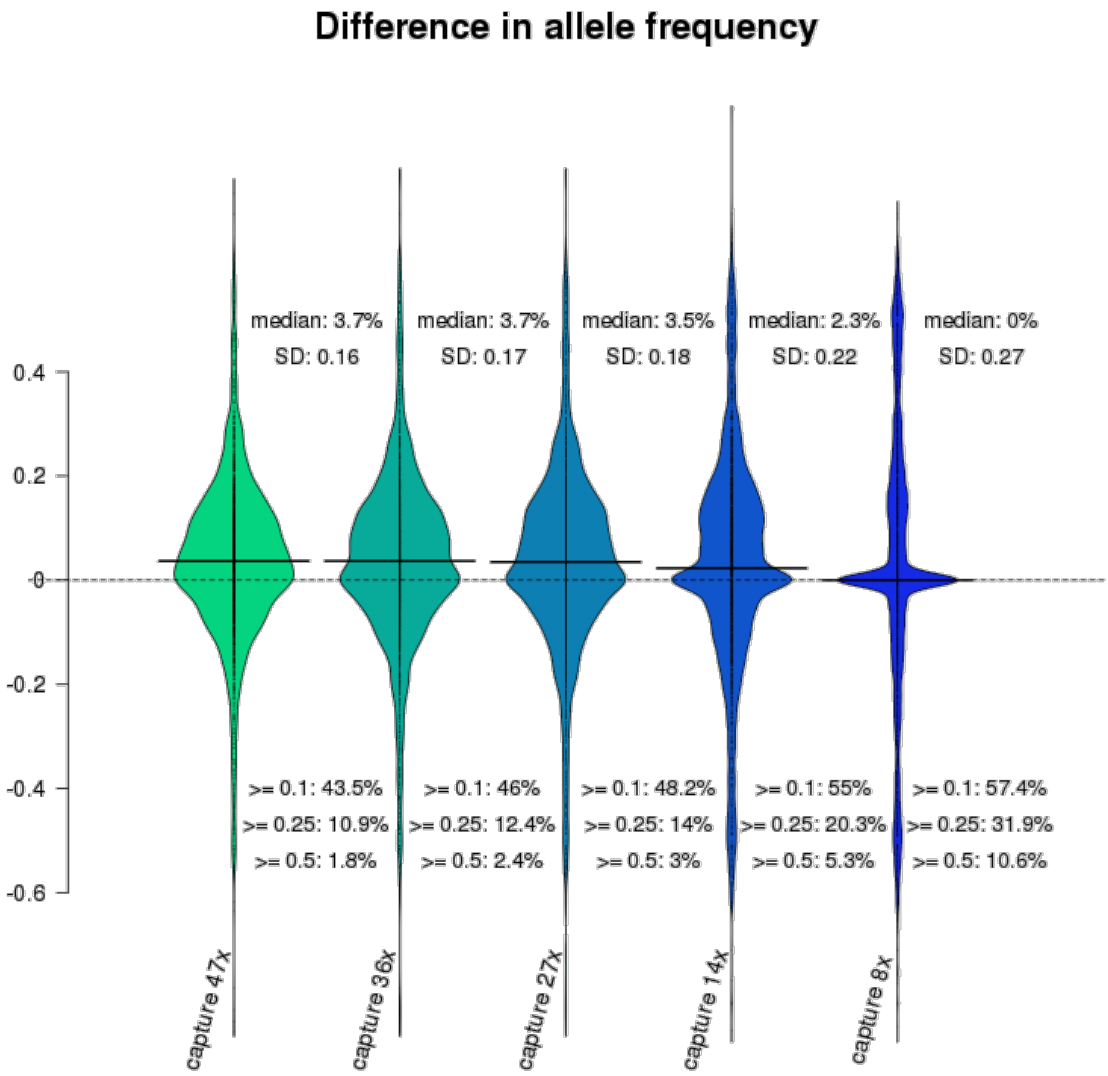

Figure S5. Difference in allele frequency between shotgun sequencing and sequencing after capture in the Altai Neanderthal. SD = standard deviations

SI 5. Archaics and present-day humans relationships

Sample relationships

We analyzed the relationships among the archaic and present-day samples using Principal Component Analysis (PCA) as provided by the R package *adegenet* (*21*). We only used sites that are variable in the dataset of four archaic individuals and 25 present-day human individuals and passed all filters in all individuals. The observations are in agreement with the PCA from exome data (*1*), with the first PC separating the archaic individuals from present-day humans (Figure S6A), the second PC separating non-Africans from Africans, with the Neanderthals shifted to the side of the non-Africans, and the third PC separating the Denisovan individual from the other hominins, with the Oceanians being closer. The fourth PC separates between the different African populations.

We calculated the pairwise spearman correlations of variable sites to generate a heatmap (R *lattice* package) displaying the relationships among the samples (Figure S7). The present-day human samples cluster according to their geographic localization, and the correlation within Africa is lower, which resembles worldwide patterns of diversity (*22*, *23*). The correlations between the different Neanderthal samples are higher than between present-day humans (0.85-0.90 in Neanderthals vs. 0.42-0.80 in present-day humans, mean = 0.56). The correlation between Neanderthals and the Denisovan individual is slightly lower than between distant present-day human samples (0.41), and much smaller between archaic individuals and present-day humans (0.27 for Altai and Vindija, 0.29 for El Sidrón and 0.23 for Denisova, with >0.25 for Oceanians). This resembles the previously described relationships of the sequenced individuals (*3*, *6*).

Variable sites were also used to infer a phylogenetic tree using the neighbor-joining method in the R package *phangorn* (pairwise differences) (*24*). The chimpanzee was used as a root, and 100 bootstrap replicates were generated (Figure S8). The tree groups together the present-day humans, while the Denisovan forms a clade with Neanderthals.

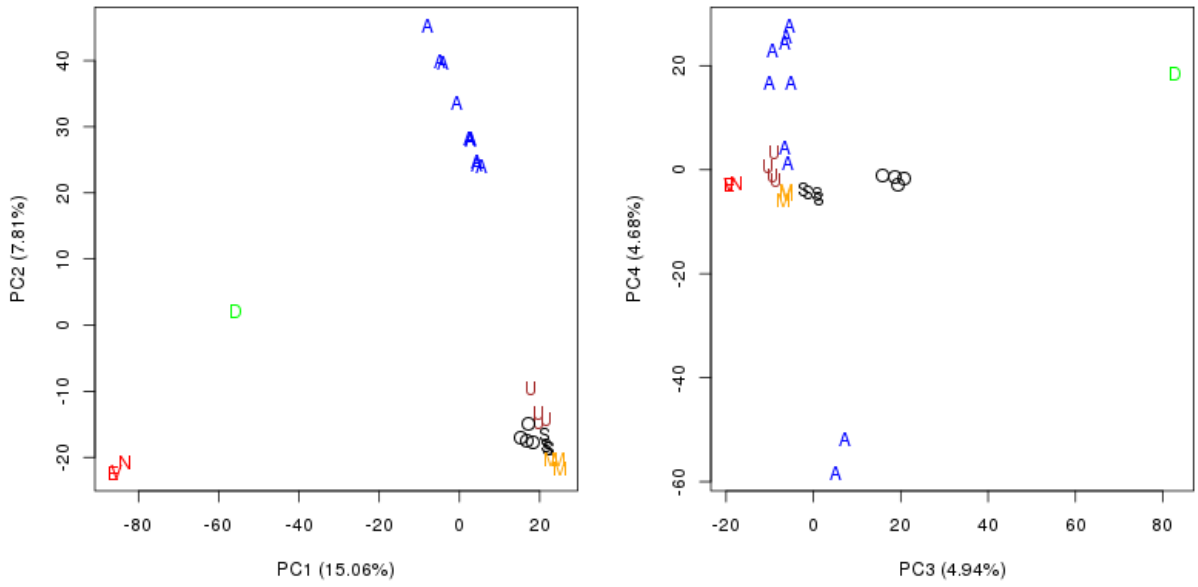

Figure S6. PCA from variable sites among archaic and present-day human individuals (*21*), considering sites that pass all filters in all individuals and are polymorphic. N=Altai Neanderthal, E=El Sidrón Neanderthal, V=Vindija Neanderthal, D=Denisovan, A=African, U=European, S=Asian, O=Oceanian, M=American. Notice that the first PC separates the archaic and present-day humans, the second PC separates non-Africans from Africans, the third PC separates the Denisovan from the others, and the fourth PC separates the San (bottom two), Mbuti (clustered with other individuals), and the other African individuals.

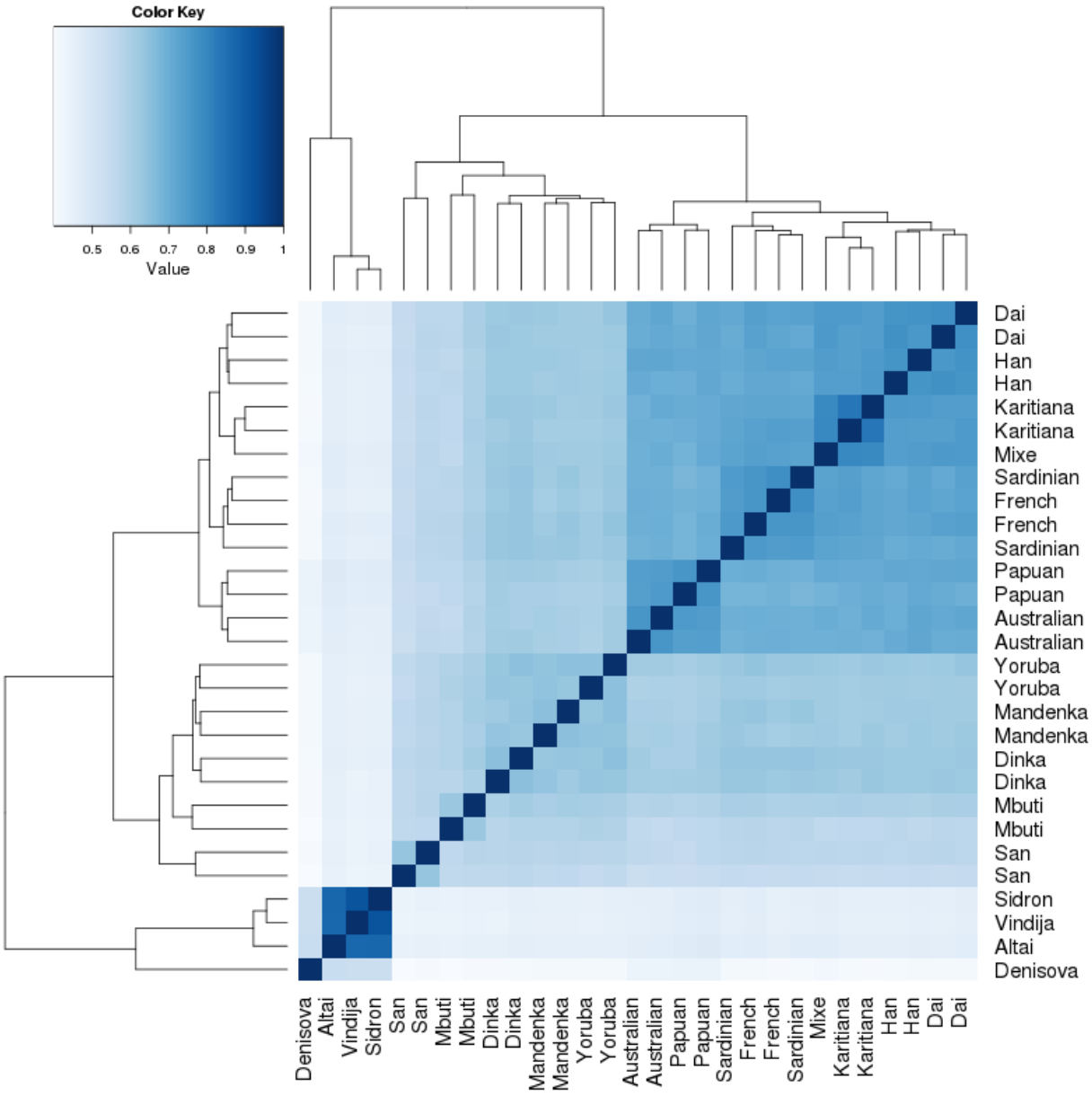

Figure S7. Distance matrix from pairwise spearman correlations between individuals, considering polymorphic sites that pass all filters in all individuals.

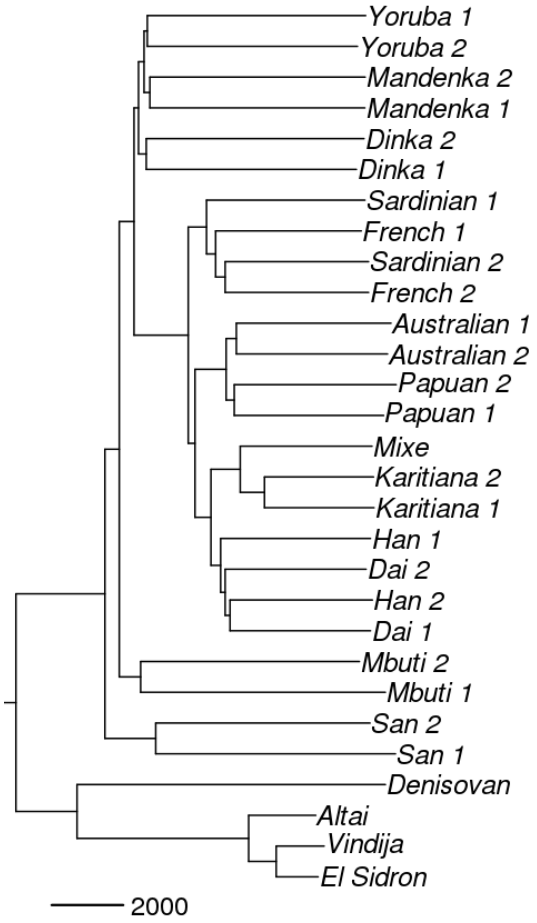

Figure S8. Neighbor-joining tree based on the number of pairwise differences between individuals (*24*).

SI 6. Heterozygosity and mating patterns

Heterozygosity

Table S7 lists the heterozygous calls for each individual. Heterozygosity is given as the number of heterozygous calls per 1,000 bases. Based on the counts of heterozygous sites in chromosome 21, the Altai Neanderthal has the lowest heterozygosity (0.131). When using mlRho (*25*), a maximum likelihood estimator of population mutation rate which approximates heterozygosity, it also has the lowest value (0.095). This is lower than the genome-wide average (0.176, based on the counts of heterozygous sites) (*3*) and slightly higher than the exome-wide average (0.113, based on the counts of heterozygous sites) (*1*). Despite capture bias (see Supplementary Information 4) the heterozygosity of the Altai Neanderthal shotgun (from 53.7-fold down to 15.1-fold coverage) and capture (from 46.9-fold and 14-fold coverage) data is comparable (Table S7). We conclude that the heterozygosity of the captured Vindija individual (35.9-fold coverage) is not strongly affected by coverage and capture bias. Lower coverage in the capture data of the Altai Neanderthal, however, results in many missed genotype calls in heterozygous sites due to their lower quality (Table S7). This is expected, because the effect of capture bias should be greater in sites covered by fewer sequences (more likely to miss sequences with alternative alleles). Thus, the heterozygosity of the El Sidrón individual is likely to be underestimated due to its 14.1-fold average coverage. Additionally, at lower coverage heterozygosity is also lower in the shotgun-sequenced Altai Neanderthal. We conclude that the contribution of capture bias to heterozygosity estimates is indeed small, compared to the effect of reduction in coverage.

If we now compare the heterozygosity estimates between the shotgun (53.7-fold coverage) and the low coverage capture data (14-fold coverage) from the Altai sample, we observe a decrease (0.131 – 0.109, a 16.8% drop based on the counts of heterozygous sites; 0.095 – 0.087, a 8.4% drop based on mlRho) in the capture data. If we correct the heterozygosity of the El Sidrón individual by this much, the estimate is similar to that of the Vindija Neanderthal. That is 0.242 and 0.263 (based on counts of heterozygous sites) for El Sidrón and Vindija, respectively. Thus, these European Neanderthals have higher genetic diversity than the Neanderthal and Denisovan individuals from the Altai cave in Asia. In any case, Neanderthal and Denisovan heterozygosities are much lower than the lowest values for present-day humans.

Inbreeding

The Altai Neanderthal is a recently inbred individual, with parents being related as closely as half-siblings (*3*). The low heterozygosity of this individual is likely the result of such inbreeding [reviewed in (*26*)]. However, while a low population size reduces diversity across the chromosome, recent inbreeding results in long stretches of homozygosity. These Runs of Homozygosity (ROH) are large chunks of the genome inherited from closely related parents. In order to analyze patterns of inbreeding, we screened the chromosome 21 of the archaic individuals and present-day humans for such ROH.

Given the small size of chromosome 21, we compared ROH of the following lengths: short ROH of length 10-100 kilobase (kb) and long ROH (>100kb). ROH of hundreds of Kb in length are likely to arise from recent inbreeding, while ROH of shorter lengths may arise from background relatedness when mating in a population of small effective size, as a result of reduced heterozygosity (*27, 28*). In order to use all possible information, we used all heterozygous sites that pass the filters described in Supplementary information 3. Since we did not join consecutive ROH, very long segments (>1Mb) are very rare on this chromosome.

The inbred Altai Neanderthal has an excess of long ROH compared to the other archaic samples (cumulative length of 14.5 Mb vs. 2.9-5 Mb) which, in turn, have a higher cumulative length of long ROH than most present-day humans (0.6-3 Mb, median 0.98 Mb). A large fraction of chromosome 21 is contained in long homozygous stretches in the Altai Neanderthal, and large fractions are contained in short ROH in the other archaic individuals (19.8-22.6Mb) compared to present-day humans (4.5-15.2Mb, median 11.3Mb). All archaic individuals show a significant excess in the distribution of shorter ROH lengths compared to present-day humans (Table S8). Within present-day humans, the reduced diversity of non-African populations led to an excess of short ROH compared to African populations, as a result of the out-of-Africa bottleneck [reviewed for example here: (*29*)]. We can identify this effect by using the two categories.

The excess of long ROH over short ROH is remarkable in the Altai Neanderthal (Figure S9). The Vindija, El Sidrón and Denisovan individuals show an excess of short ROH compared to present-day humans, but have few long ROH. The Denisovan individual, for which recent inbreeding has been rejected (*6*), shows only slightly more long ROH than El Sidrón and Vindija. Thus, Neanderthals other than the Altai lack a signal of recent inbreeding. A shift towards longer ROH compared to shorter ROH is also observed for the Karitiana, which belongs to a population with a known history of recent inbreeding (*3, 28*). We conclude that using two categories is suitable for the comparison between individuals based on only one chromosome.

Capture and coverage effects

Low sequence coverage may result in missed heterozygous calls and thus longer ROH, while wrong heterozygous calls may break longer tracts and lead to shorter ROH along the chromosome. We compared the captured sequence data of the Altai Neanderthal with the shotgun sequence data, and after capture we observe a shift towards long ROH (Figure S9A). This shift does not lead to significant change in the distribution of ROH for the range of coverages from 14-fold to 46.9-fold (P = 0.51-0.94; two-sided Mann-Whitney U test). At a coverage of 8.1-fold, the excess of long ROH is significant ($P = 4.1 \times 10^{-8}$; two-sided Mann-Whitney U test), hence a genome at this coverage would not allow this kind of comparison. However, the cumulative length of long ROH and the ratio of long to short ROH in the captured Altai sequences at any average sequence coverage above 10-fold is far outside the variation of present-day humans and other archaic individuals, and closer to the shotgun sequenced from the Altai Neanderthal than to any other sample. The variation introduced by different coverages after shotgun sequencing is comparable, as well as the strong effect of a very low coverage of 7.7-fold (Figure S9B).

Comparison to great apes

We analyzed data from all extant great ape species, in which the effects of population size differences and recent inbreeding have been described on the scale of subspecies (*30*). In order to compare datasets, we applied the general filters on the genotypes of all great apes. We used the *liftOver* function in the R package *rtracklayer* (*31*) to transfer the great ape genotypes from the human genome version hg18 to hg19, and used only genomes of wild-born animals (Table S9). Furthermore, the hominin genotypes were filtered for regions in which the great apes align without uncertainty to the human genome (*30*). The results are shown in Figure 4A, and in Figure S10 separately for each great ape species. The effects of population bottlenecks lead to an excess of short ROH in western chimpanzees and bonobos compared to central and eastern chimpanzees, and also in bornean orangutans compared to sumatran orangutans. Recent inbreeding leads to an excess of long ROH in a single chimpanzee individual and several gorillas, and the additive effect of a low effective population size and recent inbreeding in eastern lowland gorillas results in a strong excess of long ROH similar to what we observe in Altai Neanderthals. The other Neanderthal individuals are outside the range of variation of present-day humans as well as other great ape species, indicating a particularly low population size.

We used the complete autosomal genome sequences of the great apes, the 25 present-day humans, the Denisovan and the Altai Neanderthal to compare the genome-wide signatures of inbreeding with those observed on chromosome 21. We performed the same filtering on the genotype calls of all individuals, and calculated the cumulative lengths of short and long ROH. The overall patterns are similar to the patterns on chromosome 21 (Figure S11). However, as previously reported, we see that the Altai Neanderthal shows a stronger signal of inbreeding on chromosome 21 compared with the genome-wide average (*3*). Otherwise, the relative patterns are quite similar. The chimpanzee and orangutan populations separate the same way, single great ape individuals show signals of recent inbreeding, and eastern lowland gorillas are most inbred. African humans have much less short ROH than non-Africans, only the Native American group shows a slightly stronger shift towards long ROH as a result of recent inbreeding. Although the total coverage of long ROH is slightly smaller in the Altai Neanderthal than eastern lowland gorillas, this individual is far outside the range of present-day humans in terms of long ROH. The Denisovan individual is outside the range of present-day humans in terms of short ROH.

Table S7: Numbers of heterozygous and homozygous derived sites, and heterozygosity estimates from counts and mlRho (*25*). Group averages are calculated across all samples with the same geographic origin. mlRho estimates were calculated using the filtering described in (*3*).

Individual	Origin	Heterozygous sites	Homozygous sites	Derived sites	Heterozygosity	Exome-wide heterozygosity (*1*)	Genome-wide Heterozygosity (*3*)
Altai shotgun 53.7-fold	Archaic	3,022	23,020,748	36,081	0.131	0.113	0.176
Altai shotgun 44.3-fold	Archaic	3,073	23,120,676	36,231	0.133	-	-
Altai shotgun 34.5-fold	Archaic	3,011	23,054,091	35,837	0.131	-	-
Altai shotgun 28.5-fold	Archaic	3,035	22,927,957	35,028	0.132	-	-
Altai shotgun 15.1-fold	Archaic	2,811	22,635,656	33,930	0.124	-	-
Altai shotgun 7.7-fold	Archaic	1,192	13,477,765	19,383	0.088	-	-
Altai capture 46.9-fold	Archaic	2,752	21,196,172	31,754	0.13	-	-
Altai capture 35.7-fold	Archaic	2,529	20,605,964	30,239	0.123	-	-
Altai capture 26.7-fold	Archaic	2,365	20,016,548	28,780	0.118	-	-
Altai capture 14-fold	Archaic	1,930	17,749,434	24,179	0.109	-	-
Altai capture 8.1-fold	Archaic	1,005	7,316,366	7,542	0.137	-	-
El Sidrón 14.1-fold	Archaic	3,413	17,011,210	21,071	0.201	0.143	-
Vindija 35.9-fold	Archaic	5,130	20,577,269	29,369	0.249	0.127	-
Denisova	Archaic	4,879	22,940,739	36,103	0.213	0.145	0.215
HGDP00998	America	15,281	23,079,413	16,418	0.662	-	0.577
HGDP00546	Oceania	17,191	23,025,748	17,116	0.747	-	0.599
MIXE0007	America	17,287	23,099,317	14,950	0.748	-	0.613
HGDP01015	America	17,447	23,052,357	15,469	0.757	-	0.553
WONM	Oceania	19,420	23,023,170	15,461	0.843	-	0.66

doi:10.1038/nature16544

BURE	Oceania	19,506	23,051,428	16,394	0.846	-	0.667
HGDP00542	Oceania	19,668	23,001,857	15,766	0.855	0.321	0.639
HGDP00778	Asia	20,171	23,090,124	13,758	0.874	0.378	0.745
HGDP00533	Europe	20,210	23,058,330	13,752	0.876	-	0.758
HGDP00521	Europe	20,412	23,072,696	13,392	0.885	0.4	0.782
HGDP01076	Europe	20,584	23,128,199	13,270	0.89	-	0.735
HGDP00775	Asia	20,636	23,073,120	13,811	0.894	-	0.724
HGDP01308	Asia	20,662	23,070,946	13,662	0.896	-	0.72
HGDP01307	Asia	21,581	23,092,449	13,624	0.935	0.374	0.745
HGDP00665	Europe	22,389	22,996,392	12,526	0.974	0.39	0.781
HGDP0456	Africa	26,353	23,024,238	18,430	1.145	-	1.024
HGDP00936	Africa	27,083	23,078,687	15,790	1.174	-	1.007
DNK07	Africa	27,485	23,078,094	14,557	1.191	-	0.968
HGDP01284	Africa	28,178	23,103,682	14,318	1.22	0.511	1.033
DNK02	Africa	28,141	23,020,893	14,713	1.222	0.503	1
HGDP00927	Africa	28,490	23,094,154	15,840	1.234	0.508	1.02
HGDP01029	Africa	28,520	23,052,349	18,360	1.237	-	1.07
HGDP01036	Africa	28,766	23,069,722	17,918	1.247	-	1.022
HGDP01286	Africa	28,908	23,082,201	14,933	1.252	-	1.002
HGDP00982	Africa	29,842	23,076,134	15,348	1.293	-	1.01
Archaics					0.199	0.132	-
Americans					0.722	-	0.581
Oceanians					0.812	-	0.64125
Asians					0.900	-	0.7335
Europeans					0.906	-	0.764
Africans					1.222	-	1.0156

doi:10.1038/nature16544

Table S8: Two-sided Mann-Whitney U test, distribution of short (10-100kb) ROH in archaic individuals vs. present-day humans.

Individual	P-value
Altai	2×10^{-06}
El Sidrón	7×10^{-09}
Vindija	9.1×10^{-05}
Denisova	5.3×10^{-05}

Table S9: Number of individuals used per subpopulation of great apes and humans.

Population	Number of individuals
Eastern lowland Gorilla	2
Western lowland Gorilla	19
Cross river Gorilla	1
Central Chimpanzee	4
Eastern Chimpanzee	6
Western Chimpanzee	3
Nigeria-Cameroon Chimpanzee	10
Bonobo	10
Sumatran Orangutan	4
Bornean Orangutan	2
African humans	10
Eurasian humans	8
Oceanian humans	4
Native American humans	3

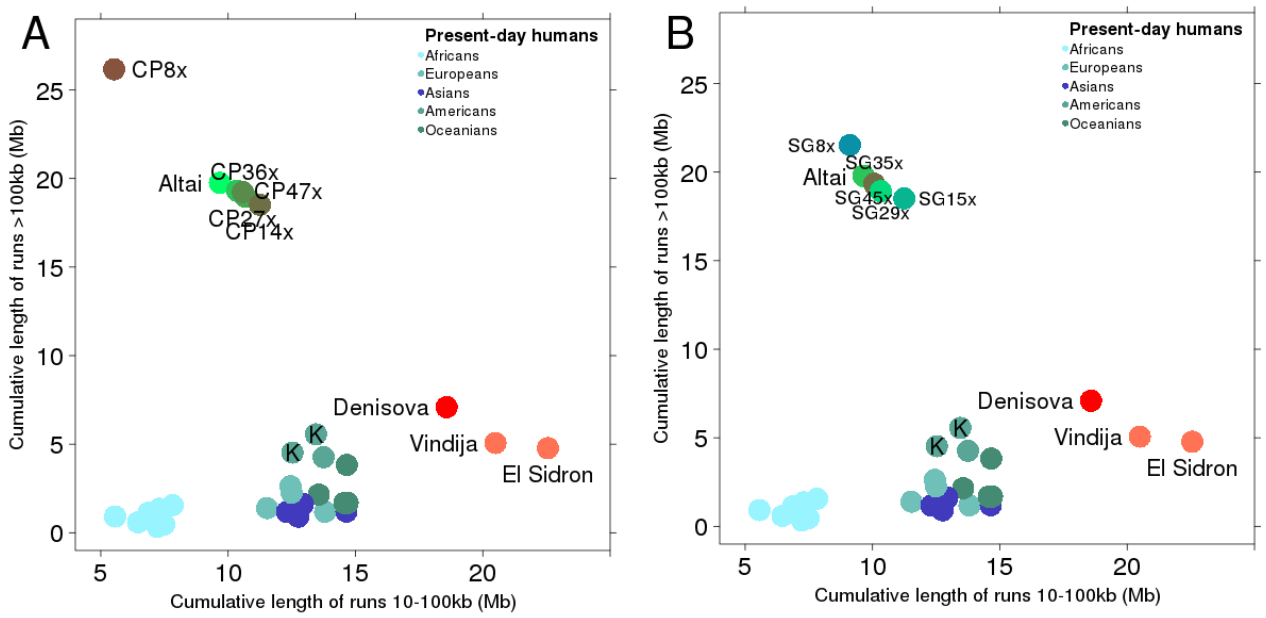

Figure S9. Short (10-100kb) vs long (>100kb) ROH on chromosome 21 in archaic and present-day humans. A) Including capture ("CP") at different coverages. B) Including shotgun ("SG") sequencing at different coverages (Supplementary Information 3).

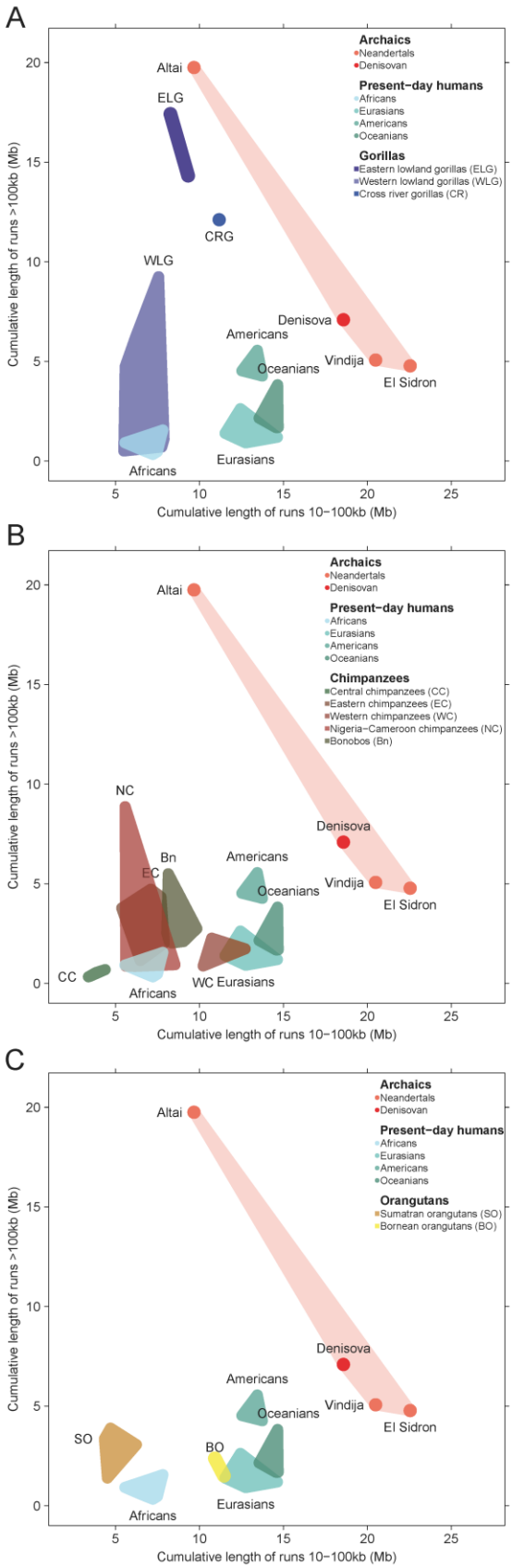

Figure S10. Short (10-100kb) vs long (>100kb) ROH on chromosome 21 in archaic and present-day humans and different great ape species. A) Gorillas. B) Chimpanzees and Bonobos. C) Orang-Utans.

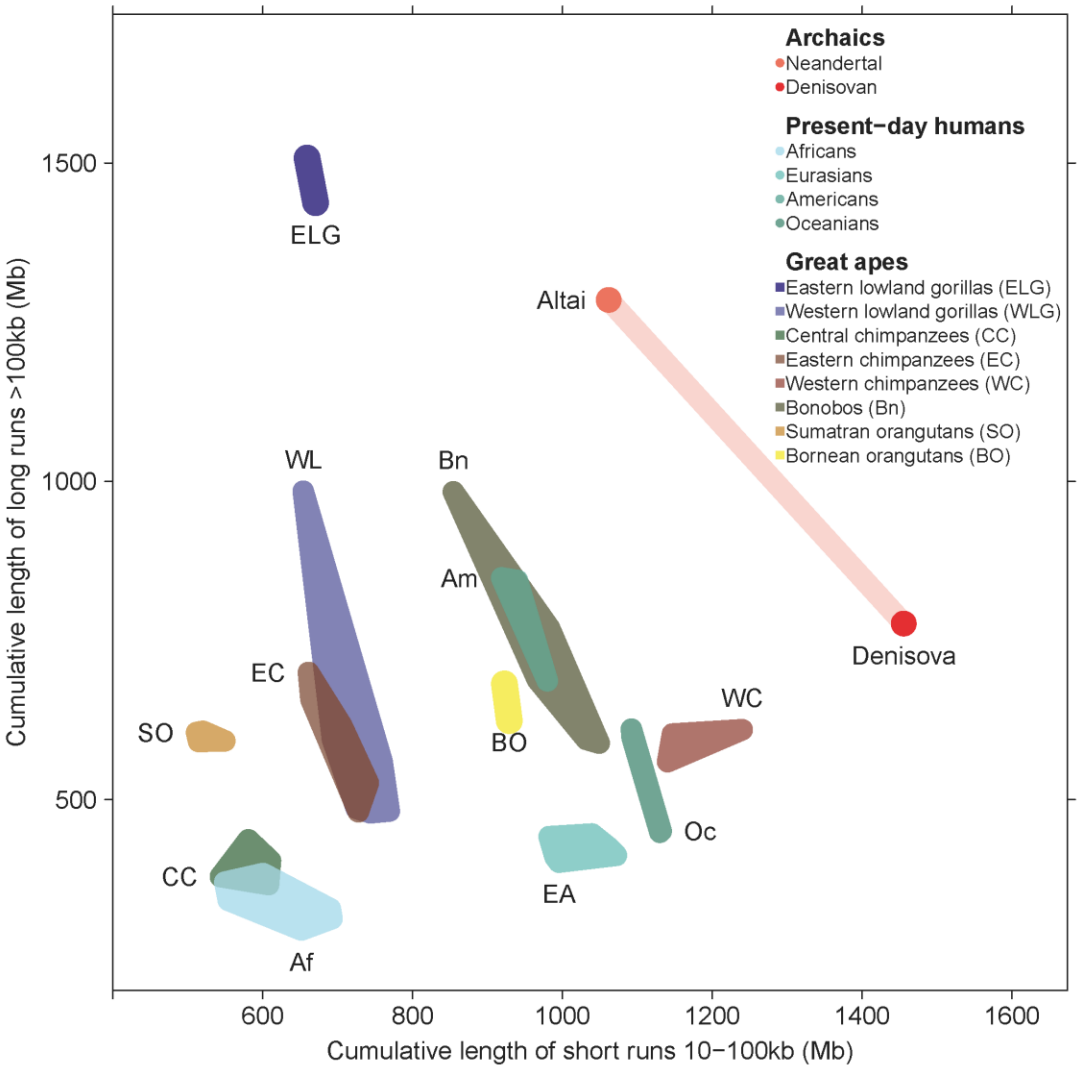

Figure S11. Short (10-100kb) vs long (>100kb) ROH across the whole genome in archaic and present-day humans and different great ape species.

SI 7. Efficacy of natural selection

A low population size over time will reduce the efficacy of purifying selection and result in a larger fraction of putatively deleterious alleles in Neanderthals than in present-day humans. Indeed, it has been shown previously that Neanderthals as a group carried a larger proportion of non-synonymous alleles inferred to alter the structure or function of proteins than present-day humans (*1*). The majority of chromosome 21 consists of non-coding regions, which are likely to have evolved neutrally, but also contain functional elements like untranslated transcribed regions (UTRs), non-coding RNAs and transcription factor binding sites (TFBS). Non-coding elements like TFBS are less conserved throughout evolution than coding regions (*32*). Here, we assess the patterns of deleterious variation in the non-coding parts of chromosome 21. We used three individuals per group for the following origins: Africans 1 (HGDP01029/San, HGDP01284/Mandenka, HGDP0456/Mbuti), Africans 2 (DNK02/Dinka, HGDP01036/San, HGDP00936/Yoruba), Europeans (HGDP00521/French, HGDP00665/Sardinian, HGDP00533/French), Asians (HGDP00778/Han, HGDP01307/Dai, HGDP00775/Han), Americans (HGDP00998/Karitiana, HGDP01015/Karitiana, MIXE0007/Mixe) and Oceanians (HGDP00546/Papuan, WONM/Australian, BURE/Australian).

Conservation and deleteriousness scores

We examined positions that are conserved among mammals according to two different conservation scores: phastCons (*33*) and phyloP (*34*). PhastCons scores >= 0.9 and phyloP scores >= 2 were defined as conserved. We calculated the fraction of polymorphic sites and homozygous derived sites with high conservation and low conservation for each annotation group. The fraction of conserved polymorphic sites in Neanderthals is higher than in modern humans for both conservation scores (Figure 4 and Figure S12A-B). However, this is not true for homozygous sites. We further used the recently published method CADD (*35*) to infer deleterious alleles along the chromosome 21 of Neanderthals. CADD provides PHRED-scaled C-scores as a measure of deleteriousness along a chromosome. Higher C-scores are indicative of higher predicted deleteriousness. Here, we also observe an excess of mutations at deleterious sites (C-scores >=10) in Neanderthals as a group compared to groups of present-day humans (Figure 4 and Figure S12C). This is also true for homozygous derived sites. We used another classifier of non-coding alleles, GWAVA (*36*), and repeated the above analyses. Mutations in deleterious alleles (GWAVA-score >=0.8) show an excess in Neanderthals (Figure S12D).

We also calculated C-scores for the genotype calls from the capture data of the Altai Neanderthal and a range of coverages from the shotgun sequencing data. We observe a slight shift towards higher C-scores throughout the range of coverage (17.0%-19.0% of scores >=5) compared to the genotypes from shotgun sequencing (17.0%), but this effect is not significant (P = 0.11, two-sided Mann-Whitney U test) and does not reach the extent of sites with deleterious alleles in the other Neanderthal individuals (21-21.3%). Only at a coverage of below 10-fold, we observe an excess of sites with high C-scores (Figure S13).

Excess of polymorphism in functional and conserved elements

We further focused on those regions, coding and non-coding, that are likely to have a functional role in chromosome 21, and assessed their putatively deleterious alleles. To define these regions, we relied on the transcripts (including UTRs) from ENSEMBL (*37*) as well as conserved TFBS (*38*). We also analyzed 5,000 bases upstream of any transcription start site as promoter regions, and 5,000 bases downstream of a transcription end site. We used the two conservation scores described above to define positions that are strongly conserved, with the top 10% of the empirical distribution of conservation values across chromosome 21 used to define functional regions within each functional class. For each of these classes, we retrieved polymorphic and homozygous derived alleles in sites that passed all filters in the three individuals of a given group. We also sampled the same number of sites from the putatively neutral regions which were used in our demography analysis (see Supplementary information 8). This enabled us to examine the reduction in polymorphic sites in functional regions compared to those observed in neutral regions, which is a measure of the amount of purifying selection acting on the different functional categories.

In coding regions, the ratio of non-synonymous to synonymous polymorphism is defined as P_n/P_s. We define the ratio of polymorphism in functional sites to polymorphism in neutral sites as $P_{(func)}/P_{(neu)}$. We computed this ratio for each functional class and for the different population groups (Figure S14) and find that it is significantly larger for Neanderthals in most functional classes (P-value = 6×10^{-3} - 3.9×10^{-7}; two-sided t-test). Thus, the fraction of polymorphic sites likely to be functional and putatively deleterious is higher in Neanderthals than in humans in all functional classes. A caveat of this approach is that the numbers of sites analyzed is often small (Table S10), and the functional definition of non-coding regions is less strict than coding ones.

Table S10: Numbers of sites in chromosome 21 falling within functional categories

Upstream	1,771,604
Downstream	1,710,162
UTRs	443,543
TFBS	212,082
Coding sites	1,383,182
PhastCons Top 10%	2,974,544
PhyloP Top 10%	2,971,209
Neutral	7,666,943

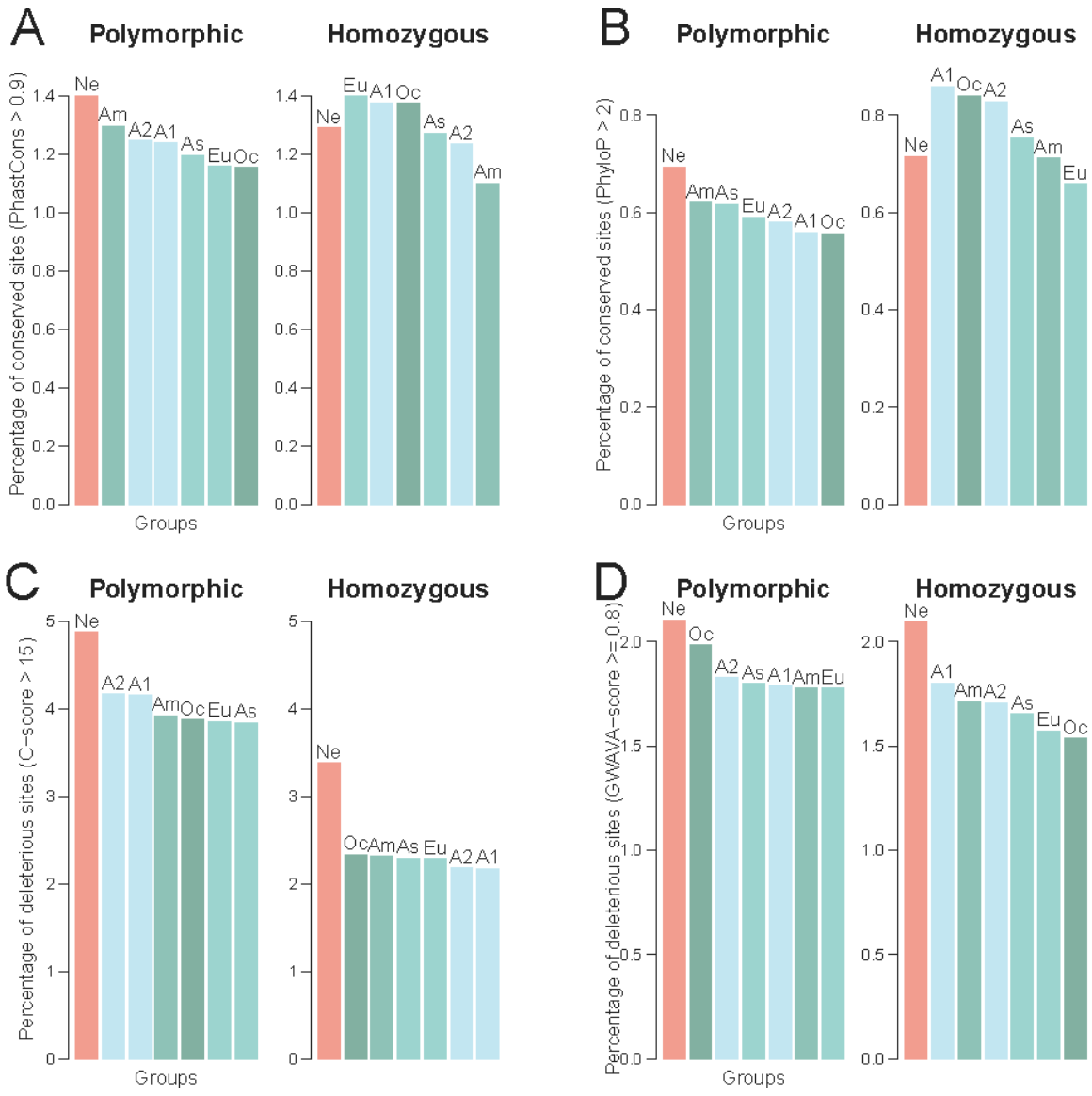

Figure S12: Proportion of derived alleles likely to be deleterious in Neanderthals or present-day humans. (A) Percentage of derived alleles, polymorphic or homozygous ("fixed"), that falls in conserved positions in the chromosome 21 of mammals according to PhastCons (*33*) posterior probabilities. Groups of present-day humans are shown in decreasing order. Ne = Neanderthals; A1 = Africans 1; A2 = Africans 2; Eu = Europeans; As = Asians; Oc = Oceanians; Am = Americans. **(B)** Percentage of derived alleles, polymorphic or homozygous ("fixed"), that falls in conserved positions in the chromosome 21 of mammals according to PhyloP (*34*) posterior probabilities. **(C)** Percentage of derived alleles, polymorphic or homozygous ("fixed"), inferred to be deleterious according to CADD (*35*) C-scores in chromosome 21. **(D)** Percentage of derived alleles, polymorphic or homozygous ("fixed"), inferred to be deleterious according to GWAVA-scores (*36*) in chromosome 21.

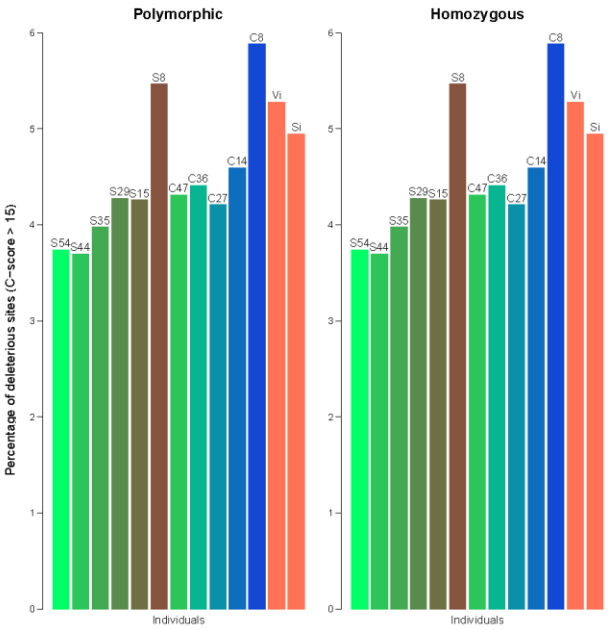

Figure S13: Percentage of derived alleles, polymorphic or homozygous, inferred to be deleterious according to CADD (*35*) C-scores in chromosome 21 across a range of coverages. S = Shotgun sequencing of Altai Neanderthal + depth; C = Sequencing after capture of Altai Neanderthal + depth; Vi = Vindija Neanderthal. Si = El Sidrón Neanderthal.

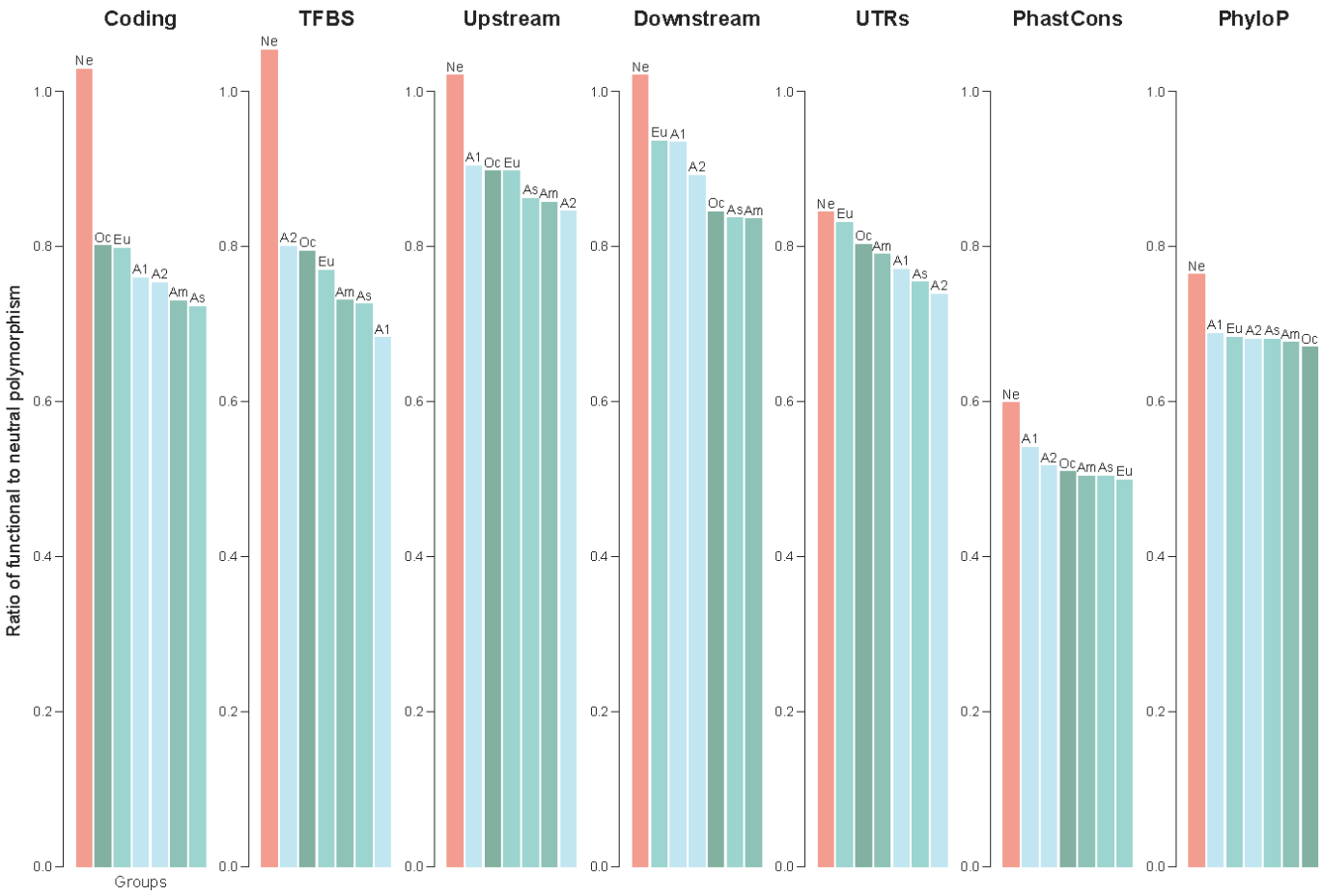

Figure S14. Ratio of derived polymorphism associated with coding or non-coding regions in genes to neutral polymorphism in chromosome 21. TFBS = Transcription Factor Binding Sites; UTRs = UnTranslated Regions. Ne = Neanderthals; Af = Africans; Eu = Europeans; As = Asians; Oc = Oceanians; Am = Americans. A simpler version of this analysis is shown in Figure 4.

SI 8. Demography inference

We conducted demography inference using the Generalized Phylogenetic Coalescent Sampler (G-PhoCS (*39*). Inference by G-PhoCS is based on examination of patterns of variation in a large number of short, putatively neutral loci in approximate linkage equilibrium. The method summarizes the information in sequence variation by approximately integrating over local genealogies at these loci using a Bayesian sampling strategy. Our analysis followed the basic guidelines developed in previous studies (*39*, *40*). In this section we provide a detailed account of the analysis, followed by a summary of our results and additional validation.

Genomic filters

Various genomic filters were applied to minimize the influence of sequencing errors, alignment errors, and direct natural selection on the demography inference. We eliminated the following regions: **1)** simple repeats identified by Tandem Repeats Finder (TRF) (*41*) (Simple Repeats track for GRCh37/hg19 downloaded from the UCSC Genome Browser); **2)** recent segmental duplications in the human genome (*42*) (Segmental Dups tracks for GRCh37/hg19), **3)** transposable elements identified by Repeat Masker (http://www.repeatmasker.org) with ≤20% divergence from their consensus sequences, **4)** regions with a mappability score in the Duke 20mer uniqueness score different from 1; **5)** sites flagged as systematic errors (*16*); **6)** regions not showing conserved synteny between human and chimpanzee (according to the UCSC syntenic net of the alignment between GRCh37/hg19 and panTro2); and **7)** sites with invalid Human-Chimpanzee ancestry information (see **Filtering** in Supplementary information 3). To reduce the influence of direct natural selection on our demography inference, we also filtered out exons of protein coding genes and RNA genes annotated by GENCODE v.13 (*43*) together with the 1,000 bp flanking these genes in each direction, and conserved non coding sequences corresponding to PhastCons elements (based on the 46-way Conservation track in the UCSC Genome Browser) and 100 bp flanking these sequences. Finally, we filtered out recombination hotspots (*44*) to avoid recombination within loci. In parts of the analysis, we also filtered out positions that may be affected by recent inbreeding in the Altai Neanderthal (*3*). (see **"Neutral Loci"** below).

Neutral loci

Because G-PhoCS assumes a model with no intra-locus recombination and no linkage between loci, we identified a collection of short loci, 1 Kb long, that were separated by at least 30 Kb and contained a sufficient number of unfiltered positions (at least 700 bp out of 1,000 bp in each locus). We applied a greedy strategy that aims to maximize the total number of informative sites under these constraints. This procedure resulted in 33,812 loci covering 30.6 million unfiltered positions (906 positions on average per 1 Kb locus). We further subsampled loci by selecting every third locus, resulting in 11,271 loci. We applied a slightly more relaxed procedure for chromosome 21 with the minimum distance between loci set to 2 Kb, which resulted in a total of 954 loci covering 824,000 unfiltered positions. It is important to note that reducing

inter-locus distances increases the dependency between loci, but this mostly affects the credible intervals of parameter estimates (by artificially reducing their size) and not the mean posterior estimates. Additionally, while the minimum distance between loci on chromosome 21 is set to 2 Kb, the mean distance is 10 kb. Thus our preliminary analysis without the two Western Neanderthals was done on the union set of 12,225 loci. Because nearly 40% of chromosome 21 (18.8 Mb) is covered by a genomic segment inferred to be influenced by recent inbreeding in the Altai Neanderthal, when analyzing the two European Neanderthals, we further relaxed our constraints by removing this filter from our set. This resulted in a total of 2,960 loci on chromosome 21 and 13,753 loci genome-wide. Our analysis indicates that these putatively inbred segments mostly influence estimates of the Altai effective population size (see **"Influence of inbreeding in the Altai Neanderthal"**).

Sequence data

Our demography inference is based on analysis of multiple sequence alignments of the four archaic genomes, several genomes from present-day humans, and the chimpanzee genome (panTro2). Each of the archaic and present-day genomes was filtered for quality, coverage, and mappability using 'N' genotypes (see **Filtering** in Supplementary information 3). Heterozygous genotypes were converted to the appropriate IUPAC ambiguity symbols (R, Y, S, W, M, and K) to enable G-PhoCS to consider the two chromosome copies for each individual (no phasing is needed, since G-PhoCS sums over all possible phases, see (*39*)). Alignment to chimpanzee was extracted from the 46-way alignment of mammalian genomes from the UCSC Genome Browser. Sub-alignments were computed for the neutral loci and subsequently filtered at positions covered by our global filters (defined above).

Population phylogeny and model of gene flow

Our demography inference focuses on the history of archaic humans. To make the analysis more efficient, and avoid the confounding influence of the complex demography of modern human populations, we divided the main analysis into five separate runs. In each run we analyzed archaic humans together with two present-day humans from one of five different populations covering a broad geographic range (Table S11). This strategy also allowed us also to validate the robustness of our estimates. In each separate analysis, we assumed a population phylogeny with the topology of the neighbor joining tree (Figure S8). We ran a series of preliminary analyses only including the Altai Neanderthal and the Denisovan as archaic samples, and a separate series of analyses adding the chromosome 21 sequences from the two European Neanderthals. To model post-divergence gene flow, the population phylogeny was augmented with a series of migration bands, each represented by an ordered pair of branches in the phylogeny. In our initial analysis of the Altai Neanderthal and the Denisovan genomes, we considered all 2x3 ordered pairs of sampled populations. In the main analysis including the chromosome capture sequences from the two European Neanderthals, we considered all 2x4 pairs of sampled archaic and modern populations as well as all 2x3 pairs of Denisovan and Neanderthal populations, for a total of 14 migration bands per run. In a separate run we also considered

gene flow from an unsampled archaic population into the Denisovan population (see **"Admixture with unsampled archaic population"**).

Uncertainty in ancient DNA sample age

One of the challenges of analyzing archaic individuals is that their genomes stopped accumulating mutations once the individuals that carried them died tens of thousands of years ago. Thus, the terminal branches in the genealogies leading to these individuals are shorter and do not reach present time. To account for this, we modified the probabilistic model of G-PhoCS to treat the individual ages as additional free parameters with exponential prior distributions (see below), and added a series of steps to each iteration of the sampling algorithm, which suggest changes to the ages of the archaic individuals (one at a time). This update step is similar in nature to the step of changing a divergence time parameter. Importantly, we kept the age of the chimpanzee outgroup and the present-day human individuals at zero, and sampled only the ages of the archaic individuals. As initialization points for the archaic ages, we chose the number of missing mutations on the path between each archaic individual and the chimpanzee reference, when compared to the mean divergence of present-day humans to chimpanzee (Table S12). We also tested our method and found it to be robust to the changes in the initial values chosen for the archaic ages (see **"Examination of sample ages**"; Figure S17). This new method is implemented in G-PhoCS v.1.2.3 (http://compgen.cshl.edu/GPhoCS/). An important thing to note is that we model the archaic populations (e.g. "Altai Neanderthal" and "Denisovan") all the way until present time, to allow gene flow from these populations to occur after the time in which these individuals are sampled. This is consistent, for instance, with gene flow from Neanderthals to modern humans out of Africa occurring much after the lifetime of the Altai Neanderthal.

MCMC setup

Each G-PhoCS run took as input the sequence alignment file (see **"Sequence data"** above) and a control file defining the population phylogeny and migration bands (see **"Population phylogeny and model of gene flow"** above), as well as features of the sampling procedure and probabilistic model. A standard prior distribution was defined over all model parameters (*39, 40*): an exponential distribution with mean 0.0001 was used for all θ and τ parameters (N_e and T scaled by mutation rate) and sample ages, and a Gamma (α=0.002, β=0.00001) distribution was used for all mutation-scaled migration rates. Additionally, we assumed variable mutation rates across loci with a Dirichlet (α=1) prior distribution. All parameters were randomly initialized in an interval within 0.1 standard deviation from their prior mean. After running a series of preliminary runs confirming that initialization does not influence parameter estimates, we settled on a set of fixed initialization values for divergence times: 0.0001 for the European Neanderthal divergence, 0.00012 for the divergence between the European and Altai Neanderthals, 0.00015 for the Neanderthal-Denisovan divergence, 0.0002 for the archaic-modern divergence, and 0.004 for the human-chimpanzee divergence. The first 10,000 sampling iterations were devoted to fine-tuning the MCMC update steps (by setting the `find-finetunes` attribute in the control file), and parameter sampling started after an additional 90,000

iterations, every 50 iterations for the following 200,000 iterations, resulting in 401 values sampled for each parameter from an approximate posterior distribution. Convergence was confirmed visually separately for each run by observing traces of the parameter values. We ran G-PhoCS v.1.2.3 (http://compgen.cshl.edu/GPhoCS/) on a Linux computer cluster with Intel Xeon E5-2665 2.40GHz CPU. An average run took 5 or 10 days to complete (for the three or five population runs, respectively).

Bayesian estimates and calibration

Using the 401 values sampled for each parameter from the approximate posterior distribution (see above), we computed for each parameter the mean posterior estimate and 95% Bayesian credible intervals. When examining combined results across runs, we aggregate the MCMC traces of different runs and then compute the mean and the 95% Bayesian credible interval of the aggregated trace. Estimates are produced by G-PhoCS in mutation units. Thus, to obtain estimates of effective population size in numbers of individuals and divergence times in years we must make additional assumptions about the mutation rate and average generation time. For generation time, we assumed 29 years on average (*45*) throughout the history of modern and archaic humans (assumptions on generation time only influence our calibrated estimates of N_e). For mutation rate, we assumed an estimate of the human mutation rate based on parent-offspring genome comparisons, which put it at about an average of 0.5×10^{-9} mutations per bp per year (*46-48*). This rate was recently corroborated by analysis of the complete genome sequence of an ancient modern human (*49*). Estimates reported in our study were calibrated using this rate, but it is important to note that there still is an ongoing debate about the sex-averaged human germline mutation rate, with older estimates based on calibration with species divergence in primates implying a rate that is roughly twice as fast as the estimate used here (1.0×10^{-9} mutations per bp per year; see (*50-52*)). Because the mutation rate acts as a scaling factor applied to our raw estimates, assuming such a rate would simply reduce all estimates of numbers of years by a factor of two.

Total migration rates

To provide meaningful measures of migration rates, we multiplied the migration rate estimated for each migration band by the total time duration of that band (which is typically the life span of a given population). For instance, for the migration band from the Denisovan population into the modern human population, we multiply the migration rate by the time of divergence between the Denisovan and the Altai Neanderthal (or all three Neanderthals in the five population analysis). This results in a measure of total migration rate approximately equal to the probability that a lineage from the target population (modern humans in the above example) originated in the source population (Denisovan in the example). Note that the mutation units cancel in this calculation, so it is independent of the calibration described above.

Preliminary analysis with the Altai Neanderthal and the Denisovan

We started with a series of analyses including the Altai Neanderthal, the Denisovan, two present-day humans for a single populations (considering five different populations), and the chimpanzee outgroup. As

expected, discrepancies were mainly observed in the estimates for the present-day human population size (θ_{Mod}) due to the use of individuals from different present-day populations in different runs (Figure S15; Table S13). Interestingly, there were also slight differences observed in the estimates of the ancestral population sizes (θ_{HUM} and θ_{ARC}) and the divergence times (τ_{HUM} and τ_{ARC}). The differences were mostly between estimates obtained using African versus non-African individuals. These differences could reflect compensation for the simplified model with constant population size along each branch of the population phylogeny. While this simplified model was shown in simulations to be robust to complex changes in N_e, including population bottlenecks and rapid expansions, a slight influence was observed in some extreme cases (*40*). Thus it is possible that the population bottlenecks and super-exponential expansion that characterize demographic changes in non-African populations could cause overestimation of the ancestral population size (θ_{HUM}) in runs using non-African individuals, which would consequently lead to underestimation of the divergence time (τ_{HUM}). In Table S13, we report the estimates obtained in the analysis of the Yoruba individuals as well as the mean estimate across all five runs and the union of the five separate credible intervals for these parameters.

Our estimates of migration rates are summarized in a matrix in Extended data figure 1, which presents the estimated total migration rates in all cases for which the 95% Bayesian credible interval of the total rate did not overlap 0, and its upper bound was above 0.3%. We identified four clusters of migration events: Admixture of Neanderthals into modern non-African humans, admixture of Denisovans into present-day humans from Oceania, admixture between the Denisovan and the Neanderthal populations, and gene flow from modern humans (African) into the Altai Neanderthal population. We note that the directionality of gene flow between the Altai Neanderthal and the Denisovan is difficult to infer in this scenario, because these are sister populations in our phylogeny. This event, and the two introgression events from archaic humans into modern humans were reported in previous studies. The final event of gene flow from modern humans into Neanderthals has not been previously reported (Supplementary Information 9 and 10).

Influence of inbreeding in the Altai Neanderthal

In our analysis we filtered out genomic positions that show evidence of recent inbreeding in the Altai Neanderthal, meaning that they belong to long runs of homozygosity (ROH) (*3*). To understand the potential influence of inbreeding on our demographic estimates, we re-ran the analysis with two Yoruba individuals on the set of 13,753 putative neutral loci identified without filtering the putatively inbred positions. Estimates in these runs were very similar to the ones obtained in our original set of 12,525 loci (Figure S15B). The only parameter estimate that seemed to be significantly influenced was the effective population size of the Altai Neanderthal, $\theta_{AltaiNea}$, whose estimate dropped from 2,200 (CI: 2,000-2,400) to 1,500 (CI: 1,400-1,600), due to the inclusion of long ROH. Importantly, the inferred migration rate from modern humans into the Altai Neanderthal population remains high at 5.8% (CI: 3.2-8.8%). We take this to imply

that patterns in genetic variation caused by recent inbreeding do not influence our inference in any substantial way.

Admixture with unsampled archaic population.

It was suggested in previous studies that the Denisovan population received gene flow from an unsampled archaic population with very ancient divergence (*3*). Scenarios of this sort are often informally termed admixture from a "ghost population". We tested this scenario using G-PhoCS to ensure that such gene flow would not significantly change our other estimates. We added a "ghost" population (Ghost) to the population phylogeny and attached it to the branch above the divergence of modern and archaic humans (Figure S15A). This population was not associated with any sampled individual, and we introduced a migration band from Ghost to the Denisovan population. We ran a separate analysis using this setting and two Yoruba individuals in the "Modern" population. We inferred migration from the ghost population into Denisovans at a low total rate of 0% - 0.5% (95% Bayesian credible intervals). When comparing estimates from these runs with our main inference we see that modeling ghost admixture does not influence estimates for any of the other parameters. Importantly, it does not influence our estimates of gene flow from modern humans into the Altai Neanderthal population (CI: 1.4%-7.8%). Interestingly, the unsampled population is inferred to have diverged from the ancestors of all human populations at around 2.4-3.1 million years before present, consistent with some of the previously reported estimates (*3*) (there were also earlier estimates at around 1 million year).

Five populations analysis

We added the chromosome 21 sequences from El Sidrón and Vindija Neanderthals to our data set and re-ran the demographic inference. Because nearly 40% of chromosome 21 (18.8 Mb) is covered by a genomic segment inferred to be recently inbred in the Altai Neanderthal, we relaxed our filters and included in this analysis regions that were putatively inbred in the Altai Neanderthal. As showed previously, these genomic segments do not significantly influence our inference (see **"Influence of inbreeding in the Altai Neanderthal"**). Thus, the five populations analysis was done on a total of 13,753 putative neutral loci. Our parameter estimates are consistent with those obtained in the preliminary analysis described above, with minor fluctuations in the estimates parameters common to both models (Extended Data Fig. 6; Table S14). The parameters pertaining to Neanderthal demography show a decline in effective population size continuing the trend we observed from θ_{HUM} to θ_{ARC} and $\theta_{Denisovan}$. Interestingly, $\theta_{Vindija}$ is higher than other population size parameters in the archaic subtree, suggesting a possible increase in N_e of Western (European) Neanderthals after their divergence from Eastern populations. Analyzing Neanderthal individuals from different populations enables us to estimate that these populations diverged from each other during a time period between 53,800 and 167,100 year ago (see **"Examination of sample ages"** below for a more detailed discussion).

The European Neanderthals helped us refine the collection of admixture events we found in the three populations analysis. Gene flow into non-African humans appears to come predominantly from a population more closely related to the European Neanderthals than to the Altai individual (Figure S16). We do note that the source of gene flow is often difficult to pinpoint using coalescent models due to incomplete lineage sorting. For this reason, we cannot confidently determine the source of gene flow from Neanderthals into Denisovans, since we estimate significant rates from both the Altai and El Sidrón Neanderthals. We also see traces of gene flow from Denisovans into present-day East Asians, which we did not see in the analysis without the two European Neanderthals. Evidence of such gene flow was previously proposed to be either a result of low levels of Denisovan admixture into the ancestors of present-day Asians (*53*, *54*), or later migration from the ancestors of Oceanian populations into East Asia (*6*, *55*). Another explanation suggested for these patterns has been a second wave of gene flow into Asians from a Neanderthal population close to Denisovans (*56*). Importantly, we see significant rates of migration from modern humans into Neanderthals, and in all cases the target population was the one ancestral to the Altai Neanderthal. It is important to note here the target of admixture is easier to determine than its source, which is confounded by incomplete lineage sorting. Still, as noted in Supplementary information 10, more high quality sequence data is needed to conclusively determine the influence of modern human admixture in Neanderthal individuals other than the Altai Neanderthal.

Examination of sample ages

As noted above (see **"Uncertainty in ancient DNA sample age"**), a key challenge in the analysis of archaic genomes is to account for differences in the individual ages. In our analysis we treated the age of each of the four archaic individuals as a free parameter ($\tau_{Denisovan}$, $\tau_{AltaiNea}$, $\tau_{Sidrón}$, and $\tau_{Vindija}$). In each of the runs described above, we initialized the sampler by setting these parameters based on missing mutations on the path between the archaic individual and the chimpanzee reference genome (Table S12). To test the robustness of our sampling technique to the initial values and the consequence on the inferred individual ages, we ran three additional analyses using alternative initialization values. In each of these runs, we used the Yoruba individuals in the present-day human population and all four archaic individuals were initialized to the same age in mutation scale. The three runs used the three following initial values covering the range of ages estimated from missing mutations: 0.00003, 0.000045, and 0.00006. We observed a high level of agreement across the four runs (the main run and the three additional runs) in estimates of the four sample ages (Figure S17A). The influence we see of the initial values is a very slight negative correlation between the initial value and the four estimated individual ages (most apparent in $\tau_{Sidrón}$).

The resulting individual age estimates are consistently smaller than those estimated using missing mutations and consequently more similar to estimates obtained from the archaeological record (Table S15). This implies that information on the age of the individuals in our model comes from comparisons among the archaic individuals and not only from comparisons with the present-day humans and the chimpanzee

outgroup. We note that the reduced heterozygosity in individuals that were sequenced after capture might contribute to a reduced number of observed mutations (Table S7). This could explain the relatively high values we obtain for the age of the individuals, in particularly for the El Sidrón Neanderthal, which is sequenced at relatively low coverage. Using the individuals age estimates, we can also examine the divergence times relative to the period in time in which the different archaic individuals lived. For each divergence time parameter, we computed the difference between its value and the maximum of the two times corresponding to its two daughter populations. We examined the approximate posterior distribution of the four derived parameters: $\Delta\tau_{W.NEA}$, $\Delta\tau_{NEA}$, $\Delta\tau_{ARC}$, and $\Delta\tau_{HUM}$ (Figure S17A and B). We see that $\Delta\tau_{W.NEA}$=2,600 years (CI: 100–7,600 years), implying that El Sidrón Neanderthal belonged to a population nearly directly ancestral to the Vindija Neanderthal. The divergence between the Eastern and Western (European) Neanderthals ($\Delta\tau_{NEA}$) is inferred to have occurred 14,400 years before that time (CI: 8,700–25,300), and roughly 38,000 years before the time of the Altai Neanderthal. Interestingly, these divergence levels are similar to those observed between present-day humans from East Asia and Europe (*39*).

Simulations examining the accuracy of G-PhoCS inferences

We generated simulated data sets to examine the accuracy of demographic estimates obtained by G-PhoCS in this setting. The simulations were conducted using the software *ms* (*57*), and using a demographic model consistent with the one inferred by our main demographic inference (see Extended Data Fig. 6 and Figure S21). The simulation generated 10,000 loci of length 1 Kb. We simulated the Altai Neanderthal, the Denisovan, and three modern human populations corresponding to the San, Yoruba, and French, assuming divergence times as inferred by recent studies (*39*), constant effective population sizes for the African populations, as inferred by our analysis (Table S13), and exponential growth for the European population, as inferred by other recent studies (*58*). Introgression from modern humans into the Altai Neanderthal was modeled from a fourth modern human population that split 300,000 years from the population ancestral to all present-day humans. The simulations also modeled gene flow from the Altai Neanderthal population to the Denisovan, and gene flow from a deeply divergent archaic population (2.6 million years ago) into the Denisovan. This divergent population and the modern population contributing gene flow to the Altai Neanderthal did not contribute samples to the simulations themselves, treating them as unsampled 'ghost' populations. We used the following command line to generate trees in ms, then shortened the external branches leading to the Altai Neanderthal and Denisovan chromosomes (samples 1-4) by 0.0000359 and 0.0000256 (resp.) to simulate their estimated ages, and ran *seq-gen* (*59*) on the resulting trees. (Note that N_e of the two archaic populations is set to an arbitrary high value to ensure that the two lineages from each individual do not coalesce until the sampling time).

```
ms 11 10000 -T  -r 0.1 1000 -seeds 96963 78582 56776 -I 8 2 2 2 2 2 0 0 1
-n 1 10 -n 2 10 -n 3 0.001442 -n 4 0.001238 -n 5 0.003570 -n 6 0.00015 -n 7 0.00015 -n 8
0.0012    -g 5 84624
-en 0.0000359 1 0.00013 -en 0.0000256 2 0.00015
-em 0.00004563793 2 1 260000 -em 0.00004566293 2 1 0
-eg 0.000049975 5 0 -en 0.000049975 5 0.000052
```

```
-ej 0.0000500 5 3 -en 0.0000500 3 0.001442
-em 0.00005127586 1 6 710000 -em 0.00005130086 1 6 0
-ej 0.0001200 4 3 -en 0.0001200 3 0.001442
-ej 0.0001500 6 3 -en 0.0001500 3 0.001442
-em 0.00015381774 2 7 400000 -em 0.00015384274 2 7 0
-ej 0.000204    2 1 -en 0.000204    1 0.0006186
-ej 0.000312    3 1 -en 0.000312    1 0.0009873
-ej 0.001293103 7 1 -en 0.001293103 1 0.0009873
-ej 0.008620690 8 1 -en 0.008620690 1 0.001189
```

Using these guidelines, we generated two different data sets: one simulated under the full model (as defined by the above command), and one without gene flow from modern humans into the Altai Neanderthal population (removed line highlighted in bold). We ran G-PhoCS three times on each of the two data sets, using different present-day samples in each run. Parameter estimates are summarized in Extended data figure 2. First, we see that most parameters are estimated accurately in all six runs. As expected, the main difference between the two data sets are the values inferred for $m_{Mod->AltaiNea}$, thus validating the ability of G-PhoCS to detect low levels of gene flow between modern humans and the Altai Neanderthal population even in the presence of archaic introgression into Denisovans. We do note, however, that the rates of migration that G-PhoCS infers for this archaic admixture event are significantly higher than the ones used in simulations (4-7% inferred versus 1% simulated). When we compare runs that examine African and non-African samples we see patterns similar to those observed in the data analysis. The divergence of modern and archaic humans (τ_{HUM}) is under-estimated when using the European sample, likely due to the fact that non-African populations experienced bottlenecks and subsequent exponential expansion, which violate the constant population size assumption made by G-PhoCS. Also under-estimated is the rate of migration from the modern human to the Altai Neanderthal population, consistent with the low rates estimated in our main G-PhoCS runs using non-African individuals. This finding provides initial support for our hypothesis that gene flow originated in a population that diverged from ancestral human populations in Africa.

Explicitly modeling the source population for modern introgression into the Altai Neanderthal

In order to examine the possible source population for the modern introgression into the Altai Neanderthal, we conducted a series of additional demographic inferences, in which we explicitly modeled that population. We modified the population phylogeny assumed in our main analysis (Extended Data Fig. 6a) by adding a 'ghost' population (ModSRC) that diverged from the modern human population and replacing the migration band Mod->AltaiNea with a migration band ModSRC->AltaiNea (Figure S18A). All other settings were maintained. We repeated the analysis with French, Chinese, Yoruba, and San individuals in four separate runs and compared parameter estimates with the ones obtained in our main data analysis (Figure S18B and Extended Data Fig. 6b). Consistent estimates were obtained for the common parameters in both sets of runs. Interestingly, modeling gene flow from the ghost population and not from the sampled present-day population resulted in elevated estimates of migration rates for non-African populations, which are now more consistent across the four runs. In particular, very similar rates were inferred for the French, Yoruba, and San populations (somewhat lower rates were inferred when using Chinese individuals). This provides

further support for our conjecture that later demographic changes not accounted for in the model assumed by G-PhoCS are the main cause for differences in estimated migration rates (see also simulation analysis above). This additional analysis also provides estimates for the time of divergence of the source population from present-day human populations. Because there is fairly weak information in the data to support such inference, the uncertainty in the inferred values is quite high, and different values are obtained in the four runs (lowest in the 'Chinese' analysis and highest in the 'San' analysis). However, if we take the union of the 95% Bayesian credible intervals for the four runs, we can conclude that the source population likely diverged from present-day humans between 138,000 and 433,000 years ago, which is consistent with divergence either before or slightly after the divergence of the San from other present-day populations.

Alternative source populations for modern introgression into the Altai Neanderthal

As indicated by the analysis summarized in Figure S18, modern introgression into the Altai Neanderthal lineage likely originated from a population that diverged from the ancestors of present-day humans around the time of the earliest reported divergence events in modern human history. Furthermore, the analysis of simulated data (Extended data figure 2) indicates that differences between African and non-African populations in inferred rates of gene flow into the Altai Neanderthal population do not indicate different levels of relation between present-day humans and the source population, and are more likely attributed to model misspecification caused by dramatic changes in the N_e of non-Africans. To examine this point more closely, we generated three simulated data sets in addition to the two analyzed in our initial simulation study. In each of these three simulations, we had the source population for gene flow diverging at different points in the population phylogeny: (1) From the population ancestral to Yoruba (and Europeans), 80,000 years after the San divergence; (2) From the population ancestral to the San, 80,000 years after the San divergence; (3) From the population ancestral to Europeans, 8,000 years after the divergence of Europeans and Africans. Recall that one of the two initial simulated sets had no modern introgression into the Altai Neanderthal, and the other had introgression from a population that diverged from present-day humans 60,000 years prior to the San divergence.

G-PhoCS was executed on each of the three additional data sets three times with different present-day samples, and estimates of total migration rate from the modern human population to the Altai Neanderthal population were examined across the 5x3 runs (Extended data figure 3). First, we note that only the simulation without modern introgression into Neanderthals resulted in no significant estimates of gene flow for all three present-day populations, providing additional support for the specificity and sensitivity of G-PhoCS to such introgression regardless of its exact origin. Secondly, assuming that the source population is non-African ('European' data set) results in a high inferred rate of migration into the Altai Neanderthal, which appears to be inconsistent with the very low rates inferred for non-Africans in our data analysis. Thus based on these simulations, we conclude that the source population diverged from present-day Africans before the divergence of present-day Europeans. Estimates obtained for the other three data sets were higher

for the two simulated African populations than the European one, consistent with the rates inferred from real data (Extended Data Fig. 6b). The 'ancestral' simulation produced estimates that were the most similar to the ones obtained in our data analysis, however, the differences between estimates obtained in the three data sets are too subtle to indicate a clear better fit for any of the models. We thus conclude that the source population diverged from present-day Africans at around the time of the San divergence, but this could be either before this divergence event or slightly after it.

Table S11. Present-day human individuals from five populations analyzed using G-PhoCS (see Table S2)

Population	Individual 1	Individual 2
Yoruba	HGDP00927	HGDP00936
San	HGDP01029	HGDP01036
French	HGDP00521	HGDP00533
Han Chinese	HGDP00775	HGDP00778
Papuan	HGDP00542	HGDP00546

Table S12. Divergence from the Chimpanzee reference genome (panTro2) computed for the archaic individuals and eight present-day humans at the neutral loci used for demography inference (without filtering putatively inbred regions in the Altai Neanderthal). All quality, alignment, and selection filters applied for the G-PhoCS analysis were applied here as well. Additionally, sites with missing data in any of the individuals were removed.

Individual	Divergence on 13,753 autosomal loci	Divergence on 2,960 loci on chromosome 21	Difference from mean human divergence
HGDP00927 (Yoruba)	0.012831	–	
HGDP00936 (Yoruba)	0.012822	–	
HGDP01029 (San)	0.012829	–	
HGDP01036 (San)	0.012822	–	
HGDP00521 (French)	0.012823	–	
HGDP00533 (French)	0.012826	–	
HGDP00775 (Han Chinese)	0.012840	–	
HGDP00778 (Han Chinese)	0.012833	–	
Human average	0.012828	–	
Denisovan	0.012794	–	0.000034
Altai Neanderthal	0.012773	0.013951	0.000056
El Sidrón Neanderthal	0.012753 *	0.013817	0.000075
Vindija Neanderthal	0.012786 *	0.013965	0.000043

* Divergence estimates for the two Western Neanderthals on chromosome 21 are elevated because chromosome 21 has higher overall levels of genetic variation (see Table S7). To correct for this effect, we computed the divergence of the Altai Neanderthal on the 2.960 loci on chromosome 21, and used it to extrapolate the divergence of the other two Neanderthal individuals across all 13,753 autosomal loci.

Table S13. Summary of estimates of effective population size (θ) and divergence time (τ) across five preliminary G-PhoCS runs on the genomes of the Altai Neanderthal, Denisovan, and two present-day human (see Figure S15). Estimates of migration rates are depicted separately in Extended Data Fig. 1.

Parameter	Estimates in run with Yoruban individuals		Aggregated across five runs *	
	Posterior mean	95% Bayesian credible interval	**Posterior mean**	95% Bayesian credible interval
θ_{French}	–	–	11,100	10,800 – 11,500
$\theta_{Chinese}$	–	–	10,100	9,800 – 10,400
θ_{Papuan}	–	–	7,500	7,300 – 7,700
θ_{Yoruba}	–	–	26,600	25,600 – 27,500
θ_{San}	–	–	24,200	23,400 – 25,000
$\theta_{AltaiNea}$ *	2,500	2,400 – 2,700	2,500	2,300 – 2,700
$\theta_{Denisovan}$ *	2,200	2,000 – 2,400	2,300	2,1000 – 2,500
θ_{ARC} *	10,300	8,200 – 12,100	9,700	7,500 – 11,800
θ_{HUM} *	16,500	16,100 – 17,000	17,200	16,200 – 18,100
τ_{ARC} *	408,400	368,900 – 453,300	376,600	334,600 – 436,800
τ_{HUM} *	624,500	603,200 – 647,200	576,700	516,200 – 637,700

* For parameters common to all five analyses, we computed estimates based on an aggregation of the five MCMC traces to account for variance across runs. For the effective population size estimates of modern human populations, estimates are taken from the run containing individuals from that population.

Table S14. Summary of estimates of effective population size (θ) and divergence time (τ) across five G-PhoCS runs in our main analysis of the genome sequences of the Altai, Vindija, and El Sidrón Neanderthals, the Denisovan, and two present-day humans (see Extended Data Fig. 6). Estimates of migration rates are depicted separately in Figure S16.

Parameter	Estimates in run with Yoruban individuals		Aggregated across five runs*	
	Posterior mean	95% Bayesian credible interval	**Posterior mean**	95% Bayesian credible interval
θ_{French}	–	–	10,700	10,400 – 11,100
$\theta_{Chinese}$	–	–	9,800	9,500 – 10,100
θ_{Papuan}	–	–	7,400	7,200 – 7,700
θ_{Yoruba}	–	–	27,600	26,700 – 28,500
θ_{San}	–	–	23,700	23,000 – 24,500
$\theta_{AltaiNea}$	700	500 – 1,000	700	400 – 1,000
$\theta_{Vindija}$	14,800	9,400 – 22,600	14,700	9,200 – 22,700
$\theta_{Sidrón}$	1,400	100 – 5,500	1,500	100 – 5,500
$\theta_{Denisovan}$	2,500	2,300 – 2,600	2,500	2,300 – 2,700
$\theta_{W.NEA}$	1,000	600 – 1,700	700	200 – 1,600
θ_{NEA}	3,400	3,000 – 3,700	3,400	3,000 – 3,900
θ_{ARC}	8,200	6,700 – 9,800	7,100	3,900 – 10,100
θ_{HUM}	17,800	17,400 – 18,200	18,500	17,300 – 19,700
$\tau_{W.NEA}$	114,200	90,100 – 143,500	99,300	58,200 – 158,400
τ_{NEA}	128,600	101,600 – 160,200	109,800	68,300 – 167,100
τ_{ARC}	434,200	400,800 – 468,300	411,700	366,300 – 464,900
τ_{HUM}	605,600	585,900 – 624,600	555,200	484,100 – 640,200

* For parameters common to all five analyses, we computed estimates based on an aggregation of the five MCMC traces to account for variance across runs. For the effective population size estimates of modern human populations, estimates are taken from the run containing individuals from that population.

Table S15. Estimates of the ages of the four archaic individuals. All estimates assume an average mutation rate of $\mu=0.5\times10^{-8}$.

Individual	Based on divergence to chimpanzee [a]	Estimated using G-PhoCS [b]	Based on archaeological record
Denisovan	68,000	55,200 (30,300 –71,400)	> 50,000 (*55*)
Altai Neanderthal	112,000	90,400 (61,700 – 121,400)	> 50,000 (*3*)
El Sidrón Neanderthal	150,000	111,600 (87,800 – 142,700)	~49,000 (*60*)
Vindija Neanderthal	86,000	52,100 (15,700 –87,100)	~44,000 (*61*)

[a] See missing mutation computation in Table S12.

[b] Posterior mean and 95% Bayesian credible interval obtained in the G-PhoCS run with four archaic populations and a present-day human population with two sampled Yoruban individuals.

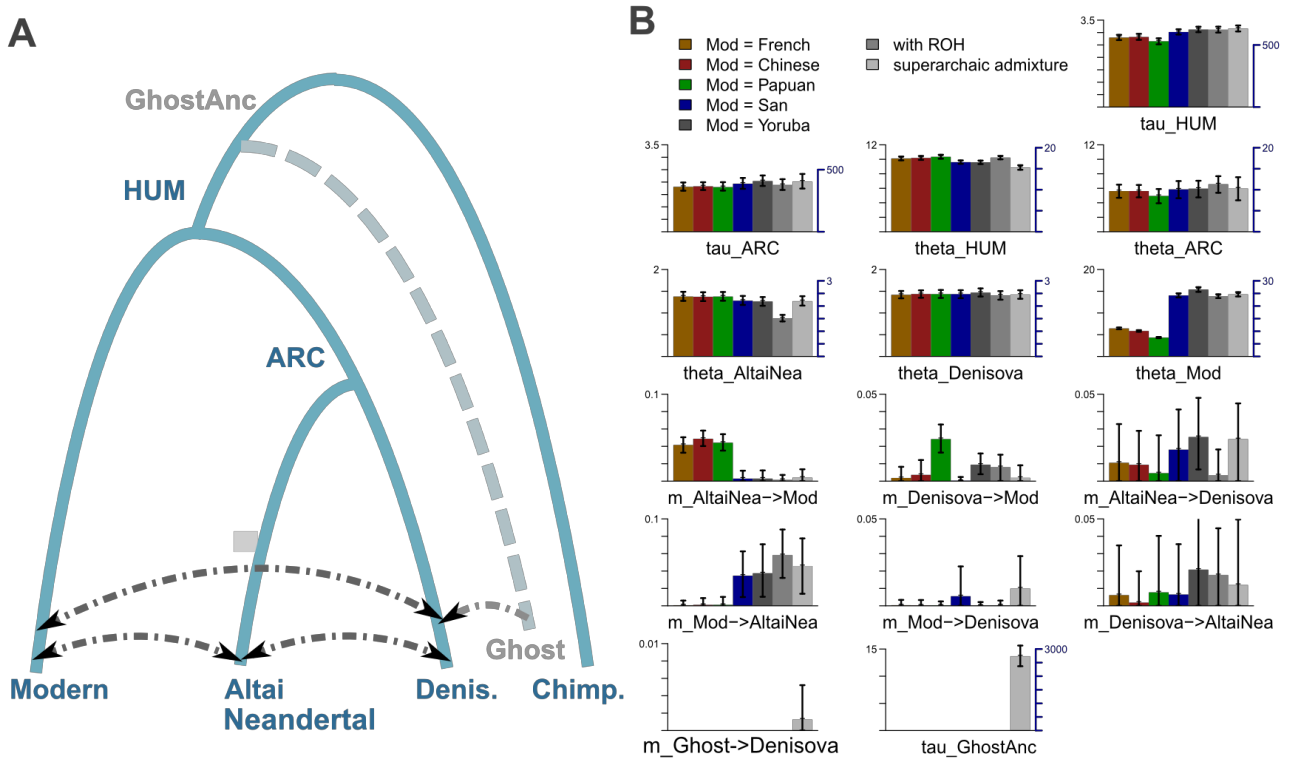

Figure S15. Summary of preliminary demographic inference using G-PhoCS for two archaic populations and one modern human population. **(A)** The population phylogeny assumed in each of the G-PhoCS runs. Labels on internal edges indicate names of the two ancestral populations of archaic humans (ARC), and all human samples (HUM). We assumed the tree topology inferred by neighbor joining based on pairwise distances computed from the complete genome sequences (Figure S8), and augmented the phylogeny with six directional migration bands (arrows) between all pairs of sampled populations. In one of the runs we added a "ghost" population and a migration band from that population into the Denisovan population. **(B)** Parameter estimates obtained by G-PhoCS in seven separate runs analyzing 12,525 neutral and loosely linked loci, substituting samples in the 'Modern' population with pairs of present-day humans from five different modern populations (Table S11). The two last runs: one without filtering runs of homozygosity (ROH), and one with gene flow from a "ghost" population, both using two Yoruban individuals in the 'Modern' population. Bar heights indicate posterior mean and error bars correspond to 95% Bayesian credible intervals. Estimates of divergence times (τ) and population sizes (θ) are given in raw form, scaled by number of mutations per 10 kilobases (left axis), and calibrated to absolute units, 1,000 years for time, and 1,000 individuals for N_e, (right axis) assuming an average mutation rate of 0.5×10^{-9} mutations per year per bp and an average generation time of 29 years. For each of the six migration bands, we are showing the estimated total migration rates. See text for more information on parameter calibration and setup for G-PhoCS. Estimates are largely concordant across the six runs, with the main exception being the effective size of the modern human population (θ_{Mod}), and rates of gene flow into modern humans from archaic populations. We also observe slight differences in estimates of the time of divergence of modern humans from the archaic populations (τ_{HUM}).

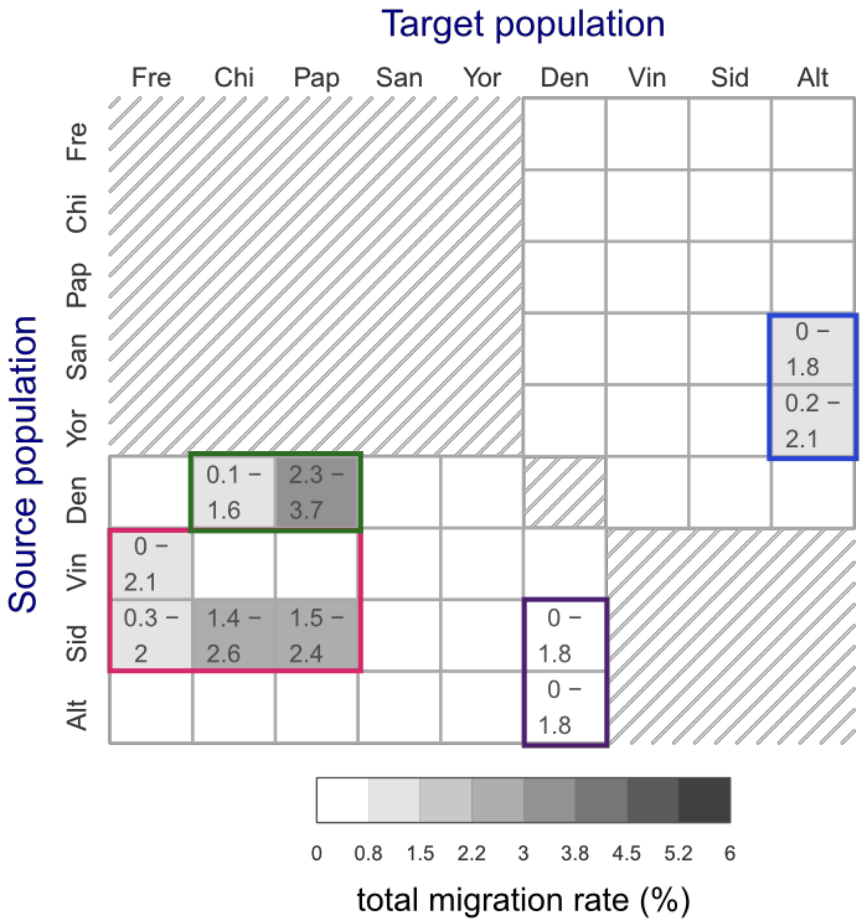

Figure S16. Total migration rates estimated for 46 directional migration bands in five separate G-PhoCS runs. Rows correspond to source populations and columns to the target populations. The 40 migration bands between modern (present-day) and archaic populations were considered in five separate runs, each containing the eight bands associated with a different modern human population (Extended Data Fig. 6a). The six migration bands between the Denisovan population and the three Neanderthal populations were considered in all six runs, and the values shown here were estimated as an aggregate of all five runs. The estimates are as shown in Extended Data Fig. 6b. Shade indicates the posterior mean total migration rate (legend), which approximates the probability that a lineage in the target population originated in the source population. The 95% Bayesian credible intervals are indicated for migration bands whose upper credible interval bound is above 0.3%. We identified four clusters of migration bands, corresponding to what were likely at least four different cases of introgression between populations: **(1)** Western (European) Neanderthals into non-African modern humans (red box), **(2)** Denisovans into East Asian and Oceanians (green box), **(3)** Neanderthals into Denisovans (magenta), and **(4)** modern humans into Eastern Neanderthals (blue box). These are depicted by directed arrows in Figure 3a.

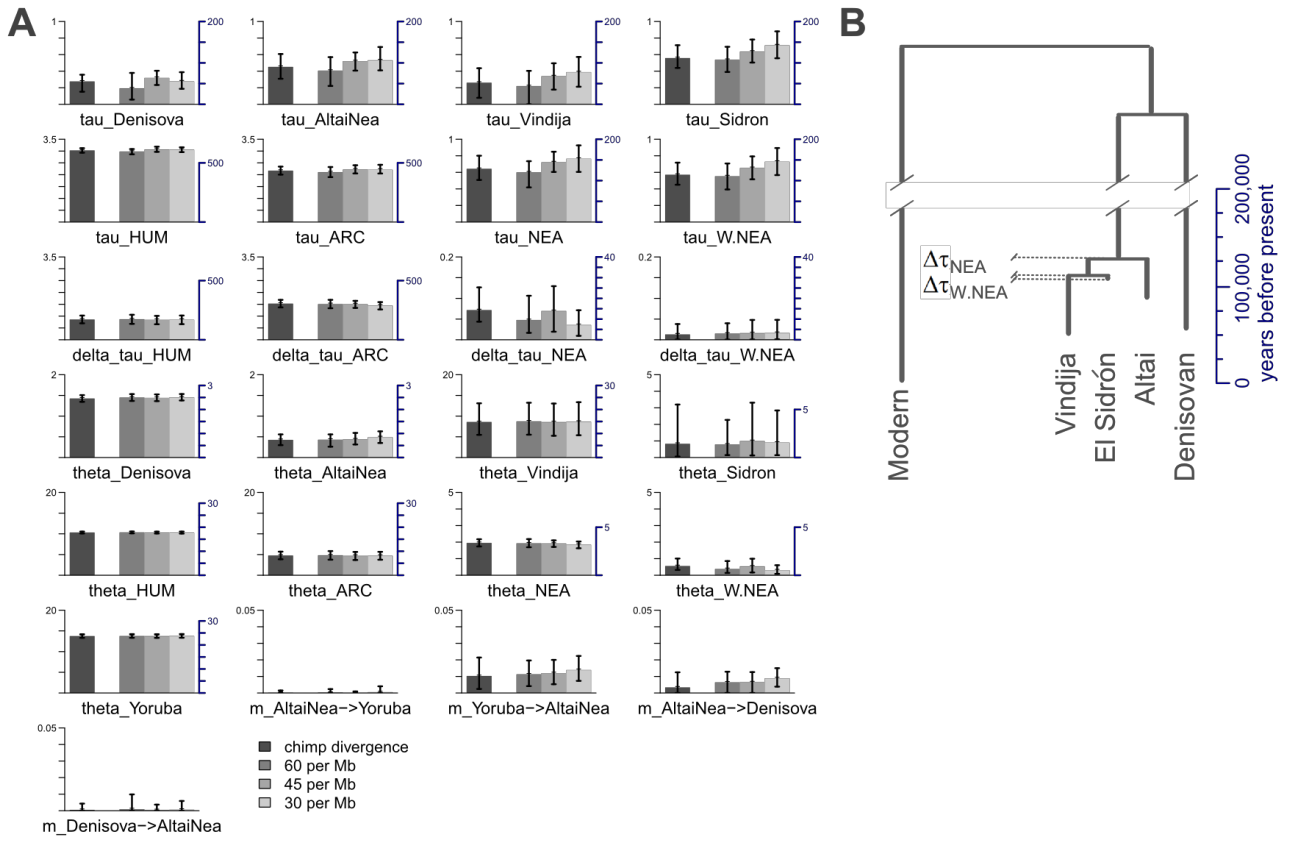

Figure S17. Influence of assumptions on ancient DNA sample age on parameter estimates. **(A)** Parameter estimates obtained by G-PhoCS in four separate runs analyzing 13,754 neutral and loosely linked loci, with different initial values chosen for the sample ages of the four archaic humans. Our main set of runs (Extended Data Fig. 6) used estimates based on divergence from chimpanzee (Table S12), and the three alternative runs use the same initial value for each of the four archaic samples: 0.00003, 0.000045, and 0.00006. In all four runs, two present-day Yoruban individuals were used in the modern human population. Bar heights indicate posterior mean and error bars correspond to 95% Bayesian credible intervals. Estimates of divergence times (τ) and population sizes (θ) are given in raw form, scaled by number of mutations per 10 kilobases (left axis), and calibrated to absolute units, 1,000 years for time, and 1,000 individuals for N_e, (right axis) assuming an average mutation rate of 0.5×10^{-9} mutations per year per bp and an average generation time of 29 years. For each of the 14 migration bands, we are showing the estimated total migration rates. See text for more information on parameter calibration and setup for G-PhoCS. The comparison shows little influence of the initial values on any of the parameter estimates. **(B)** Schematic depiction of sample age estimates and times of divergence between Neanderthal populations. The derived parameters $\Delta\tau_{W.NEA}$ and $\Delta\tau_{NEA}$ describe the difference between the age of an ancestral population and the maximum age of its most ancient daughter population.

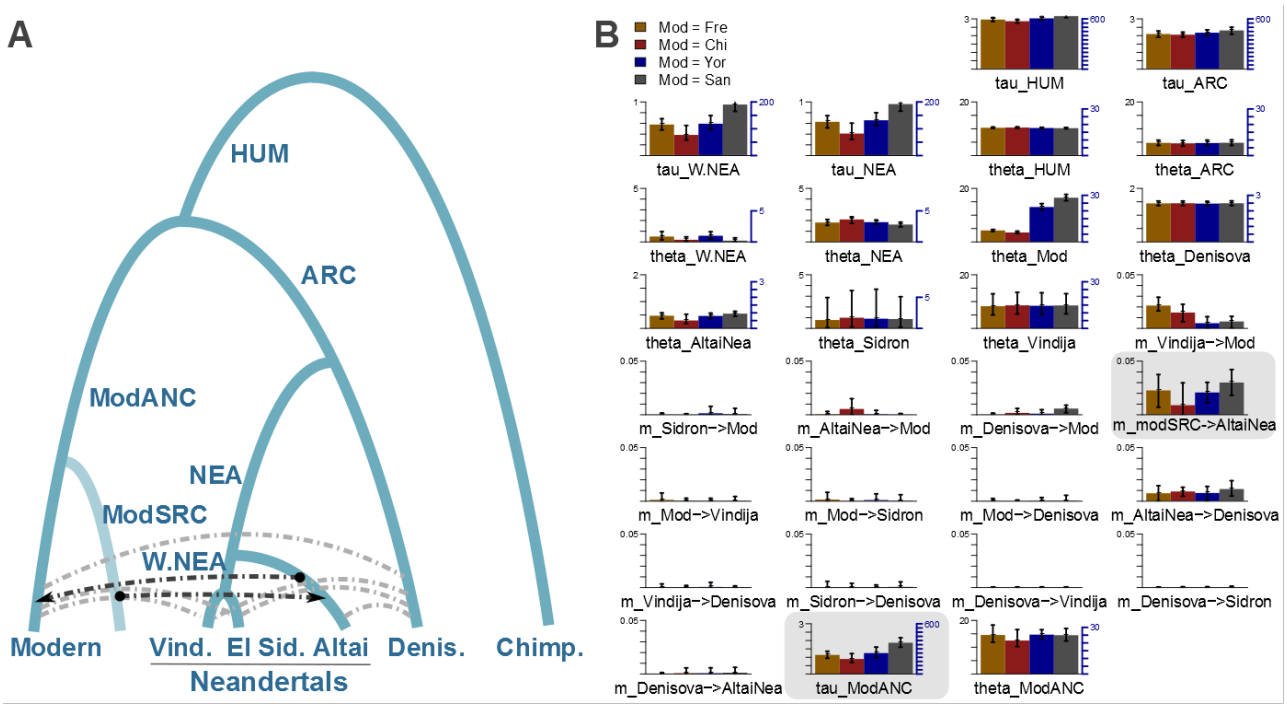

Figure S18. Demographic inference explicitly modeling source population for introgression from modern humans into the Altai Neandertal population. **(A)** The population phylogeny assumed in four G-PhoCS runs. We modified the population phylogeny assumed in our main analysis (Extended Data Fig. 6a) by adding a 'ghost' population (ModSRC) and by replacing the migration band Mod->AltaiNea with a migration band ModSRC ->AltaiNea (highlighted). **(B)** Parameter estimates obtained by G-PhoCS in four separate runs analyzing 13,754 neutral and loosely linked loci, substituting samples in the 'Modern' population with pairs of present-day humans from four different modern populations (French, Chinese, Yoruba, and San). Bar heights indicate posterior mean and error bars correspond to 95% Bayesian credible intervals. Estimates of divergence times (τ) and population sizes (θ) are given in raw form, scaled by number of mutations per 10 kilobases (left axis), and calibrated to absolute units, 1000 years for time, and 1000 individuals for N_e, (right axis) assuming an average mutation rate of 0.5×10^{-9} mutations per year per bp and an average generation time of 29 years. For each of the 14 migration bands, we are showing the estimated total migration rates. See text for more information on parameter calibration and setup for G-PhoCS. Estimates of all shared parameters are consistent with the ones estimated in the main set of runs (Extended Data Fig. 6b). Using an explicit source population for the introgression into the Altai Neandertal, rates of migration become much more consistent across the four runs ($m_{ModSRC->AltaiNea}$), and we infer a divergence time of the source population from present-day humans in the range of 138,000 – 433,000 years ago (τ_{ModANC}).

SI 9. Sequence patterns of modern human introgression into the Altai Neanderthal

G-PhoCS consistently infers gene flow from modern humans into the Altai Neanderthal lineage, but not into the Denisovan or European Neanderthal lineages (see Supplementary information 8). In addition, we infer gene flow from a deeply divergent archaic population into the ancestors of the Denisovan. This latter admixture event has been previously reported (*3*). We describe here the sequence patterns underlying these inferences, in particular those that allow us to distinguish modern human gene flow into the ancestors of the Altai Neanderthal from archaic gene flow into the ancestors of the Denisovan from a deeply divergent hominin (super-archaic admixture).

Proportion of shared derived alleles with African genomes from the 1000 genomes project

We calculated how many derived alleles in one archaic genome (Altai Neanderthal or Denisovan) are shared with Africans in sites that are homozygous ancestral in the other archaic genome. To do this, we used 504 individuals from five African populations (Yoruba, Mende, Luhya, Gambian and Esan) in the 1000 Genomes phase III release (*62*) and determined derived alleles using the inferred ancestral base in the EPO six-primate alignments (*18*). To avoid sequence errors in these low-coverage African genomes and the possibility of derived-allele sharing due to admixture with non-African populations carrying derived alleles from Neanderthals, we required an allele frequency in Africans of >0.1 for a derived allele to be counted as shared. As previously reported (*3*), we find that the Altai Neanderthal genome shares more derived alleles with Africans than the Denisovan genome (5.4% more). This is particularly the case for derived alleles at >0.9 frequency in Africans (Extended Data Table 1).

Divergence between the Altai Neanderthal and Denisovan genomes in windows of 100Kb

The larger proportion of high-frequency derived alleles shared between the Altai Neanderthal and Africans could result from either super-archaic introgression into the Denisovan lineage or modern human introgression into this Neanderthal lineage. Assuming both introgressions took place, the Denisovan genome should bear introgressed genetic material from an unknown archaic group and the Altai Neanderthal genome should bear introgressed genetic material from modern humans. Regions in the Denisovan genome introgressed from an archaic population should have, on average, unusually high divergence to both humans and Neanderthals. Regions of the Altai genome introgressed from modern humans should have unusually low divergence with modern humans and higher divergence with the Denisovan than non-introgressed genomic regions. Since the rate of introgression is likely to be low in both cases (Supplementary information 8), the introgressed alleles would have a high probability of being heterozygous.

To test these expectations, we analyzed the Altai Neanderthal and Denisovan genomes in windows of 100Kb. Regions of the genome described as inbred in the Altai Neanderthal (Supplementary Information 10 in (*3*)) were excluded from this analysis. These are 103 regions > 2.5cM depleted in heterozygous sites. Each window was required to have high-quality genotypes (as described in Supplementary information 3) in at least 50% of its length in both archaic genomes. This resulted in a total of 15,881 windows in each archaic

genome. We calculated in each window the divergence to Africans in those high-quality genotypes with a derived allele frequency >0.9 as follows: **1)** in the absence of information about the phase of the archaic alleles, we chose the alleles within each archaic window that gives the minimum divergence to Africans. That is, only homozygous ancestral genotypes in the archaic individuals count as one difference, while heterozygous sites carry a human and an archaic allele and do not contribute to the number of differences; and **2)** we divided this number by the number of high-quality genotypes in the window. Using the minimum divergence to Africans allows introgressed segments from modern humans to be more easily identified.

We first compared the windows of the Altai Neanderthal to those in the Denisovan genome binned according to their minimum divergence to Africans. We find that windows in the Altai Neanderthal genome are less divergent to Africans than windows in the Denisovan genome ($P < 2.2 \times 10^{-16}$, Mann-Whitney U test). This difference, however, could be caused by archaic admixture alone (*3*), which increases the divergence of the Denisovan to modern humans. We therefore tested whether windows in the Altai Neanderthal at the lowest divergence to Africans have elevated divergence to the Denisovan, as expected from modern human introgression into the Altai Neanderthal, and whether windows in the Denisovan at the highest divergence to Africans have elevated divergence to the Altai Neanderthal, as expected from archaic introgression into the Denisovan. To do this, we plotted the windows in each archaic genome (Altai Neanderthal or Denisovan) according to their divergence to Africans (see above) against their divergence to the other archaic genome. We computed the divergence between the two archaic individuals as follows: **1)** in the absence of information about the phase of the archaic alleles, we chose the alleles within each archaic window that gives the maximum divergence to the other archaic. That is, we counted differences between high-quality genotypes in the two archaic individuals, so that a homozygous derived genotype in one archaic and a homozygous ancestral genotype in the other archaic counts as one difference, and a heterozygous genotype (both derived and ancestral alleles are present) in one archaic and any other genotype in the other archaic counts also as one difference; and **2)** we divided this number by the number of high-quality genotypes in the window. Using the maximum divergence between the archaic windows allows introgressed segments in either of the two archaic individuals to be more easily identified.

Indeed, we find that the windows most divergent to Africans in the Denisovan genome show elevated divergence to the Altai Neanderthal (Figure S19A), when compared with windows of the same divergence to Africans in the Altai Neanderthal. This is consistent with archaic introgression into the Denisovan increasing divergence to both modern human and Neanderthal genomes. In contrast, in windows least divergent to Africans, the Altai Neanderthal genome has significantly elevated divergence to the Denisovan (Figure S19A). This is also true when we use only the subset of derived alleles that are fixed in Africans to compute the divergence of the archaic individuals to Africans (Figure S19A). This observation is not expected from super-archaic introgression into the ancestors of the Denisovan alone (see simulations below).

In addition, computing the divergence of each archaic to individual African genomes previously sequenced at high-coverage (*3*) at homozygous derived sites in these genomes supports the observed high divergence of the Altai Neanderthal in windows at the lowest divergence to Africans (Figure S20).

Heterozygosity in the Altai Neanderthal and Denisovan genomes in windows of 100Kb

If the windows least divergent to Africans in the Altai Neanderthal genome are due to introgression from modern humans into the ancestors of this Neanderthal, then we expect these windows to have elevated heterozygosity compared to windows of the same divergence to Africans in the Denisovan genome. We find this to be the case (Figure S19B). This observation is also inconsistent with super-archaic introgression into the Denisovan lineage alone (see simulations below), as this introgression should not affect the heterozygosity in the Altai Neanderthal genome.

If the elevated heterozygosity of windows least divergent to Africans in the Altai Neanderthal genome is the result of introgression of modern human haplotypes, these heterozygous sites should be mostly due to introgressed alleles, and thus be enriched in African derived alleles. Indeed, when we compute heterozygosity considering only sites with derived African alleles, the pattern remains (not shown). The proportion of heterozygous sites with African derived alleles in windows least divergent to Africans is larger in the Altai Neanderthal (40.7%) than in the Denisovan (24.2%), which is not expected from super-archaic introgression into the Denisovan lineage alone. If we require an allele frequency in Africans of >0.1 for a derived allele to be counted as shared (to avoid sequence errors and the possibility of admixture with non-African populations carrying derived alleles from Neanderthals), the proportion of heterozygous sites with African derived alleles is still larger in the Altai Neanderthal (28.0%) than in the Denisovan (16.6%). Finally, the heterozygosity patterns above in the Altai Neanderthal and Denisovan using Africans from the 1000 genome project are consistent with those found using individual high-quality African genomes (Figure S20).

Simulations of the Altai Neanderthal and Denisovan genomes in windows of 100Kb

We tested whether the observations above and shown in Figure S19 are expected from the demographic scenario inferred by G-PhoCS (Table S13 and Supplementary information 8). To do this, we used the software *ms* (*57*) to simulate windows of 100Kb under four models of gene flow: **1)** No gene flow; **2)** Only super-archaic gene flow into the Denisovan lineage; **3)** Super-archaic gene flow into the Denisovan lineage and Altai Neanderthal gene flow into the Denisovan lineage; and **4)** Super-archaic gene flow into the Denisovan lineage, Altai Neanderthal gene flow into the Denisovan lineage and **modern human gene flow into the Altai Neanderthal lineage**.

Simulation parameters were chosen to be consistent with G-PhoCS estimates for the divergence times, effective population sizes and rates of gene flow (Supplementary information 8). The mutation rate of 0.5×10^{-9} mutations per bp and year and an average generation time of 29 years (as assumed when calibrating the G-PhoCS estimates) were also used. We assumed gene flow lasted for one generation and happened

50,000 years ago for the Altai Neanderthal gene flow into the Denisovan lineage, 100,000 years ago for the modern human gene flow into the Altai Neanderthal lineage and 200,000 years ago for the super-archaic gene flow into the Denisovan lineage. For each of these scenarios, we simulated 15,881 sequence windows of 100Kb in length. The number of chromosomes simulated were 1,008 for the Africans, two for the Neanderthal, two for the Denisovan, one for the unknown archaic and one for the chimpanzee. The unknown archaic hominin is assumed to have diverged from the other lineages 1.5 Million years ago. The *ms* command for scenario 4, the most complex one, is as follows:

```
ms 1014 15881 -seeds <x> <x> <x>  -t 5.8 -r 5.19948 100000 -I 5 2 2 1008 1
1 -n 1 2.2 -n 2 2.5 -n 3 24.25 -n 4 2.5 -n 5 20 -em 0.4310345 2 1 26 -em
0.4312845 2 1 0 -em 0.862069 1 3 142 -em 0.862319 1 3 0 -em 2.586207 2 4 40 -em
2.586457 2 4 0 -ej 3.43 2 1 -en 3.43 1 10.4 -ej 5.25 3 1 -en 5.25 1 16.6 -ej
12.93103 4 1 -en 12.93103 1 16.6 -ej 86.2069 5 1 -en 86.2069 1 20
```

Where N0 was set to 1,000. For each of the four simulated models of gene flow, and for each simulated window we computed the divergence between the Altai Neanderthal and Denisovan, the heterozygosity, and the divergence of each of the archaic individuals to the Africans, and plot these measures as in Figure S19 (African derived alleles at >0.9 frequency). These calculations were done as described above for the real data.

First, we notice that the slope of the divergence and heterozygosity plots is more pronounced in the actual archaic genomes than in the simulated scenarios, owing to mutation rate variation along the genome, which is not incorporated in the simulations. Comparing the different scenarios, we observe that a model with no gene flow (model 1) cannot explain the divergence and heterozygosity patterns found in these archaic genomes (Figure S21A). Including the super-archaic gene flow into the Denisovan lineage (models 2 and 3), results in the windows of the Denisovan genome with the highest divergence to Africans showing elevated divergence with the Altai Neanderthal (Figures S21B and C), but fail to reproduce the divergence and heterozygosity patterns in the Altai Neanderthal. Only when modern human gene flow into the ancestors of the Altai Neanderthal is included (model 4), we observe that windows of the Neanderthal genome with the lowest divergence to Africans have both elevated divergence to the Denisovan and elevated heterozygosity (Figure S21D), as observed in the real sequences (Figure S19). These results hold when the rate of modern human introgression into the Altai Neanderthal assumed to be half of the point estimate. This value is more consistent with the inference including European Neanderthals (Figure 3), and the simulated sequences under this lower rate of modern human gene flow into the Altai Neanderthal lineage resembles more the real observations (Figure S22A and B).

Present-day human contamination in DNA fragments of the Altai Neanderthal has been estimated to be below 1% (*3*). We tested whether simulating a higher amount of present-day human contamination could cause the observed sequence patterns in the simulated windows of the Altai Neanderthal. We assigned a

probability of 0.05 to each segregating site in the simulated Altai Neanderthal sequences of carrying an African allele. We note that this would resemble a contamination of 5% at the genotype level, which would require substantial contamination (larger than 5%) on the sequences at the DNA fragment level (Supplementary Information 4). We simulated two models with contamination and different gene flows: **1)** Super-archaic gene flow into the Denisovan lineage and Altai Neanderthal gene flow into the Denisovan lineage; and **2)** Super-archaic gene flow into the Denisovan lineage, Altai Neanderthal gene flow into the Denisovan lineage and **modern human gene flow into the Altai Neanderthal lineage**. We find that contamination has no effect on the divergence between the Altai Neanderthal and Denisovan in either model (Extended Data Figure 4a and b), but generally increases the heterozygosity across the simulated windows in the Altai Neanderthal in both models (Extended Data Fig. 4a and b). The increase of heterozygosity in windows with low divergence to Africans is however modest, which contrasts with the sharp increase in heterozygosity observed in the actual Altai Neanderthal genome (Figure S19B).

The archaic individuals died thousands of years ago but our simulations treated them as if they were present-day individuals. We explored the effect of their age by removing derived alleles in the archaic individuals that are not shared with the simulated African individuals. Because the Altai Neanderthal is thought to be older than the Denisovan, we removed 11.6% of derived alleles in the Neanderthal lineage, and 5.8% of derived alleles in the Denisovan lineage. This would resemble 70,000 years and 35,000 years back in time for the Altai Neanderthal and Denisovan, respectively. We find that the divergence between the archaic individuals and present-day Africans and their heterozygosities in our simulations are not affected by this (Figure S23A and B) and, hence, cannot account for the sequence patterns observed in the Altai Neanderthal genome.

We conclude that both archaic gene flow into the Denisovan and modern human gene flow into the Altai Neanderthal are necessary to fully explain the patterns of divergence and heterozygosity in these archaic genomes.

Frequency-stratified D-statistics (D_j)

We calculated frequency-stratified D_j statistics as described in Supplementary information 16a in (*3*). This measure has been used to describe an excess of shared derived alleles between Africans and one archaic over the other archaic. Such excess has been demonstrated for the Altai Neanderthal over the Denisovan, particularly at sites that are fixed derived in present-day Africans (Figure S16a.1 in (*3*)). This has been interpreted as evidence for super-archaic admixture into the Denisovan. However, the scenarios of modern human introgression into the Altai Neanderthal lineage and archaic introgression into the Denisovan lineage were considered to be mutually exclusive. As modeled previously (Figure S16a.3 in (*3*)), each of these scenarios did not fully explain the observations in real data.

We computed the same statistic for 504 African individuals in bins of 10% (Figure S24A). We observe on average elevated levels of D_j, and an increase particularly at sites that are fixed derived in Africans. This is consistent with the observations in (*3*). We also calculated D_j for the simulated data described above. In the absence of gene flow, no differences between the individuals could be observed (Figure S24B). Archaic introgression introduces a slope towards high frequency in Africans with a discontinuous jump at fixed derived sites (Figure S24C). Neanderthal introgression into the Denisovan lineage weakens this slope (Figure S24D). This aspect of the data has not been modeled in (*3*), and here we show that this gene flow event decreases differences between the two archaic individuals. Only a model that also includes human introgression into the Altai Neanderthal lineage introduces a general shift of D_j towards the Neanderthal, and a slope that is similar to the real data (Figure S24E).

In the real data, sites at low frequency in present-day Africans are also more shared with the Altai Neanderthal than the Denisovan (Figure S21A and Figure S16a.4 in (*3*)). This has been described as the result of small amounts of back-migration of Eurasians into Africa. We simulated a small amount of introgression from the Neanderthal into Africans (0.1%), in addition to the previously described parameters. We confirmed that this does not influence the divergence and heterozygosity statistics explored above (not shown). It introduces an excess of allele-sharing at low frequency in Africans similar to the real data (Figure S24F). Adding super-archaic admixture (Figure S24G) and introgression from the Neanderthal into the Denisovan lineage (Figure S24H) do not explain the shift and slope observed in the real data, while adding modern human introgression into the Neanderthal resembles the real observations (Figure S24I).

We conclude that a model including both super-archaic admixture and modern human introgression into the Altai Neanderthal explains best the patterns observed in the archaic genomes.

Proportion of shared derived alleles with African genomes in the chromosome 21

We also find that the chromosome 21 of the Altai Neanderthal shares more derived alleles with Africans from the 1000 genomes project than the chromosome 21 of El Sidrón (3.5% more) and Vindija (4.9% more) Neanderthals, with the European Neanderthals sharing also more derived alleles with Africans than the chromosome 21 of the Denisovan (9.8% more for El Sidrón and 8.8% more for Vindija). This is particularly the case for derived alleles at >0.9 frequency in Africans (Table S16). Although these observations are based on small numbers, they are consistent with modern human gene flow into the Altai Neanderthal lineage contributing to the differences between the Altai and the European Neanderthals and super-archaic gene flow into the Denisovan lineage contributing to the differences between Neanderthals and the Denisovan. Both the shotgun and capture sequences of chromosome 21 in the Altai Neanderthal have similar proportions of shared derived alleles with Africans (Table S16), suggesting that capture bias is not responsible for the differences observed among the Neanderthals.

We calculated D_j on chromosome 21 for derived sites in the Altai and Vindija Neanderthals and the Denisovan. We calculated the summary statistic across sites with African allele frequency > 0.1, due to small amounts of data. The obtained value is 0.075 for Altai Neanderthal vs. Denisova, 0.073 for Vindija vs. Denisova, and 0.019 for Altai Neanderthal vs. Vindija. This is consistent with super-archaic introgression into the Denisovan lineage, and modern human introgression into the Altai Neanderthal lineage.

Proportion of derived alleles in heterozygous sites shared with high-quality African genomes

We further investigated the differences between the Altai and the European Neanderthals using the chromosome 21 of five African individuals previously sequenced at high-coverage (*3*). We specifically focused on the Neanderthal lineage after its split from the Denisovan lineage and in regions that may contain introgressed haplotypes and, hence, be heterozygous in the Neanderthal. We determined for each African chromosome 21 those positions with derived alleles that are homozygous ancestral in the chromosome 21 of the Denisovan and heterozygous in one or more chromosome 21 of the Neanderthals. Regions of chromosome 21 described as inbred in the Altai Neanderthal (*3*) were excluded from this analysis. We find that each of the five chromosomes 21 from Africa share significantly more derived alleles in heterozygous sites with the Altai Neanderthal than with El Sidrón or Vindija Neanderthals (Table S17). This is consistent with modern human gene flow predominantly into the Altai Neanderthal lineage (Figure 3) but we caution that the complete genomes of these and other Neanderthals will be needed to resolve the differences in the extent of modern human introgression among Neanderthal lineages.

A screen for introgressed segments from modern humans into the Altai Neanderthal genome

We searched for segments that may have been introgressed into the Altai Neanderthal from modern humans. To do this, we first calculated the frequency in Africans of the derived alleles in sites that are heterozygous in one archaic genome (Altai Neanderthal or Denisovan) and homozygous ancestral in the other archaic genome. This allows us to identify segments that carry an archaic haplotype on three chromosomes, and a human haplotype only on one chromosome. Derived alleles were determined using the inferred ancestral base in the EPO six-primate alignments (*18*). We calculated the derived allele frequency as follows: **1**) Derived alleles shared with Africans are given the frequency of the allele in 504 individuals from Africa described above; and **2)** Derived alleles in each archaic genome which are ancestral in all Africans are given a frequency of zero. Private mutations, sequence errors and ancient damage in the archaic genomes will tend to have a frequency of zero.

We fitted the frequencies of the derived alleles along each of the archaic genomes using a locally weighted polynomial regression (*loess* function in *R*). This non-linear regression was conducted in (local) windows of 20 sites with alpha = 20 / number of heterozygous sites in a chromosome. Derived alleles in the Neanderthal genome that are the result of present-day human contamination may be shared across humans and have a high allele-frequency in Africans, but are unlikely to concentrate in such short windows, and should not affect our approach (Figure S25). For each archaic genome, we then selected those segments where the fitted

curve to the derived African allele frequencies consistently stayed over a frequency of 0.25 along the segment. We further selected those segments in each archaic genome that: **1)** were 5Kb or longer; **2)** had at least 10 derived alleles that are no more than 25Kb apart from each other; **3)** were in regions with no more than one incompatible site with introgression per 100Kb. Incompatible sites are defined as sites that are homozygous and derived in both the Altai Neanderthal and Denisovan genomes, and have a derived allele frequency below 0.05 in Africans. Derived alleles in these sites are unlikely to be the result of modern human introgression into the Altai Neanderthal lineage only; and **4)** segments within a 50Kb region were joined.

We find 163 segments of more than 50 Kb in the Altai Neanderthal genome (Table S18), compared to only 48 segments in the Denisovan genome. The Altai Neanderthal segments are enriched in heterozygous sites by 4.9-fold compared to random genomic regions, and are significantly more heterozygous in the Altai Neanderthal than in the Denisovan ($P = 0.026$, Mann-Whitney U test). The cumulative length of heterozygous segments longer than 50 Kb in the Altai Neanderthal is 3.9-fold higher than in the Denisovan genome. The longest heterozygous segment in the genome is in chromosome 1, which has 161 derived alleles shared with Africans (Table S18 and Figure S26). A gene ontology enrichment test was performed on heterozygous segments longer than 100 Kb using a hypergeometric test in the software *FUNC* (*63*). Three Gene Ontology categories were found to have more segments than expected in the Altai Neanderthal genome (Table S19), including 'spermatogenesis'. We note that for the MHC category, two genes are in tandem in the genome. For the spermatogenesis and phosphorylation categories, however, genes are on different chromosomes or megabases apart from each other.

Finally, because the Altai Neanderthal individual was recently inbred, we also analyzed sites that are homozygous derived in one archaic genome and homozygous ancestral in the other. In this case, we required homozygous derived sites to be no more than 10 Kb apart, with heterozygous sites considered inconsistent with introgression. We find 697 segments longer than 50 Kb in the genome of the Altai Neanderthal, for only 318 segments in the genome of the Denisovan. Out of these, 28 segments exceed 250 Kb in the Altai Neanderthal genome, and only eight in the Denisovan genome. The cumulative length of homozygous segments longer than 50 Kb in the Altai Neanderthal genome is 2.4-fold higher than in Denisovan genome. These observations agree with those in the non-inbred region of the Altai Neanderthal genome and are consistent with modern human introgression into the ancestors of the Altai Neanderthal.

A screen for introgressed segments from modern humans into the chromosome 21 of Neanderthals

We searched for segments that may have been introgressed from modern humans into Neanderthals on chromosome 21. Here, we required that the Denisovan and two out of three Neanderthals were homozygous ancestral, while only the third Neanderthal individual carrying the African derived allele. We used the parameters described above, and found in the Altai Neanderthal one segment of about 53 Kb (21:41,033,308-41,086,255) enriched in African derived alleles at heterozygous sites, and two segments

enriched in African derived alleles at homozygous sites of about 44 Kb each (21:20,431,532-20,475,077 and 21:30,387,418-30,431,730). Furthermore, we find one segment of about 21 Kb enriched in African derived alleles at heterozygous alleles in the Vindija Neanderthal (21:32,183,808-32,204,347), and no segments in El Sidrón Neanderthal. This supports modern human gene flow predominantly into the Altai Neanderthal lineage (Figure 3).

Natural selection in the introgressed segments of the Altai Neanderthal genome

We computed the proportion of each chromosome that is potentially introgressed from modern humans in the Altai Neanderthal genome as a measure their modern human ancestry. We find that the proportion of introgressed regions in the autosomes is 0.78%, ranging from 0.18% (chromosome 15) to 1.77% (chromosome 20). The four introgressed regions in the X chromosome of the Altai Neanderthal, however, comprise only 0.17% of the length of this chromosome. This shows that chromosome X, compared to the autosomes, is depleted in introgressed fragments from modern humans in the Altai Neanderthal ($P < 10^{-20}$; G-test). Interestingly, the reduction of modern human ancestry in the X chromosome of the Altai Neanderthal (~4.6-fold reduction) is similar to the reduction of Neanderthal ancestry in the X chromosome of non-Africans (~five-fold reduction) (*64*). The differences between the two analyses, however, make this result difficult to interpret.

Regarding the role of natural selection, the modern human introgressed fragments in the autosomes have B-scores (*65*) that are significantly higher than in randomly selected regions in the autosomes (mean of 854 in the introgressed regions vs. mean of 785 in the random regions; $P = 1.1 \times 10^{-11}$; Wilcoxon rank test). Because high B-scores are expected in regions of reduced background selection, this result suggests that modern human fragments generally introgressed in regions subjected to weak purifying selection in the genome. This is also the case in the X chromosome, with the four introgressed fragments having B-scores that are higher than in random regions in this chromosome (mean of 800 in the introgressed regions vs. mean of 522 in the random regions). The difference is not significant due to the small number of introgressed fragments in the X chromosome, but the magnitude of the difference suggest that the effect may be indeed stronger in the X chromosome than in the autosomes. These results suggest that many modern human alleles, particularly in the X chromosome but also in the autosomes, were not tolerated in the Neanderthal genetic background. If selection was responsible for this, male hybrid sterility is a possible explanation for selection against modern human DNA in the X chromosome of the Altai Neanderthal (*64*).

We caution though that other explanations cannot be ruled out at this time. Male reproductive bias could, for example, contribute to the differences observed between the autosomes and X chromosome by distorting the strength of selection in the X chromosome. In addition, differences in the population history of Neanderthals and modern humans may also result in differences between the autosomes and X chromosome that are unrelated to selection. Future work will need to examine these questions in detail, both through simulations and the analysis of additional archaic genomes.

Table S16. Percentage of derived alleles in either the Altai Neanderthal, European Neanderthals or Denisovan chromosome 21 shared with African genomes. The percentages of shared derived alleles are binned by their African allele frequency. Fixed derived alleles in Africans are included in the '$0.9 < f \leq 1$' but also shown separately in the 'Fixed' category. The Altai Neanderthal capture of chromosome 21 has an average coverage of 14-fold, making it comparable to the capture of El Sidrón Neanderthal.

African frequency	$0 \leq f \leq 0.1$	$0.1 < f \leq 0.2$	$0.2 < f \leq 0.3$	$0.3 < f \leq 0.4$	$0.4 < f \leq 0.5$	$0.5 < f \leq 0.6$	$0.6 < f \leq 0.7$	$0.7 < f \leq 0.8$	$0.8 < f \leq 0.9$	$0.9 < f \leq 1$	Fixed
Altai	57.65	5.67	4.80	4.15	3.83	3.35	3.01	4.00	4.15	**9.39**	**4.59**
Altai capture	57.59	5.67	4.75	4.14	3.83	3.37	3.01	4.04	4.14	**9.46**	**4.64**
El Sidrón	61.15	4.82	4.26	3.98	3.71	3.11	2.99	3.74	3.67	**8.56**	**4.16**
Vindija	62.50	4.95	3.86	3.80	3.36	3.20	2.98	3.53	3.53	**8.29**	**4.04**
Denisovan	70.99	5.22	3.92	3.19	2.57	2.52	2.42	2.10	2.10	**4.95**	**1.72**

Table S17. Test of the proportion among Neanderthals of the number of heterozygous sites with derived alleles shared with an African chromosome 21 in sites where the Denisovan is homozygous ancestral. P-values from a G-test are shown.

African	Altai vs. Vindija	Altai vs. El Sidrón	Vindija vs. El Sidrón
Dinka	1.4x10-4	1.2x10-6	0.29
Mandenka	0.006	2.2x10-4	0.35
Mbuti	0.003	4.8x10-8	0.01
San	8.9x10-5	1.7x10-8	0.08
Yoruba	6x10-4	1.6x10-6	0.17

Table S18. Regions in the Altai Neanderthal genome that are enriched for African derived alleles in heterozygous sites (coordinates in *hg19*). These sites are homozygous ancestral in the Denisovan genome. Regions are 50 Kb or longer.

Region	SNPs	Length (bp)	Genetic length (cM)	Genes
1:199707795-200016460	161	308,665	0.047	*NR5A2; RNU6-609P; RNU6-716P; RNU6-778P*
13:49532446-49790867	103	258,421	0.04	*COX7CP1; FNDC3A; OGFOD1P1; RAD17P2; RNU6-60P; RNY3P2*
2:88815371-89061977	116	246,606	0.023	*EIF2AK3; RPIA; TEX37*
3:89790776-90031537	70	240,761	0.017	–
3:30590736-30816806	100	226,070	0.547	*GADL1; TGFBR2*
6:42492777-42713223	67	220,446	0.088	*ATP6V0CP3; PRPH2; RNU6-890P; TBCC; UBR2*
8:93809505-94011334	122	201,829	0.07	*IRF5P1; TRIQK*
1:192267587-192466254	43	198,667	0.115	*RGS21*
6:64964495-65143725	61	179,230	0.002	*EYS*
3:184641954-184811511	63	169,557	0.042	*C3orf70; VPS8*
7:11351364-11507986	54	156,622	0.156	*THSD7A*
10:45785277-45939818	68	154,541	0.061	*ALOX5; OR13A1*
7:88668270-88819025	29	150,755	0.133	*ZNF804B*
7:113813987-113963584	37	149,597	0.055	*FOXP2*
20:3244564-3386692	83	142,128	0.01	*C20orf194; RN7SL839P; RNU6-1019P; UBE2V1P1*
6:110381003-110517506	54	136,503	0.009	*CDC40; WASF1*
4:45667803-45803054	53	135,251	0.031	–
18:24544545-24679652	40	135,107	0.097	*AQP4-AS1; CHST9*
4:31939594-32071451	50	131,857	0.026	–
7:30602991-30734819	33	131,828	0.226	*CRHR2; GARS*
6:31141209-31269154	38	127,945	0.01	*HCG27; HLA-C; POU5F1; PSORS1C3; RPL3P2; USP8P1; WASF5P*
20:25084087-25210827	35	126,740	0.046	*ENTPD6*
3:5139286-5264770	63	125,484	0.067	*ARL8B; EDEM1*
4:117771802-117895396	55	123,594	0.038	–
2:1162219-1284445	83	122,226	0	*SNTG2*
9:85811734-85932885	39	121,151	0.219	*FRMD3; RN7SKP242; RNU4-29P*
7:140681430-140800690	28	119,260	0.037	*CCT4P1; MRPS33; RNU4-74P; TMEM178B*
5:24663784-24782879	30	119,095	0.017	
10:86775252-86893256	19	118,004	0.014	
20:45280443-45396705	22	116,262	0.116	*SLC13A3; SLC2A10; TP53RK*
14:96742594-96858777	77	116,183	0.025	*AK7; ATG2B; GSKIP; RNU2-33P*
4:25069541-25183385	43	113,844	0.121	*PI4K2B; SEPSECS*
17:3551178-3664975	22	113,797	0.331	*CTNS; EMC6; GSG2; ITGAE; P2RX5; P2RX5-TAX1BP3; TAX1BP3*
6:31459636-31571894	20	112,258	0.04	*ATP6V1G2; ATP6V1G2-DDX39B; DDX39B; DDX39B-AS1; LST1; LTA;*

				LTB; MCCD1; MICB; NCR3; NFKBIL1; PPIAP9; RPL15P4; SNORD117; SNORD84; TNF
6:83969447-84081405	41	111,958	0.019	*ME1*
8:18194861-18305817	32	110,956	0.147	*NAT2; NATP*
6:75348870-75459754	43	110,884	0.025	–
10:46042945-46153540	42	110,595	0.004	*MARCH8; ZFAND4*
20:12270287-12380594	52	110,307	0.206	*PA2G4P2*
20:11966913-12073308	61	106,395	0.323	–
22:32475924-32581354	27	105,430	0.037	*AP1B1P1; AP1B1P2; C22orf42; SLC5A1*
5:178806782-178909386	24	102,604	0.052	*RN7SL71P*
5:23274898-23376708	49	101,810	0.022	–
11:60598449-60697138	16	98,689	0.044	*CCDC86; PRPF19; PTGDR2; TMEM109; TMEM132A; ZP1*
1:219484494-219582864	20	98,370	0.017	–
17:50547733-50644300	32	96,567	0.069	–
2:15594926-15691026	36	96,100	0.004	*NBAS*
1:189589634-189684800	82	95,166	0.006	*RNA5SP73*
1:88758831-88853195	21	94,364	0.064	–
11:38250791-38344560	27	93,769	0.003	–
5:173300399-173392960	24	92,561	0.007	*CPEB4*
10:44908783-45001314	41	92,531	0.015	–
2:81499134-81591163	74	92,029	0.013	–
1:79396079-79487080	53	91,001	0.019	*ELTD1*
10:123773001-123863333	18	90,332	0.233	*TACC2*
4:32162926-32252887	53	89,961	0.02	–
1:153103712-153192119	28	88,407	0.195	*LELP1; PRR9; SPRR2B; SPRR2C; SPRR2G*
1:4332602-4420804	51	88,202	0.615	–
12:18358730-18446678	55	87,948	0.04	*PIK3C2G; RERGL*
9:83998114-84086034	38	87,920	0.104	*RPS20P25*
3:112186762-112274613	18	87,851	0.024	*ATG3; BTLA; OR7E100P*
20:33770932-33858460	30	87,528	0.064	*EDEM2; MMP24; MMP24-AS1; MT1P3; RNA5SP483*
11:87831733-87918891	25	87,158	0.042	*MIR3166; RAB38*
9:13671425-13757167	34	85,742	0.149	–
5:29645558-29730372	37	84,814	0.097	–
8:71838025-71922018	19	83,993	0.007	–
4:64474004-64557762	48	83,758	0.082	–
4:187278004-187360993	31	82,989	0.019	*F11-AS1*
2:929925-1012876	60	82,951	0.012	*SNTG2*
8:106143853-106226580	31	82,727	0.029	*TMCC1P1*
1:92563373-92646021	14	82,648	0.005	*BTBD8; GAPDHP46; KIAA1107; PRKAR1AP*
11:21668858-21751076	65	82,218	0.035	–
8:75922888-76004157	32	81,269	0.01	*CRISPLD1*
6:38767559-38847685	53	80,126	0.047	*DNAH8*

11:119659753-119738622	22	78,869	0.335	–
6:49296422-49375140	51	78,718	0.013	*EEF1A1P42; RNU7-65P*
5:75096287-75174322	24	78,035	0.075	
10:55700011-55777899	37	77,888	0.051	*PCDH15*
5:71521214-71597658	24	76,444	0.003	*MRPS27*
20:12125979-12202388	25	76,409	0.271	–
11:71125387-71201562	50	76,175	0.005	*DHCR7; NADSYN1*
18:61972580-62048584	22	76,004	0.093	–
13:42704399-42780317	29	75,918	0.006	*CHCHD2P11; DGKH*
11:77714175-77789554	19	75,379	0.117	*KCTD14; NDUFC2; NDUFC2-KCTD14; THRSP*
11:24535294-24610602	35	75,308	0.24	*LUZP2*
1:102634212-102708758	26	74,546	0.032	–
13:60299552-60373988	51	74,436	0.004	*DIAPH3*
8:13639263-13713326	41	74,063	0.042	–
6:10730474-10804127	16	73,653	0.085	*MAK; RNA5SP203; SYCP2L; TMEM14B; TMEM14C*
5:180303546-180376719	39	73,173	0	*BTNL8; RPS29P12*
4:45024582-45097477	14	72,895	0.024	–
13:31158752-31231513	32	72,761	0.024	*HMGB1; USPL1*
18:1125057-1197434	19	72,377	0.039	*COX6CP3*
2:84195111-84266625	32	71,514	0.002	–
1:35133871-35204787	21	70,916	0.078	*MIR552; SMIM12*
3:154516433-154585906	18	69,473	0.034	–
6:33874378-33943495	16	69,117	0.129	–
2:57737150-57806091	27	68,941	0.074	–
4:53053707-53122296	41	68,589	0.008	–
6:32730012-32797809	59	67,797	0.038	*HLA-DOB; HLA-DQB2; TAP2*
4:78588401-78656133	29	67,732	0.056	*CNOT6L*
7:82229729-82297165	54	67,436	0.02	–
12:52881498-52948875	46	67,377	0.2	*KRT5; KRT6A; KRT71*
1:216975182-217040850	19	65,668	0.056	*ESRRG*
6:22449014-22513914	17	64,900	0.103	–
6:84147119-84211876	34	64,757	0.01	–
6:23005705-23070218	33	64,513	0.027	–
8:133056533-133120784	21	64,251	0.096	*HHLA1; OC90*
20:8427620-8491659	21	64,039	0.074	*PLCB1*
18:74267147-74330672	23	63,525	0.751	*LINC00683; LINC00908*
16:12845849-12909286	39	63,437	0.153	*CPPED1*
4:185120586-185183505	48	62,919	0.109	*ENPP6*
6:153982533-154045407	56	62,874	0.039	*MTND4P13; RNU6-896P*
15:77865287-77927945	45	62,658	0.051	*LINGO1*
3:142721893-142784321	36	62,428	0.004	*U2SURP*
4:43194839-43257176	32	62,337	0.034	–
5:41086537-41148859	25	62,322	0.001	*C6*
3:164809268-164871552	26	62,284	0.014	–
3:189770598-189832810	30	62,212	0.113	*LEPREL1; RN7SL486P*

10:55336366-55398076	18	61,710	0.022	–
1:219329499-219391205	20	61,706	0.002	*LYPLAL1; RIMKLBP2*
11:37148142-37209578	28	61,436	0.056	
15:27069737-27131066	27	61,329	0.119	*GABRA5; GABRB3*
11:120443983-120505289	20	61,306	0.279	*GRIK4; TCEB1P22*
8:37852688-37913977	13	61,289	0.056	*EIF4EBP1*
1:32367055-32426830	33	59,775	0.025	*PTP4A2*
5:154975408-155035003	24	59,595	0.019	–
3:174352220-174411008	32	58,788	0.039	*NAALADL2*
1:37241316-37299788	21	58,472	0.053	*GRIK3*
3:2925284-2983419	21	58,135	0.116	*CNTN4*
11:37281342-37339216	28	57,874	0.01	–
6:25082105-25139813	58	57,708	0.003	*CMAHP*
2:88339648-88396348	18	56,700	0.149	*KRCC1; MIR4780; SMYD1*
20:54806930-54863255	24	56,325	0.104	*MC3R*
3:14675938-14731811	16	55,873	0.011	*C3orf20; CCDC174*
13:29752354-29808169	16	55,815	0.007	*MTUS2*
3:105776780-105832057	20	55,277	0.004	–
12:95416774-95471943	20	55,169	0.004	*FGD6; NR2C1*
6:46808183-46863260	11	55,077	0.062	*GPR116*
4:92418107-92472694	24	54,587	0.009	*CCSER1*
9:83641143-83695647	23	54,504	0.038	–
3:143354316-143408707	15	54,391	0.144	*SLC9A9*
8:68683561-68737887	33	54,326	0.064	
3:125121628-125175879	16	54,251	0.058	*SNX4*
1:14214412-14268365	11	53,953	0.172	–
20:38141538-38194882	15	53,344	0.037	–
7:49675388-49728354	24	52,966	0.007	–
2:71844196-71897075	22	52,879	0.153	*DYSF*
3:153178358-153230919	13	52,561	0.013	*C3orf79; RNU6-901P*
6:97981066-98033529	21	52,463	0.008	–
5:126567785-126620193	30	52,408	0.006	–
8:51313375-51365764	36	52,389	0.028	*SNTG1*
2:14314673-14366975	27	52,302	0.111	*LINC00276*
16:13525213-13577210	24	51,997	0.039	–
4:190348013-190399763	46	51,750	0	*HSP90AA4P*
7:23946088-23997693	17	51,605	0.069	–
9:90797820-90849255	21	51,435	0.051	–
19:15808025-15859253	15	51,228	0.004	*OR10H2; OR10H3*
4:184333347-184384311	24	50,964	0.073	*CDKN2AIP*
2:111635711-111686635	15	50,924	0.006	*ACOXL*
11:21148101-21198841	37	50,740	0.021	*NELL1*
6:64201173-64251656	51	50,483	0.005	*PTP4A1*

Table S19. Biological process categories in a gene ontology enrichment test on regions of the Altai Neanderthal genome putatively introgressed from modern humans. Regions are 50Kb or longer and contain at least 20 SNPs (see Table S18).

GO ID	Category	P-value	Genes
GO:0002495	antigen processing and presentation of peptide antigen via MHC class II	0.014	*HLA-DOB; HLA-DQB2; MARCH8*
GO:0042327	positive regulation of phosphorylation	0.04	*EDEM1; EIF2AK3; PLCB1; TGFBR2*
GO:0007283	spermatogenesis	0.04	*AK7; DIAPH3; FNDC3A; UBR2*

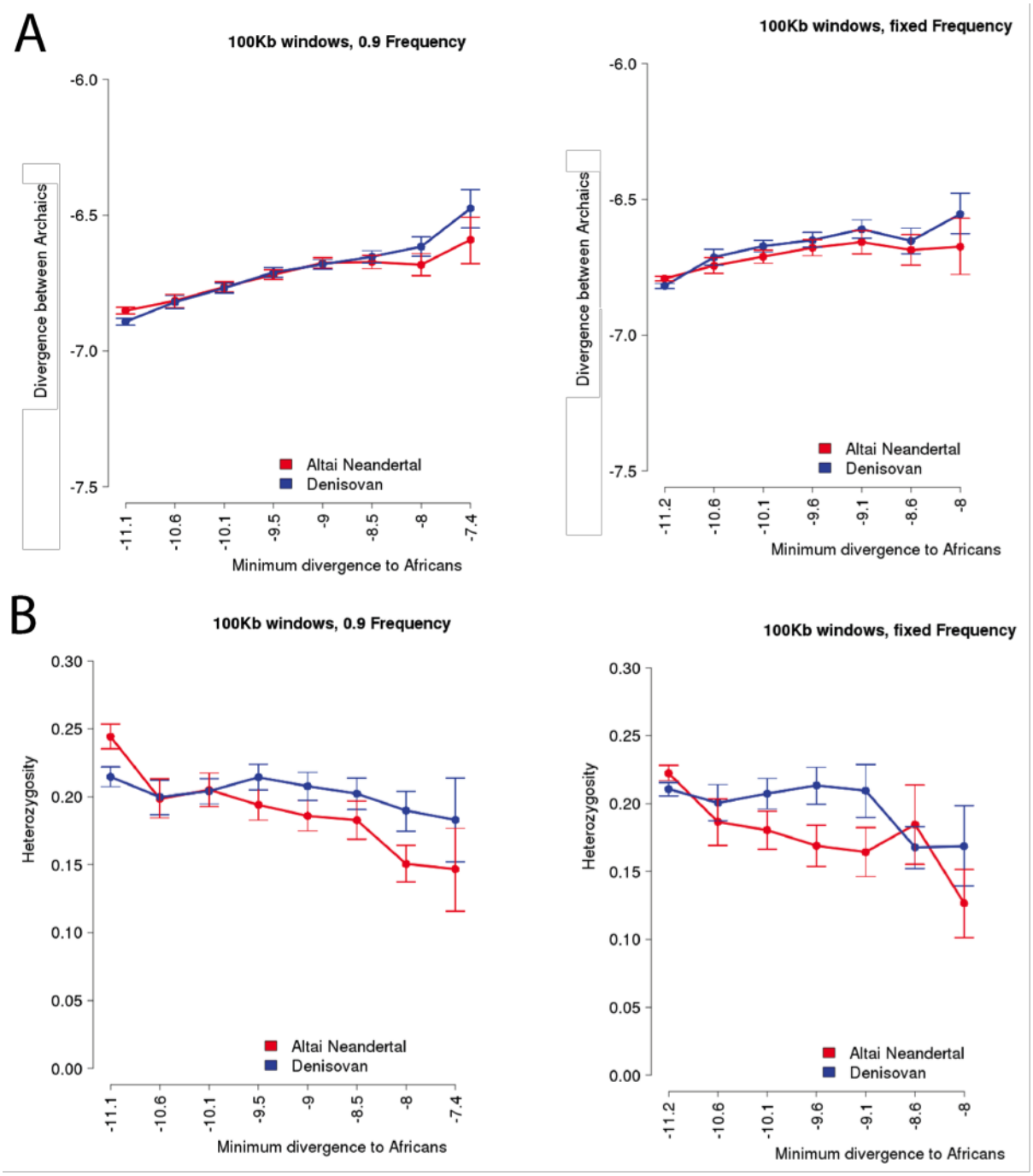

Figure S19. Windows of 100Kb across the Altai Neanderthal and Denisovan genomes binned by their minimum divergence to Africans using derived alleles at >0.9 frequency (left column) or fixed (right column) in five African populations. Bins have at least 100 windows. X-axis is in $\log_{10}$ scale. (**A**) Divergence between windows in the Altai Neanderthal and Denisovan genomes. The 95% confidence intervals are shown. The Y-axis is in $\log_{10}$ scale. (**B**) Heterozygosity (per one thousand bases) in windows of each archaic genome. The left plot of panel A is used in Figure 1a and the left side of panel B is used in Figure 1b.

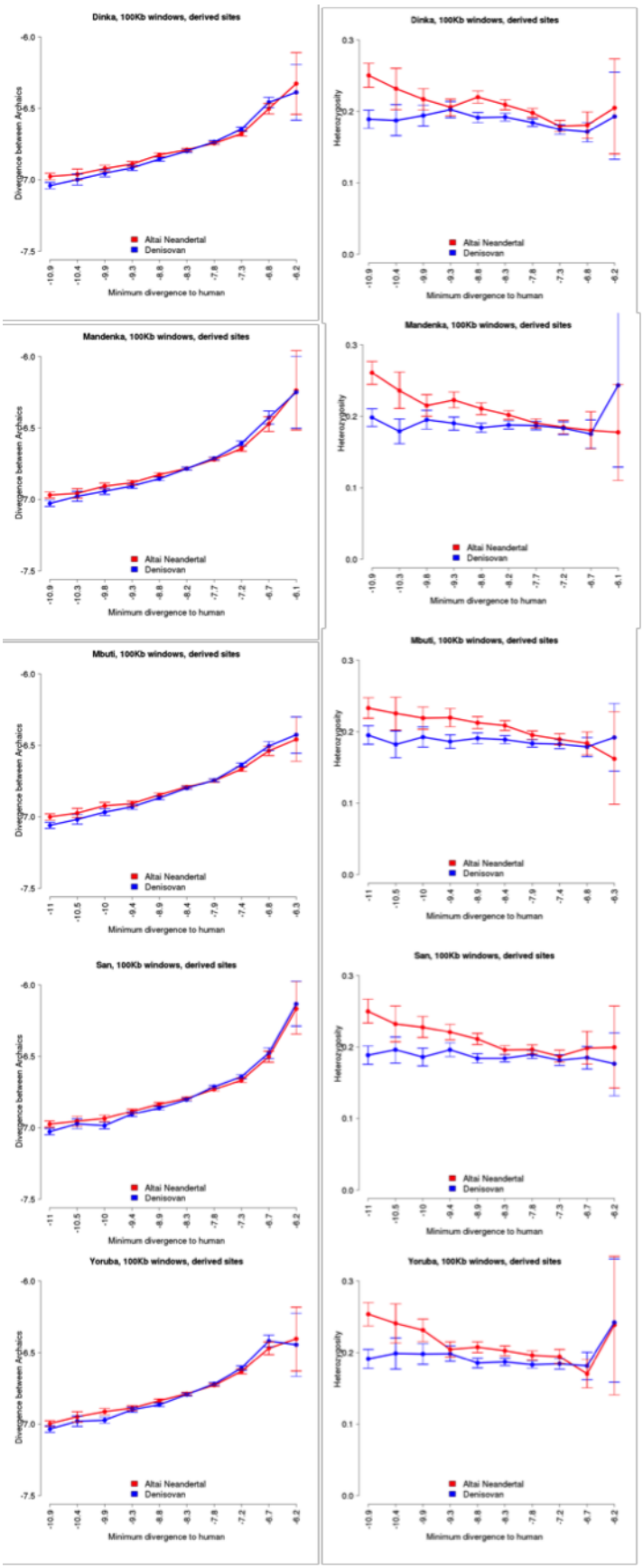

Figure S20. Windows of 100Kb across the archaic genomes binned by their minimum divergence to individual African genomes (X-axis; divergence to derived alleles in homozygous sites in each African genome). Bins have at least 100 windows. Y-axis as in Figure S19.

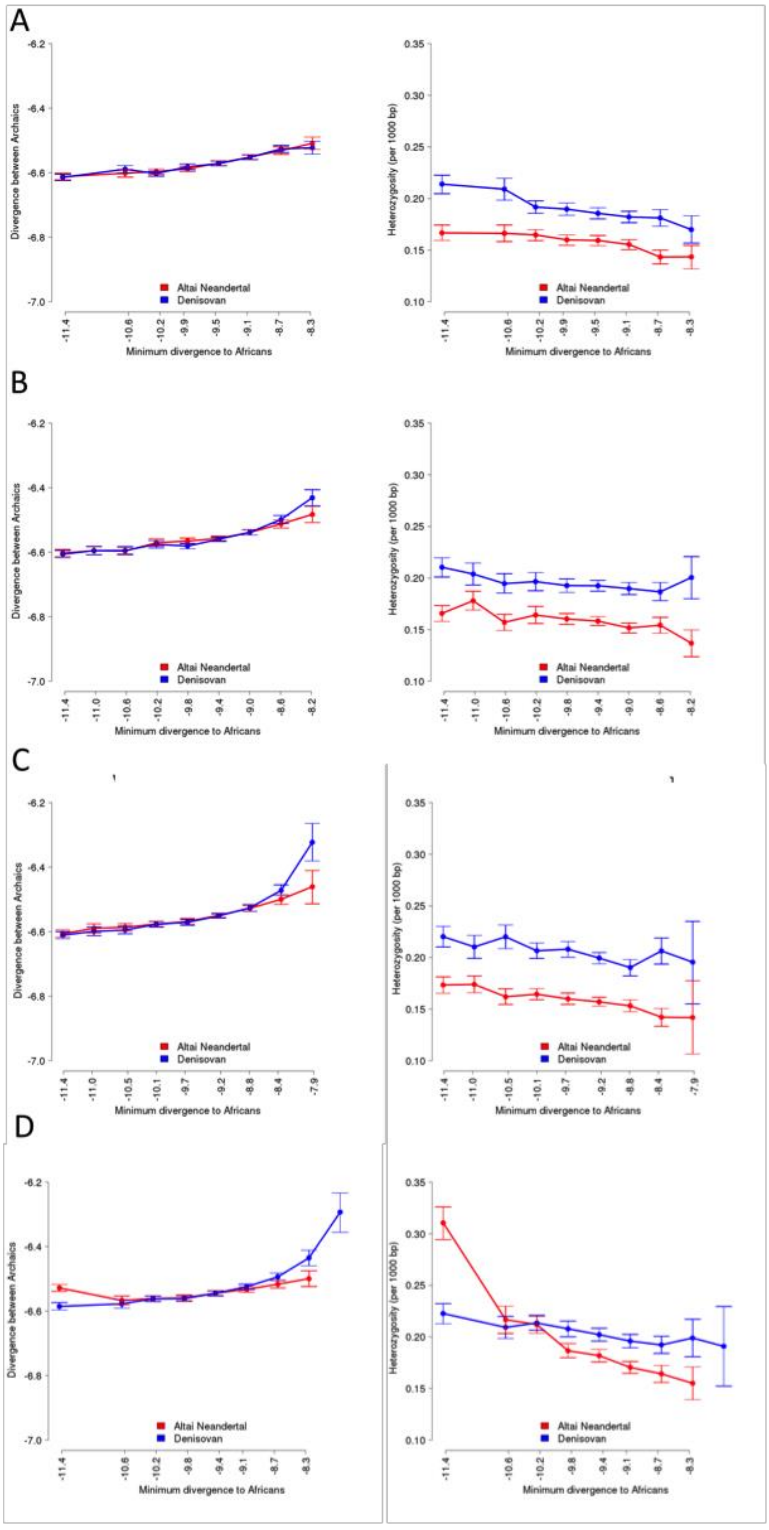

Figure S21. Simulated windows of 100 Kb for the Altai Neanderthal and Denisovan genomes. Windows are binned by their minimum divergence to Africans using derived alleles at >0.9 frequency in the simulated African population. X- and Y-axis as in Figure S19. (**A)** No gene flow; (**B)** Only super-archaic gene flow into the Denisovan lineage (1%); (**C)** Super-archaic gene flow into the Denisovan lineage and Altai Neanderthal gene flow into the Denisovan lineage (0.65%); and (**D)** Super-archaic gene flow into the Denisovan lineage, Altai Neanderthal gene flow into the Denisovan lineage and **modern human gene flow into the Altai Neanderthal lineage** (3.55%). Panel C is used in Figures 1c and 1d, and panel D is used in Figures 1e and 1f. Note though some differences in the range of the X-axis between Figure S21 and Figure 1.

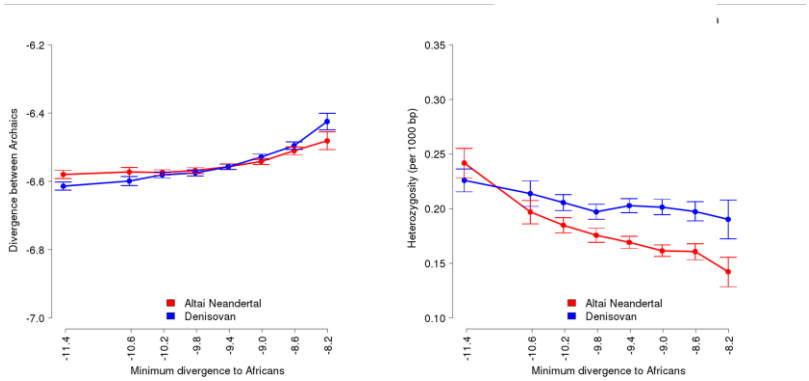

Figure S22. Simulated windows of 100Kb for the Altai Neanderthal and Denisovan genomes with a reduced rate of modern human gene flow into the Altai Neanderthal lineage. Windows are binned by their minimum divergence to Africans using derived alleles at >0.9 frequency in the simulated African population. X- and Y-axis as in Figure S19. Super-archaic gene flow into the Denisovan lineage (2%), Altai Neanderthal gene flow into the Denisovan lineage (0.65%) and **modern human gene flow into the Altai Neanderthal lineage** with a reduced rate (1.8%).

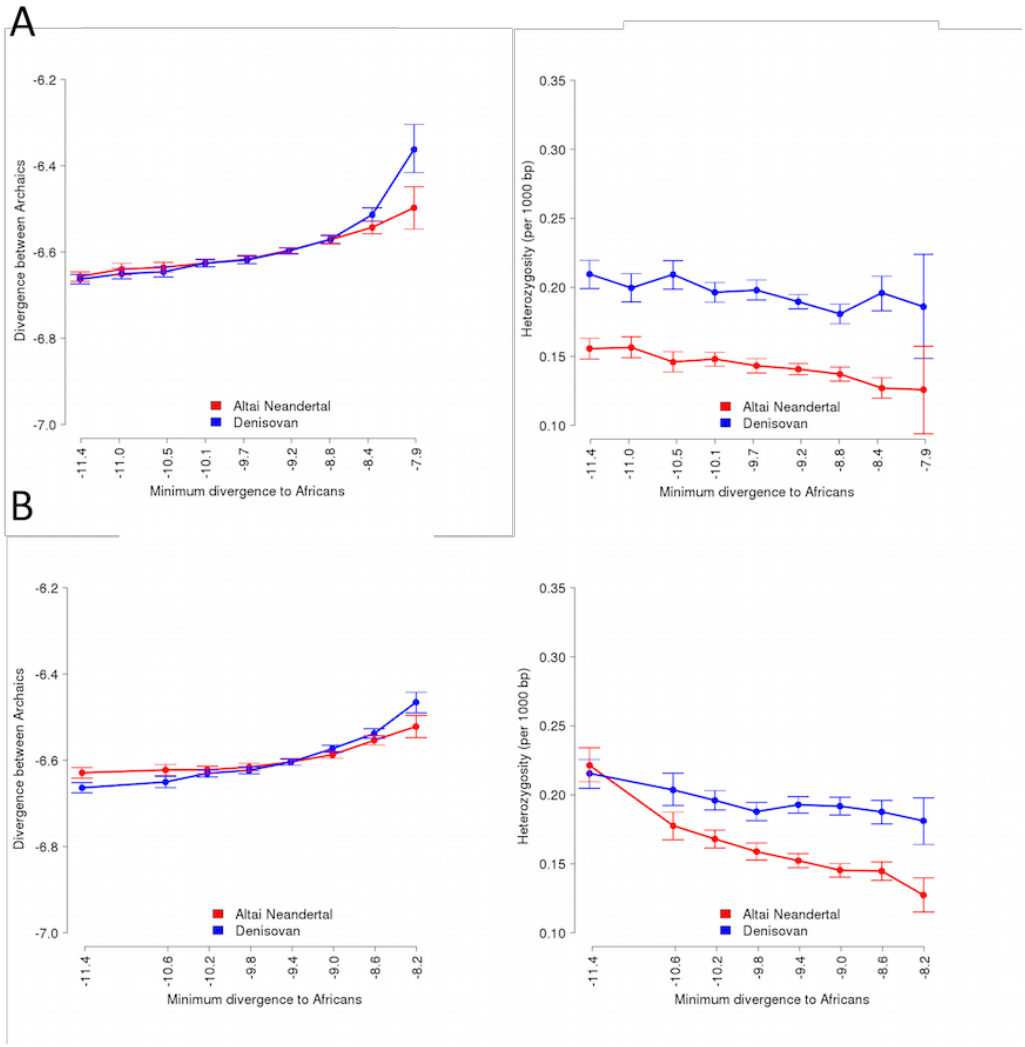

Figure S23. Simulated windows of 100Kb for the Altai Neanderthal and Denisovan genomes with the age differences between the two archaic individuals taken into account. Windows are binned by their minimum divergence to Africans using derived alleles at >0.9 frequency in the simulated African population. X- and Y-axis as in Figure S19. (**A)** Super-archaic gene flow into the Denisovan lineage (1%) and Altai Neanderthal gene flow into the Denisovan lineage (0.65%). (**B)** Super-archaic gene flow into the Denisovan lineage, Altai Neanderthal gene flow into the Denisovan lineage and **modern human gene flow into the Altai Neanderthal lineage** (1.8%).

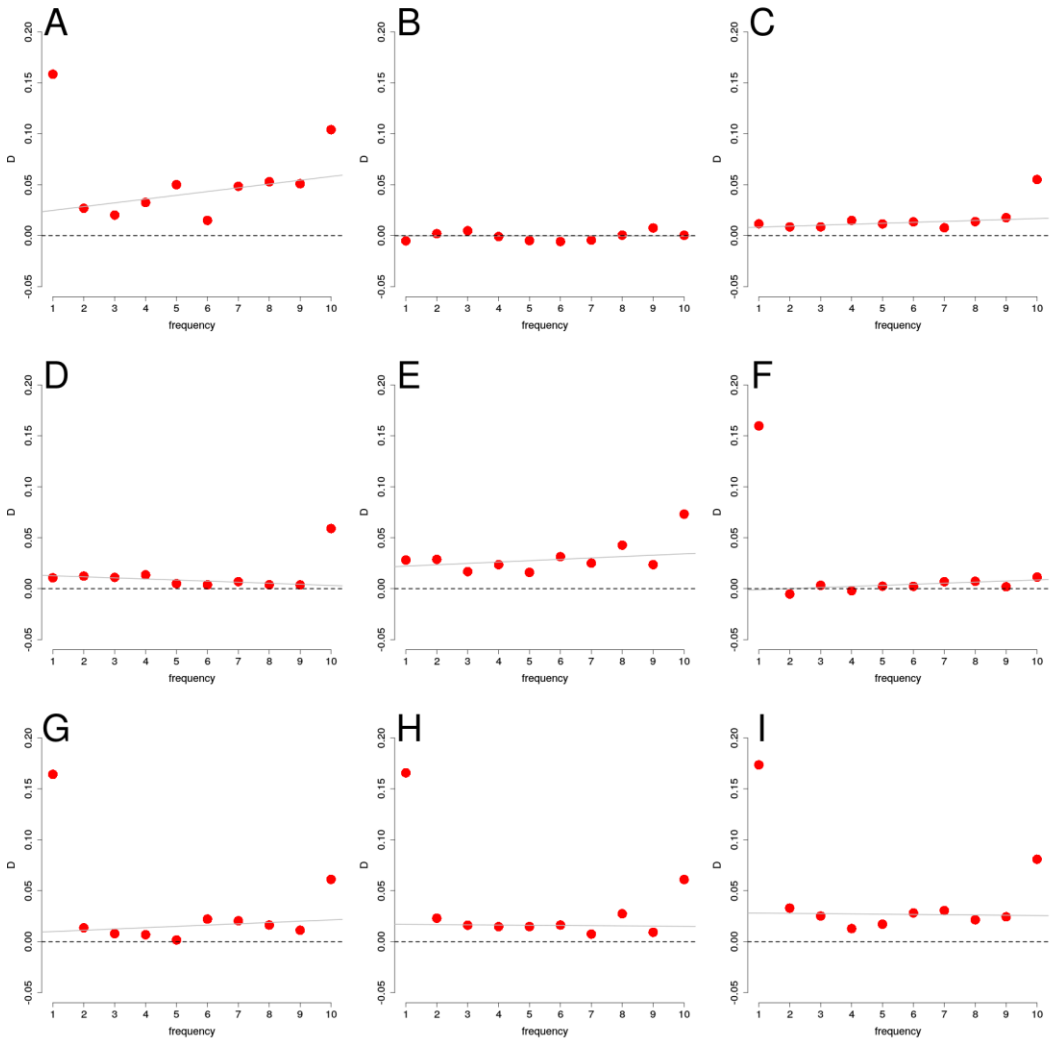

Figure S24. Dj; frequency-stratified summary statistics. Statistics were calculated using all sites at a given allele frequency in Africans in (**A**) Real sequences; (**B**) Simulation without gene flow; (**C**) Simulation with only super-archaic gene flow into the Denisovan lineage; (**D**) Simulation with super-archaic gene flow and Altai Neanderthal gene flow into the Denisovan lineage; (**E**) Simulation with super-archaic gene flow, Altai Neanderthal gene flow into the Denisovan lineage and **modern human gene flow into the Altai Neanderthal lineage**; (**F**) Simulation with Neanderthal gene flow into Africans (0.1%); (**G**) Simulation with Neanderthal gene flow into Africans and super-archaic gene flow; (**H**) Simulation with Neanderthal gene flow into Africans, super-archaic gene flow and Altai Neanderthal gene flow into the Denisovan lineage; and (**I**) Simulation with Neanderthal gene flow into Africans, super-archaic gene flow, Altai Neanderthal gene flow into the Denisovan lineage and **modern human gene flow into the Altai Neanderthal lineage**.

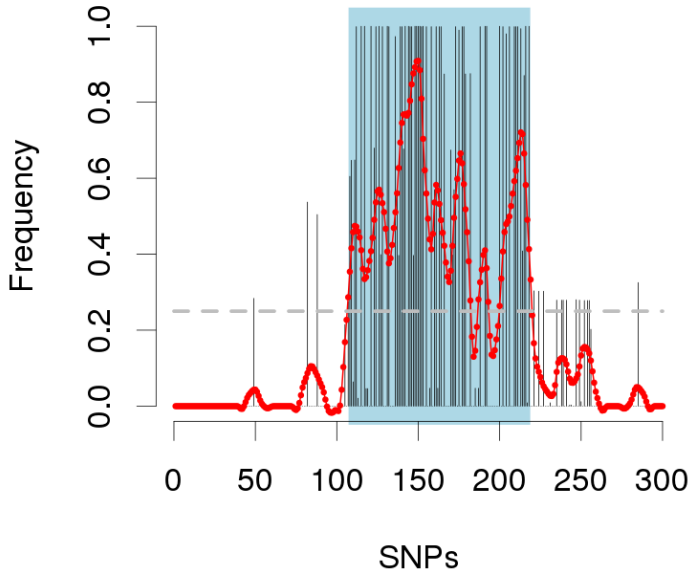

Figure S25. Screen for introgressed segments. The derived allele frequencies in Africans (Y-axis) at sites where the Altai Neanderthal is heterozygous and the Denisovan is homozygous ancestral are shown for 300 consecutive SNPs (black lines) for the region 13:48,962,446-50,360,867 (1.4 Mb), encompassing one of the largest candidate regions (259Kb, in light blue; see Table S18). We fitted a local regression curve to these frequencies (red line), and applied a cutoff of 0.25 (dashed line). Note that derived alleles in the Altai Neanderthal not shared with Africans have a derived African allele frequency of zero.

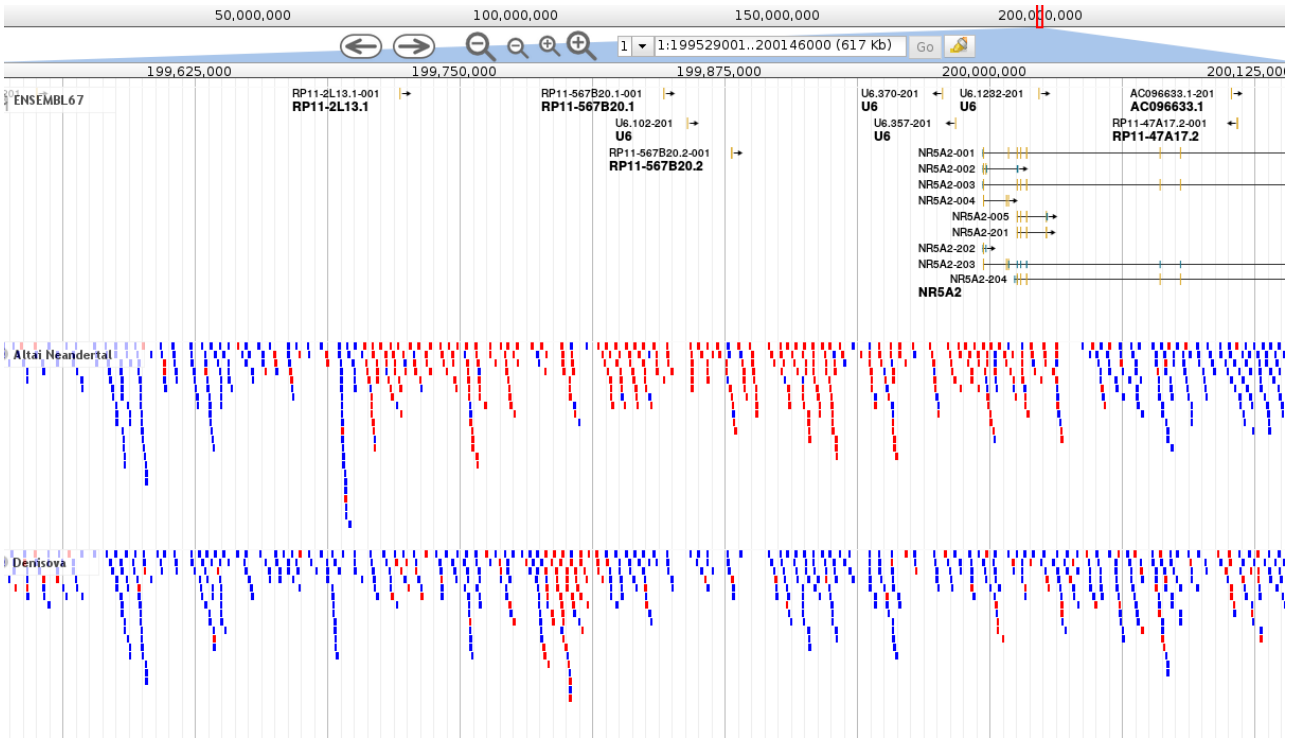

Figure S26. The longest putatively introgressed region in the genome of the Altai Neanderthal is in chromosome 1. Heterozygous sites are shown in red, homozygous differences in blue.

SI 10. ARGweaver

Overview of ARGweaver analysis

ARGweaver (*66*) is a Bayesian method for sampling ancestral recombination graphs (ARGs), which describe the evolutionary relationship between genetic samples. From the ARGs, we can obtain local trees for every non-recombining block of the genome, and we can explore these trees for signs of introgression. For this analysis, we specifically looked for long genomic blocks in which a Neanderthal lineage is inferred to coalesce with a modern African lineage more recently than the time of divergence between Neanderthals and modern humans.

ARGweaver was run genome-wide using a data set consisting of the Altai Neanderthal and Denisovan, six present-day humans and chimpanzee (panTro4). The six present-day humans included two each of Yoruban (HGDP00927, SS6004475), Mbuti (SS6004471, HGDP0456), and San (HGDP01029, SS6004473) individuals. The quality filters 1-7 described in "Genomic Filters", Supplementary information 8 were also applied for this analysis. ARGweaver requires prior distributions for the coalescence, mutation, and recombination rates, and these were chosen as in Rasmussen et al (2014) (*66*). Specifically, a population size of 11,534 was used, and the recombination rate was based on the HapMap Phase II recombination map. The average per-generation mutation rate was 1.26×10^{-8}, with the rate in every 100Kb segment scaled to reflect the observed substitution rate in that region between chimpanzee (panTro2), orangutan (ponAbe2), and macaque (rheMac2). Other ARGweaver parameters were a maximum time of 1,000,000 generations, 20 discrete time steps (distributed on a logarithmic scale, such that recent time intervals are shorter than more ancient ones, using the ARGweaver parameter δ=0.01) and 5,000 MCMC iterations. We used a site compression rate of 10 (-c 10), which decreases compute time 10-fold by combining groups of 10 sites into a single compressed site, and increasing mutation and recombination rates correspondingly. Site compression is implemented in a dynamic way, ensuring that variant sites are never compressed together, so that information is not lost. The genome was divided into 5Mb chunks with 1Mb overlap, in order to run the analysis in parallel across many processors. The ARGs for each chunk of a chromosome were then pasted together at the midpoints of the overlaps between them before they were analyzed for signs of introgression. ARGs were sampled every 20^{th} iteration starting with iteration 2,000. ARGweaver was also run separately on the chromosome 21 of the same individuals, with the addition of El Sidrón and Vindija Neanderthals. For this analysis, the chromosome was divided into 2 Mb chunks with 500Kb overlapping between chunks. ARGweaver did not take the ages of the archaic individuals into account, however we expected that the six present-day samples would dominate in determining the coalescence times. We explored the effect of this model misspecification using simulations (see the "Simulation study" section below).

Integration over phase

A new method to integrate over phase was used to run ARGweaver on unphased genomes. Recall that ARGweaver is a Markov chain Monte Carlo (MCMC) sampler in which each iteration consists of an "unthreading" and a "threading" operation, which removes and then resamples the coalescence points for one or more lineages. Half of the iterations are "leaf threading" operations, which re-thread a single randomly selected lineage, whereas the other iterations re-thread subtrees of the ARG. With phase integration, all individuals are initially assigned randomized genotype phases. However, the leaf threading operation is performed without regard to the phase of the individual whose lineage is being re-threaded, and is followed by re-sampling the phase for that individual. The genotype phases of other individuals are held constant during this step. Leaf threading can be performed on an unphased individual by summing over the two possible phase configurations of each heterozygous site when computing the probability of the sequence data for a particular ARG. These probabilities are used as the emissions probabilities in the hidden Markov Model, which is used to sample the new threading. After the threading is complete, the phase for that individual is sampled at each heterozygous site according to the relative probabilities of the two possible phasings under the newly sampled ARG. Note that the phasings are held constant during subtree threading steps. Phase sampling is implemented in the ARGweaver source code available at http://github.com/mjhubisz/argweaver, using the --sample-phase option. Phase integration was used for all samples in the data (except panTro4, which was treated as a single haploid sample). The effects of using phase integration for this analysis were explored by simulation (described below).

Sequence segments coalescing within the African subtree

Segments coalescing within the African subtree (Figure 2a) were identified for each haploid chromosome of each archaic individual, based on an ARG output by ARGweaver (representing a single MCMC sample from the posterior distribution of ARGs). The ARG defines a local tree at every position along the genome, with each tree having two leaf nodes per individual representing its two haploid chromosomes or "lineages". The 'African' haplotypes for a particular archaic lineage (the "target" lineage) are determined by looking at the times to the most recent common ancestor (TMRCA) between the target lineage and other lineages in each local tree. Let T_{Afr} be the set of TMRCAs between the target lineage and all African lineages in the tree, and let T_{Anc} be the set of TMRCAs between the target lineage and all lineages coming from other archaic individuals. Then, if $min(T_{Afr}) < min(T_{Anc})$ and $min(T_{Afr}) < max(T_{Afr})$, the local tree is considered discordant, and thus, may contain 'African' haplotypes. These two conditions guarantee that the archaic lineage is more closely related to at least one African lineage than to other archaic individuals, and that it falls within the range of African variation for the segment in question. Note that the other lineage from the target individual is not used to define T_{Anc}, so that both heterozygous and homozygous 'African' haplotypes will be detected.

Once the sequence segments with 'African' haplotypes have been identified, the age for each segment is set to $min(T_{Afr})$. Adjacent segments with 'African' haplotypes with the same age are combined into a single segment. Finally, a filter was applied which removed any segment in which the overall polymorphism level

(across all individuals in the data set excluding the chimpanzee outgroup) was less than 1 polymorphic site per 1,000 bases. This was done in order to remove segments with long stretches of masked sites.

Sequence segments coalescing beyond the African and archaic tree

The ancestral segments shown in Figure 2b of the main text were defined using the same quantities defined in the previous section; in this case choosing regions for which $min(T_{Afr})$, $max(T_{Afr})$, $min(T_{Anc})$, and $max(T_{Anc})$ are all equal. This indicates that the target lineage is an outgroup to all African lineages as well as all lineages from other archaic individuals. The age of the ancestral segments was set to the TMRCA of this lineage with all other lineages, and adjacent ancestral segments with the same age were combined. The same filter for the polymorphism level in each segment was applied to these ancestral segments.

Averaging over MCMC replicates and the effect of homozygosity

The ARGweaver analysis produced 151 sampled ARGs, as samples were taken every 20th MCMC iteration from iteration 2,000 to 5,000. Each of these 151 ARGs produced a set of 'African' and ancestral haplotypes for each haploid lineage of each archaic individual (Altai Neanderthal and Denisovan). For a given archaic individual, then, there are 302 sets of segments with 'African' haplotypes as well as 302 sets of ancestral segments. Statistics presented in this paper (such as counts or genomic coverage of these segments, or a selected subset of them) are calculated on each of the 302 replicates separately, and means and 95% confidence intervals across these values are reported.

Note that all 'African' and ancestral segments are defined for a single haploid lineage of an archaic individual, while ignoring the other lineage from that individual, so that segments are identified without regard to whether they are homozygous or heterozygous. This was done in order to fairly compare numbers between the Altai Neanderthal and the Denisovan, despite the higher level of homozygosity in the Altai Neanderthal. Homozygous segments are expected to be identified in both lineages, with the effect that the number of replicates in homozygous regions will be closer to 151 rather than 302. This may result in somewhat more noise in our estimates for the Altai Neanderthal compared to the Denisovan, but it should be a minor effect, and importantly, there should be no impact on the expected values of our statistics due to an individual's level of homozygosity.

Potentially introgressed segments in the Altai Neanderthal

We expect most of the inferred 'African' segments to be a result of incomplete lineage sorting and not necessarily the result of introgression. We thus wanted to choose a set of 'African' segments in the Altai Neanderthal that are strong candidates for being introgressed from modern humans. We chose a length cutoff of ≥50 Kb because we expect introgressed segments to be long, relative to older haplotypes resulting from incomplete lineage sorting. In addition, long haplotypes harbor more mutations, giving ARGweaver more power to accurately date coalescence events, so this length cutoff also filters out less informative regions. However, none of our results changed substantially when varying the length cutoff from 20 Kb up

to 100 Kb (affecting the overall but not relative counts between the Altai Neanderthal and Denisovan). Looking at Figure 2a in the main text, which uses a length cutoff of ≥50 Kb and shows the distribution of haplotype ages for 'African' haplotypes, the age cutoff ≤230 Ky was chosen to classify potentially introgressed segments in Altai Neanderthal, as there are few 'African' segments in the Denisovan genome meeting this criteria. There are an average of 97 (95% CI: 86-108) 'African' segments in the Altai Neanderthal genome meeting this length and age criteria, covering 7.2 Mb (95% CI: 6.5-7.9 Mb). Conversely, in the Denisovan genome, there are an average of 20 'African' segments (95% CI: 13-28) covering 1.3 Mb (95% CI: 0.9-1.9 Mb). Some of the 'African' segments in the Altai Neanderthal that are older than 230 Ky may also be due to the proposed introgression event, however, given the high levels of 'African' haplotypes in the Denisovan older than 230 Ky, it seems likely that most of these segments are better explained by incomplete lineage sorting. This observation is also confirmed by simulations (see "Simulation study" section below).

African source population of potentially introgressed segments

Looking at the set of potentially introgressed segments in the Altai Neanderthal genome, we examined whether these segments primarily coalesce within a particular African population. In Figure S27, we show the number of segments in the Altai Neanderthal defined by their coalescence time with each African individual. There appear to be somewhat fewer 'African' segments from the individuals from the Mbuti population; however this difference is not statistically significant, and the data support a model in which the three African populations contribute equally to the introgression event.

Overlap of segments with 'African' haplotypes and ancestral segments

As shown in Figure 2b of the main text, there is an excess of "ancestral" segments in the Denisovan, which is presumably due to introgression of an unknown archaic population into the Denisovan genome (*3*). This archaic introgression complicates interpretation of the ARGs. Both scenarios of introgression –super-archaic introgression into Denisovan lineage and modern human introgression into Altai Neanderthal lineage– are likely to lead to an excess of Denisovan ancestral lineages, as well as an excess of 'African' Altai Neanderthal lineages. However, the observed excess of 'African' haplotypes in the Altai Neanderthal at ≤230Ky is not expected from super-archaic introgression into the Denisovan lineage alone. Nevertheless, we wanted to check that this signal is not an artifact due to the excess of ancestral segments in the Denisovan genome.

To this end, we created a version of Figure 2a from the main text, which shows the excess of young segments in the Altai Neanderthal genome with 'African' haplotypes. In this version, we removed all 'African' segments which overlap any "ancestral" segment in either lineage of the other archaic individual. The ancestral segments used for this purpose were not filtered for informativeness or length, in order to use the most complete (rather than confident) set of ancestral segments. The results are shown in Figure S28. 67% of the Altai Neanderthal segments with 'African' haplotypes were removed, and 62% of the Denisovan

segments were removed; however the excess of young Altai Neanderthal segments with 'African' haplotypes is still statistically significant.

Argweaver analysis of the two European Neanderthals on chromosome 21

ARGweaver was also run on chromosome 21 with the addition of sequence data from El Sidrón and Vindija Neanderthals, and 'African' haplotypes were determined as described above. Having three Neanderthals in the analysis makes it less likely that a Neanderthal lineage will coalesce into the human subtree before coalescing with another Neanderthal, under a model with no modern human introgression. Therefore, we expect fewer 'African' haplotypes in any of the three Neanderthals compared to the Denisovan. Still, the analysis yielded one region on chromosome 21 which was called as a long, young homozygous 'African' haplotype in Altai Neanderthal (chr21:30,368,000-30,458,000; hg19 coordinates). This region overlaps with that found in the screen for introgressed segments on chromosome 21 (Supplementary information 9). No such region was found on chromosome 21 of the El Sidrón and Vindija Neanderthals or the Denisovan (Figure S29).

Simulation study to address the ages of the archaic individuals

One limitation of ARGweaver is that it currently does not have an option to handle the age of archaic individuals, as done in our demographic inference (Supplementary information 8). For this reason, all individuals in each data set were treated as if they were present-day individuals, but we were concerned that this approach could potentially lead to a bias in the coalescence times inferred by ARGweaver. If the archaic individuals were all of the same age, we would expect this bias to be the same for the Altai Neanderthal and Denisovan. However, since the Altai Neanderthal is likely older than the Denisovan, there is an additional concern that this could lead to a larger bias in the Altai Neanderthal compared to the Denisovan, and this differential bias could be falsely interpreted as a signal of introgression.

In order to explore the effects of this model misspecification, we conducted a simulation study. We used *ms* (*57*), to simulate one hundred 2-Mb regions consisting of four Africans, one Altai Neanderthal, and one Denisovan individual. We used demographic parameters consistent with the G-PhoCS estimates: an African population size of 24,000, an Altai Neanderthal population size of 750 from 70 Kya to 140 Kya, changing to 3,200 from 140 Kya to 450 Kya, a Denisovan population size of 2,500 from 50Kya to 450 Kya, the Altai Neanderthal and Denisovan populations coalesce at 450 Kya and have a population size of 8,000, and this population coalesces with Africa at 620Kya, with an ancestral population size of 17,800. The Altai Neanderthal age was modeled at 70 Kya, and the Denisovan at 50 Kya. In order to do the simulations with ms, we set the Altai Neanderthal and Denisovan population sizes to a very high number (10,000 4×N0 generations) from the present until the sampling time, so that the two lineages from each individual would not coalesce with each other.

A recombination rate of 1.25×10^{-8} recombs/generation/base pair was chosen (by trial and error), with the aim of producing a similar distribution of lengths of 'African' haplotypes as observed in the real data. The following is the *ms* command used, obtained by converting the above sizes into units of 4xN0, and converting times to units of 4xN0 generations by dividing by 29x4xN0. N0 can be chosen arbitrarily and was set to 1,000. The first eight samples correspond to the African population, the next two to the Altai Neanderthal, and the final two to the Denisovan. The *ms* command is as follows:

```
ms 12 1 -T -seeds <seed1> <seed2> <seed3> -r 10 2000000 -I 3 8 2 2 -n 1 24
-n 2 10000 -n 3 10000 -en 0.431 3 2.5 -en 0.603 2 0.75 -en 1.21 2 3.2 -ej 3.88 3
2 -en 3.88 2 8 -ej 5.34 2 1 -en 5.34 1 17.8
```

The trees output by *ms* were then modified (using a custom perl script) to shorten the branches of each ancient individual, subtracting the sample age. These modified trees were then given to the program *Seq-Gen* v1.3.3 (*59*) to simulate the sequences. The *Seq-Gen* call was the following:

```
seq-gen -q -z <seed4> -p <nump> -mHKY -t3.0 -f0.3,0.2,0.2,0.3 -l2000000 -s
0.00005 < trees.txt
```

where <nump> is the number of trees output by ms, and trees.txt contains the modified output from ms. The mutation rate corresponds to $4 \times N0 \times 1.2 \times 10^{-8}$. The *ms* and *seq-gen* commands above were run 100 times with different values of seed1, seed2, seed3, seed4 to produce 100 sets of 2 Mb sequences.

ARGweaver was run on each simulated data set as in the real data analysis: individual ages were ignored, haplotype phases were randomized for each individual, and the phase integration feature was used. Then, 'African' segments in the Altai Neanderthal and Denisovan were identified, and the distribution of their ages compared. Unlike in the real data analysis, there was no significant excess of young segments with 'African' haplotypes in the Altai Neanderthal genome (Figure S30). Therefore, the excess observed in the real data analysis appears not to be an artifact due to the difference in the ages of the archaic individuals.

Effect of phase integration

We analyzed the simulated data sets in two ways: once with the true haplotype phase treated as known, and once with randomized phase and phase integration. The results presented in the Supplementary Figures are from the analysis with phase integration, as this is how the real data was analyzed. Similar figures produced from the runs with known phase look extremely similar in shape (not shown). However, the absolute numbers of long 'African' haplotypes was 40% lower in the runs with phase integration. This appears to be largely a result of long haplotypes being broken up by phase errors. On a basewise level, the performance of the two runs was more similar: 'African' segments were identified with a true positive rate of 77.7% and a false positive rate of 3.9% when the true phase was used, compared to a true positive of 74.2% and false positive of 4.7% with phase integration. Overall, we expect that, if phase were known in the real data, our

analysis would have yielded more long 'African' haplotypes, but phase integration does not seem to have impacted the ages or relative counts of these segments.

Simulations with archaic introgression into the Denisovan

We conducted an additional simulation study to explore the effects of introgression into the Denisovan from an unknown archaic hominin. The simulation parameters were the same as before, except that we now include an unsampled archaic hominin population with a divergence time of 1.5 Million years from the ancestral human population. Admixture with the Denisovan was simulated to occur 300 Kya, such that 1% of the Denisovan genome came from this archaic hominin every generation for 10 generations. The *ms* command was:

```
ms 12 1 -T -seeds <seed1> <seed2> <seed3> -r 10 2000000 -I 4 8 2 2 0 -n 1
24 -n 2 100000 -n 3 100000 -n 4 5 -en 0.431 3 2.5 -en 0.603 2 0.75 -en 1.21 2
3.2 -ej 3.88 3 2 -en 3.88 2 8 -ej 5.34 2 1 -en 5.34 1 17.8 -em 2.586 3 4 40 -em
2.589 3 4 0 -ej 12.93 4 1
```

Sequences were generated from the trees created by this command as before, followed by the same ARGweaver analysis. The age distribution of 'African' haplotypes is shown in Figure S31, and the distribution for ancestral haplotypes in Figure S32. In this case, the excess of ancestral segments in Denisovan compared to Altai Neanderthal is much higher than observed in the real data, suggesting that the simulations contain an exaggerated amount of super-archaic introgression into the Denisovan. As expected, this introgression does cause the Altai Neanderthal to have more 'African' haplotypes than the Denisovan. However, it does not cause any skew in the ages of these haplotypes compared to those shown in the simulations without archaic introgression. Notably, there are no 'African' haplotypes in the Altai Neanderthal with ages $\leq$ 350 Kya, and only a small excess in the 350 Kya category compared to the Denisovan. Therefore, it is unlikely that the youngest 'African' haplotypes identified for in the Altai Neanderthal genome, could be explained by super-archaic introgression into the Denisovan.

Simulations with modern human introgression into the Altai Neanderthal

We performed a final simulation study to test the power of the ARGweaver approach to detect the type of introgression event proposed in this manuscript. These simulations included migration from a modern human population into the Altai Neanderthal lineage 100 Kya at a rate of 3.55% for a single generation. It also included migration from a deeply divergent archaic population into the Denisovan lineage at a more modest rate than the previous set of simulations (1% migration for a single generation 300 Kya). Ancient sample ages of 70 Kya for the Altai Neanderthal and 50 Kya for the Denisovan were implemented as before by post-processing the *ms* output. The *ms* command was:

```
ms 12 1 -T -seeds <seed1> <seed2> <seed3> -r 10 2000000 -I 4 8 2 2 0 -n 1
```

```
24 -n 2 100000 -n 3 100000 -n 4 5 -en 0.431 3 2.5 -en 0.603 2 0.75 -en 1.21 2
3.2 -ej 3.88 3 2 -en 3.88 2 8 -ej 5.34 2 1 -en 5.34 1 17.8 -em 0.862069 2 1 142
-em 0.862319 2 1 0 -em 2.586207 3 4 40 -em 2.586457 3 4 0 -ej 12.93 4 1
```

1,000 replicates of this simulation were created and analyzed by ARGweaver in the same manner as the real data analysis, including randomizing the initial haplotype phasings and use of ARGweaver's phase integration feature. The 'African' haplotypes ≥50 Kb are shown in Extended data figure 5. In the top panel (Extended Data Fig. 5a), the distribution of 'African' haplotype ages is shown for the Altai Neanderthal and Denisovan. These simulations show an excess of young 'African' haplotypes dated ≤234 Kya, as well as an absence of such haplotypes in the Denisovan, which is quite similar to the results from the actual archaic genomes. Therefore, a migration event similar to the one simulated can produce a signal much like the one we observe, and our ARGweaver analysis has the power to detect this signal.

These simulations also allowed us to compare the haplotype ages computed by ARGweaver to the true haplotype ages available in the trees produced by ms. For each 'African' haplotype predicted by ARGweaver, we computed its true age as the average time (from present) to the first coalescence between an African lineage and a target lineage (either the Altai Neanderthal or Denisovan) across the predicted region. In Extended Data Fig. 5b, we show the distribution of true ages for each set of 'African' haplotypes sharing a particular estimated age from ARGweaver. The figure is divided into true positives, false positives, true negatives, and false negatives based upon ARGweaver's ability to identify these introgressed haplotypes resulting from the modern human gene flow into the ancestors of the Altai Neanderthal, using an identification threshold of ≤234 Kya. Note that this figure considers only 'African' haplotypes which were identified by ARGweaver and which pass the length threshold of 50 Kb; there are many more false and true negatives which are not considered here. Overall, these simulations reinforce our choice of 234 Kya as a threshold for choosing a confident set of potential introgressed regions in the Altai Neanderthal genome with a very low false positive rate. This choice is supported both by the distribution of true ages in each age bin for the Altai Neanderthal, as well as by the contrast between the Altai Neanderthal and Denisovan. A higher threshold would identify more truly introgressed regions, but would disproportionately increase the false positive rate.

It is apparent from Extended Data Fig. 5b that the times produced by ARGweaver behave reasonably, with the expected linear relationship between estimated and true times. However, the estimated times are quite noisy, and cannot be used to precisely date a particular haplotype. It also appears from this figure that the ARGweaver age estimates may be biased downward, but this is actually an artifact of our simulation settings and the distribution of true haplotype ages. For example, because the simulated migration into Altai Neanderthal occurred at 100 Kya, all haplotypes with age estimates less than 100 Kya are necessarily underestimated under this scenario. The same effect is seen for the Denisovan, which has no haplotypes with

true ages younger than the archaic/modern human divergence time of 620 Kya. To confirm that the bias is an artifact, we show in Figure S33 a more standard view of the accuracy of the ARGweaver age estimates, with the estimated ages shown as a function of (binned) true ages. Figure S33 confirms that the estimates are largely unbiased, especially for the younger ages where ARGweaver's discrete times are sampled densely. However, Extended Data Fig. 5b demonstrates that the youngest haplotypes predicted by ARGweaver are almost certainly underestimates, due to their noise; therefore the ages of the youngest haplotypes do not provide a lower bound on the date of introgression. In the simulation, 13.2% of haplotypes with ages estimated ≤234 Kya have dates earlier than the true introgression event. In the real data, only 8.6% of haplotypes are dated more recently than 100 Kya, suggesting that the true introgression was likely somewhat older than 100 Kya.

ARGweaver conclusion

The ARGweaver analysis conclusively shows that there is an excess of young, long 'African' haplotypes in the Altai Neanderthal genome. The simulations show that this excess cannot be explained by the ages of the archaic individuals, or by introgression into the Denisovan from an unknown archaic hominin. Our simulations do find that this excess is consistent with the signal produced by an early modern human population into the Altai Neanderthal lineage 100 Kya. However, the noise in ARGweaver's haplotype ages, as well as the large number of possible migration scenarios to consider, makes it difficult to get a precise estimate of the time of this gene flow event.

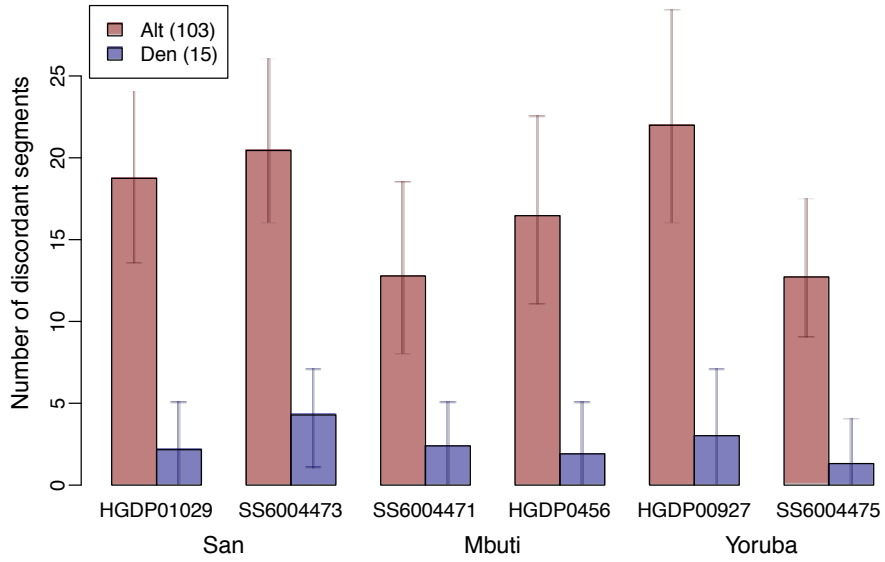

Figure S27. Number of potentially introgressed segments (≥50 Kb with ages ≤235 Ky) in the Altai Neanderthal and Denisovan genomes based on their coalescence times with each African individual. Red=Altai, blue=Denisova, bar height represents means, and error bars give 95% confidence interval.

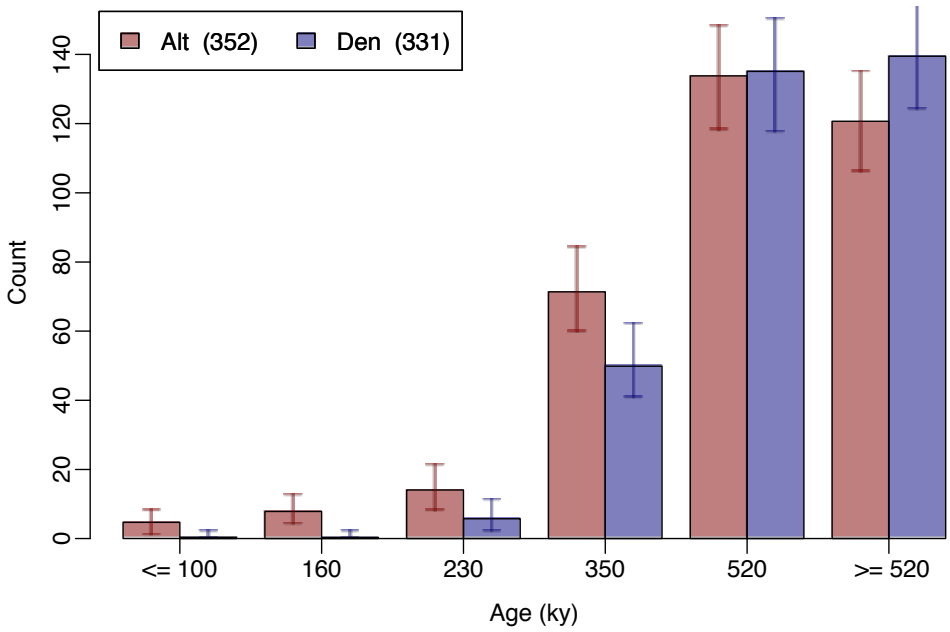

Figure S28. Distribution of ages in the Altai Neanderthal and Denisovan genomes for segments (≥ 50 Kb) with 'African' haplotypes, after removing any 'African' segment which overlaps segments where the other archaic individual is an outgroup to all other archaic and present-day humans. Numbers in the legend give total numbers of segments. Bar height represents means across all ARGweaver runs, and error bars give 95% confidence interval.

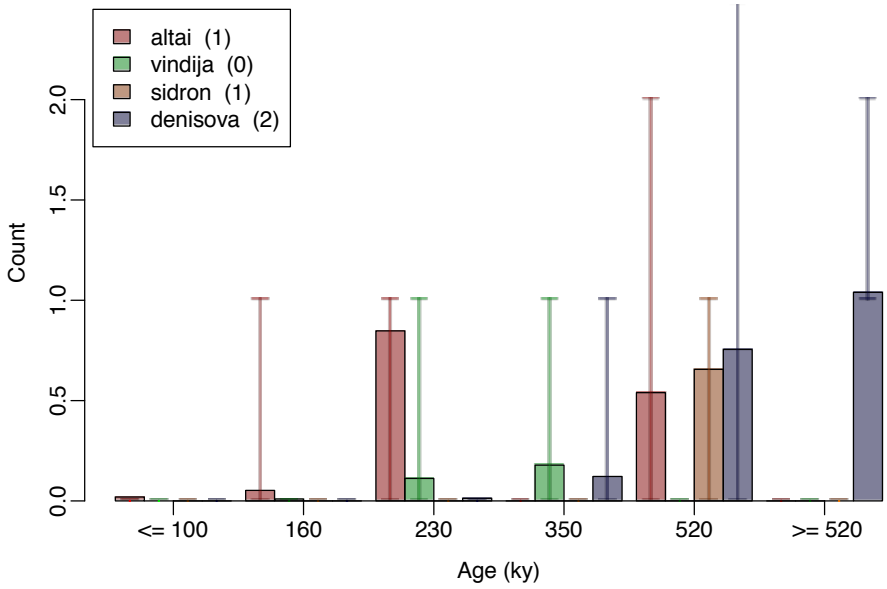

Figure S29. Number of 'African' haplotypes found in each archaic individual in the ARGweaver analysis of their chromosome 21.

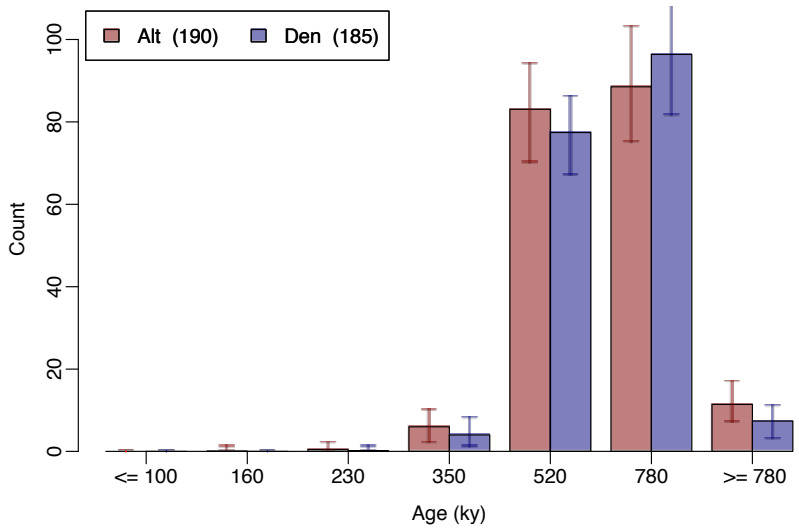

Figure S30. Distribution of the ages of segments with 'African' haplotypes in the simulated data set, which was simulated with no recent modern human admixture, but with sampling times of 70 Ky for the Altai Neanderthal and 50 Ky for the Denisovan. Bar height represents mean, and error bars give 95% confidence intervals.

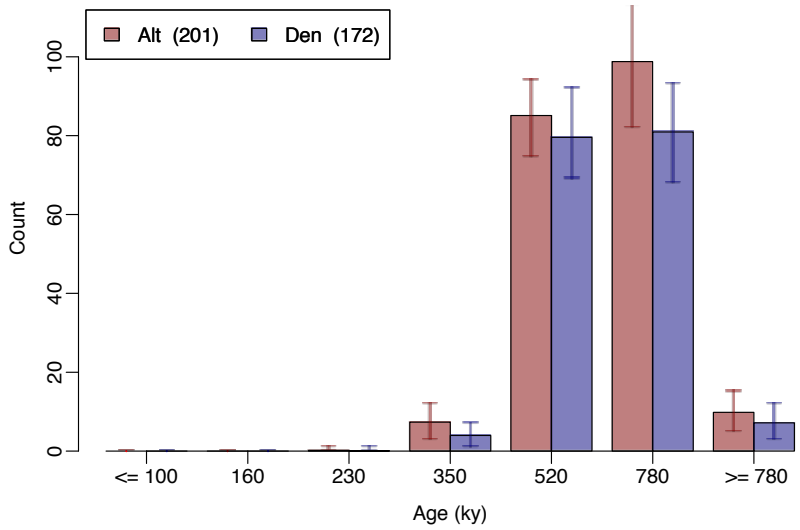

Figure S31. Distribution of 'African' haplotype ages in data simulated with introgression into the Denisovan from an unknown archaic hominin.

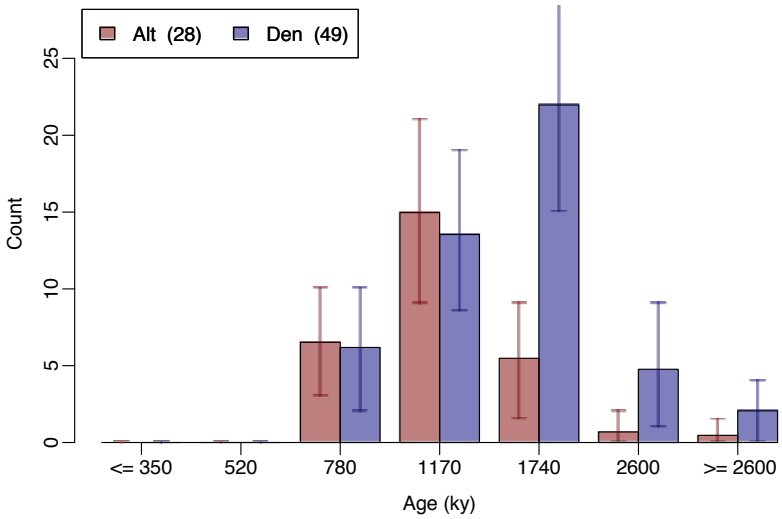

Figure S32. Distribution of ancestral segment ages in data simulated with introgression into the Denisovan from an unknown archaic hominin (super-archaic introgression).

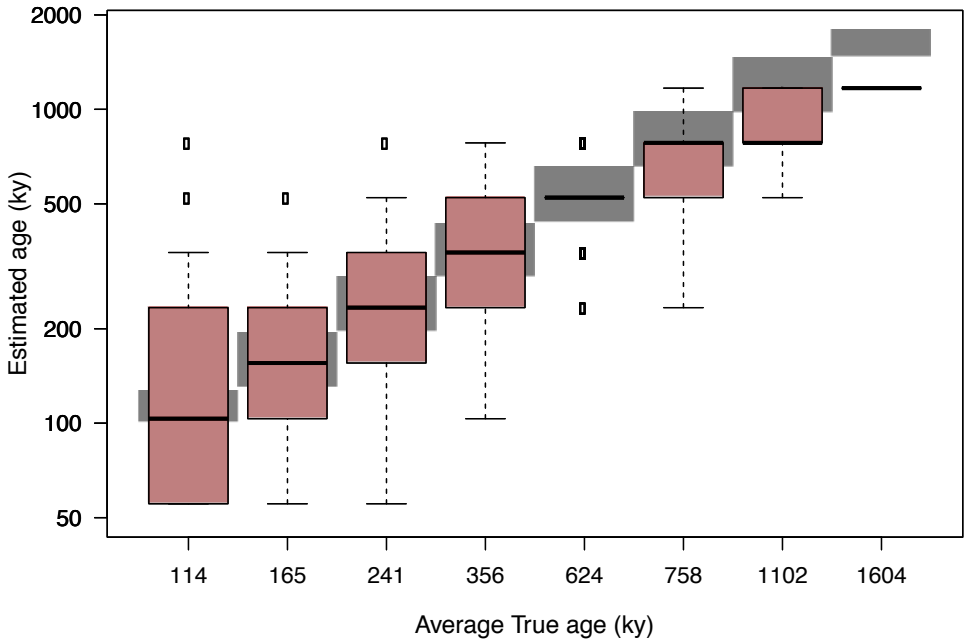

Figure S33. Distribution of estimated 'African' haplotype ages in Altai Neanderthal genome as a function of true haplotype ages, in a simulation scenario with migration from modern humans into the Altai Neanderthal lineage 100 Kya. The gray boxes in the background show the range of true haplotype ages in each bin; the boxplot shows the distribution of estimated ages for each bin. Note that the boxplots represent distributions over a somewhat coarse collection of discretized times used by ARGweaver.

SI 11. Population diversity

The rarity of Neanderthal remains and the difficulty to obtain endogenous DNA from them hinders sampling the genetic diversity of populations of Neanderthals. Neanderthals, however, tend to share a larger fraction of alleles among them (Figure S7) than present-day humans do. Furthermore, Neanderthal heterozygosities are much lower than in present-day humans (*1, 3, 67*) (see also Supplementary Information 5). This suggests that small samples of Neanderthals will be enough to study their genetic diversity across Eurasia. If so, each additional Neanderthal chromosome sampled will discover relatively fewer novel derived alleles than chromosomes of present-day humans. This is indeed the case in the six Neanderthal chromosomes studied in this work (Figure S34A). Estimates of population parameters, such as theta (population mutation rate), will also vary less with sample size (Figure S34B and C), making their calculation more reliable with samples of small size.

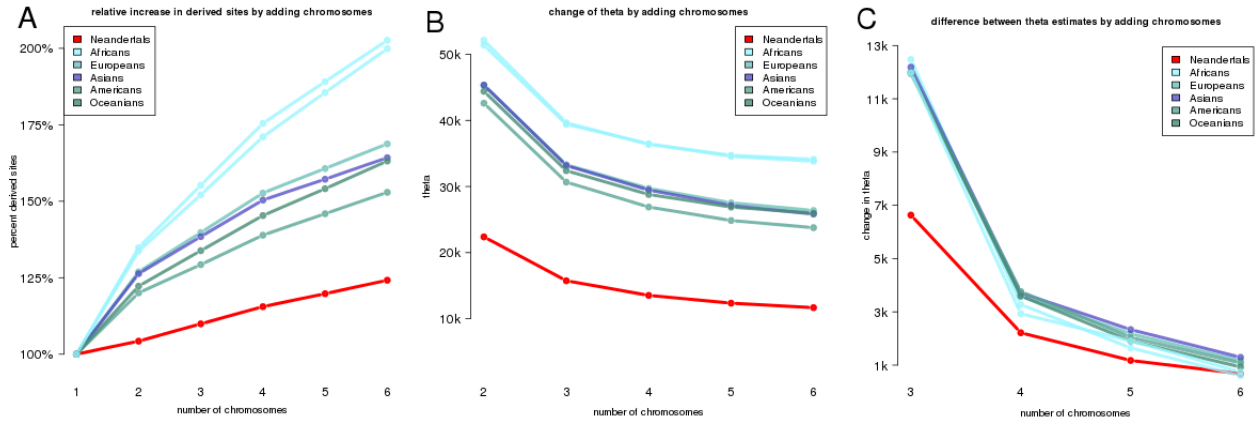

Figure S34. The discovery of derived alleles **(A)** and estimation of theta **(B and C)** with increasing number of chromosomes in Neanderthal and present-day humans. Individuals were chosen by geographic origin (see Supplementary Information 7).

1. S. Castellano *et al.*, Patterns of coding variation in the complete exomes of three Neandertals. *Proceedings of the National Academy of Sciences of the United States of America* **111**, 6666-6671 (2014).
2. H. A. Burbano *et al.*, Targeted investigation of the Neandertal genome by array-based sequence capture. *Science* **328**, 723-725 (2010).
3. K. Prufer *et al.*, The complete genome sequence of a Neanderthal from the Altai Mountains. *Nature* **505**, 43-49 (2014).
4. M. Kircher, S. Sawyer, M. Meyer, Double indexing overcomes inaccuracies in multiplex sequencing on the Illumina platform. *Nucleic acids research* **40**, e3 (2012).
5. A. W. Briggs *et al.*, Removal of deaminated cytosines and detection of in vivo methylation in ancient DNA. *Nucleic acids research* **38**, e87 (2010).
6. M. Meyer *et al.*, A high-coverage genome sequence from an archaic Denisovan individual. *Science* **338**, 222-226 (2012).
7. Q. Fu *et al.*, DNA analysis of an early modern human from Tianyuan Cave, China. *Proceedings of the National Academy of Sciences of the United States of America* **110**, 2223-2227 (2013).
8. A. Gnirke *et al.*, Solution hybrid selection with ultra-long oligonucleotides for massively parallel targeted sequencing. *Nature biotechnology* **27**, 182-189 (2009).
9. M. Kircher, U. Stenzel, J. Kelso, Improved base calling for the Illumina Genome Analyzer using machine learning strategies. *Genome biology* **10**, R83 (2009).
10. M. Meyer, M. Kircher, Illumina sequencing library preparation for highly multiplexed target capture and sequencing. *Cold Spring Harbor protocols* **2010**, pdb prot5448 (2010).
11. M. Kircher, Analysis of high-throughput ancient DNA sequencing data. *Methods in molecular biology (Clifton, N.J.)* **840**, 197-228 (2012).
12. S. F. Grant *et al.*, Follow-up analysis of genome-wide association data identifies novel loci for type 1 diabetes. *Diabetes* **58**, 290-295 (2009).
13. H. Li *et al.*, The Sequence Alignment/Map format and SAMtools. *Bioinformatics* **25**, 2078-2079 (2009).
14. A. McKenna *et al.*, The Genome Analysis Toolkit: a MapReduce framework for analyzing next-generation DNA sequencing data. *Genome research* **20**, 1297-1303 (2010).
15. M. Meyer *et al.*, A High-Coverage Genome Sequence from an Archaic Denisovan Individual. *Science*, (2012).
16. F. Meacham *et al.*, Identification and correction of systematic error in high-throughput sequence data. *BMC bioinformatics* **12**, 451 (2011).
17. B. Paten *et al.*, Genome-wide nucleotide-level mammalian ancestor reconstruction. *Genome research* **18**, 1829-1843 (2008).
18. B. Paten, J. Herrero, K. Beal, S. Fitzgerald, E. Birney, Enredo and Pecan: genome-wide mammalian consistency-based multiple alignment with paralogs. *Genome research* **18**, 1814-1828 (2008).
19. R. E. Green *et al.*, A complete Neandertal mitochondrial genome sequence determined by high-throughput sequencing. *Cell* **134**, 416-426 (2008).
20. V. Heinrich *et al.*, The allele distribution in next-generation sequencing data sets is accurately described as the result of a stochastic branching process. *Nucleic acids research* **40**, 2426-2431 (2012).
21. T. Jombart, adegenet: a R package for the multivariate analysis of genetic markers. *Bioinformatics (Oxford, England)* **24**, 1403-1405 (2008).
22. N. Yu *et al.*, Larger Genetic Differences Within Africans Than Between Africans and Eurasians. *Genetics* **161**, 269-274 (2002).
23. H. Kaessmann, F. Heissig, A. von Haeseler, S. Paabo, DNA sequence variation in a non-coding region of low recombination on the human X chromosome. *Nature genetics* **22**, 78-81 (1999).
24. K. P. Schliep, phangorn: phylogenetic analysis in R. *Bioinformatics (Oxford, England)* **27**, 592-593 (2011).

25. B. Haubold, P. Pfaffelhuber, M. Lynch, mlRho – a program for estimating the population mutation and recombination rates from shotgun-sequenced diploid genomes. *Molecular Ecology* **19**, 277-284 (2010).
26. L. F. Keller, D. M. Waller, Inbreeding effects in wild populations. *Trends in Ecology & Evolution* **17**, 230-241 (2002).
27. Trevor J. Pemberton *et al.*, Genomic Patterns of Homozygosity in Worldwide Human Populations. *The American Journal of Human Genetics* **91**, 275-292 (2012).
28. M. Kirin *et al.*, Genomic runs of homozygosity record population history and consanguinity. *PloS one* **5**, e13996 (2010).
29. S. A. Tishkoff, B. C. Verrelli, Patterns of human genetic diversity: implications for human evolutionary history and disease. *Annual review of genomics and human genetics* **4**, 293-340 (2003).
30. J. Prado-Martinez *et al.*, Great ape genetic diversity and population history. *Nature* **499**, 471-475 (2013).
31. M. Lawrence, R. Gentleman, V. Carey, rtracklayer: an R package for interfacing with genome browsers. *Bioinformatics (Oxford, England)* **25**, 1841-1842 (2009).
32. D. Schmidt *et al.*, Five-vertebrate ChIP-seq reveals the evolutionary dynamics of transcription factor binding. *Science (New York, N.Y.)* **328**, 1036-1040 (2010).
33. A. Siepel *et al.*, Evolutionarily conserved elements in vertebrate, insect, worm, and yeast genomes. *Genome research* **15**, 1034-1050 (2005).
34. K. S. Pollard, M. J. Hubisz, K. R. Rosenbloom, A. Siepel, Detection of nonneutral substitution rates on mammalian phylogenies. *Genome research* **20**, 110-121 (2010).
35. M. Kircher *et al.*, A general framework for estimating the relative pathogenicity of human genetic variants. *Nature genetics* **46**, 310-315 (2014).
36. G. R. Ritchie, I. Dunham, E. Zeggini, P. Flicek, Functional annotation of noncoding sequence variants. *Nature methods* **11**, 294-296 (2014).
37. S. Durinck *et al.*, BioMart and Bioconductor: a powerful link between biological databases and microarray data analysis. *Bioinformatics (Oxford, England)* **21**, 3439-3440 (2005).
38. L. Arbiza *et al.*, Genome-wide inference of natural selection on human transcription factor binding sites. *Nature genetics* **45**, 723-729 (2013).
39. I. Gronau, M. J. Hubisz, B. Gulko, C. G. Danko, A. Siepel, Bayesian inference of ancient human demography from individual genome sequences. *Nature genetics* **43**, 1031-1034 (2011).
40. A. H. Freedman *et al.*, Genome sequencing highlights the dynamic early history of dogs. *PLoS genetics* **10**, e1004016 (2014).
41. G. Benson, Tandem repeats finder: a program to analyze DNA sequences. *Nucleic acids research* **27**, 573-580 (1999).
42. J. A. Bailey *et al.*, Recent segmental duplications in the human genome. *Science (New York, N.Y.)* **297**, 1003-1007 (2002).
43. J. Harrow *et al.*, GENCODE: the reference human genome annotation for The ENCODE Project. *Genome research* **22**, 1760-1774 (2012).
44. 1000 Genomes Project Consortium *et al.*, A map of human genome variation from population-scale sequencing. *Nature* **467**, 1061-1073 (2010).
45. J. N. Fenner, Cross-cultural estimation of the human generation interval for use in genetics-based population divergence studies. *American journal of physical anthropology* **128**, 415-423 (2005).
46. J. C. Roach *et al.*, Analysis of genetic inheritance in a family quartet by whole-genome sequencing. *Science* **328**, 636-639 (2010).
47. M. Lynch, Rate, molecular spectrum, and consequences of human mutation. *Proceedings of the National Academy of Sciences of the United States of America* **107**, 961-968 (2010).
48. A. Scally, R. Durbin, Revising the human mutation rate: implications for understanding human evolution. *Nat Rev Genet* **13**, 745-753 (2012).
49. Q. Fu *et al.*, Genome sequence of a 45,000-year-old modern human from western Siberia. *Nature* **514**, 445-449 (2014).

50. M. W. Nachman, S. L. Crowell, Estimate of the mutation rate per nucleotide in humans. *Genetics* **156**, 297-304 (2000).
51. A. S. Kondrashov, Direct estimates of human per nucleotide mutation rates at 20 loci causing Mendelian diseases. *Human mutation* **21**, 12-27 (2003).
52. S. Y. Ho *et al.*, Time-dependent rates of molecular evolution. *Mol Ecol* **20**, 3087-3101 (2011).
53. P. Skoglund, M. Jakobsson, Archaic human ancestry in East Asia. *Proceedings of the National Academy of Sciences of the United States of America* **108**, 18301-18306 (2011).
54. E. Huerta-Sanchez *et al.*, Altitude adaptation in Tibetans caused by introgression of Denisovan-like DNA. *Nature* **512**, 194-197 (2014).
55. D. Reich *et al.*, Genetic history of an archaic hominin group from Denisova Cave in Siberia. *Nature* **468**, 1053-1060 (2010).
56. B. Vernot, J. M. Akey, Resurrecting Surviving Neandertal Lineages from Modern Human Genomes. *Science (New York, N.Y.)*, (2014).
57. R. R. Hudson, Generating samples under a Wright-Fisher neutral model of genetic variation. *Bioinformatics* **18**, 337-338 (2002).
58. S. Gravel *et al.*, Demographic history and rare allele sharing among human populations. *Proceedings of the National Academy of Sciences of the United States of America* **108**, 11983-11988 (2011).
59. A. Rambaut, N. C. Grassly, Seq-Gen: an application for the Monte Carlo simulation of DNA sequence evolution along phylogenetic trees. *Computer applications in the biosciences : CABIOS* **13**, 235-238 (1997).
60. R. E. Wood *et al.*, A NEW DATE FOR THE NEANDERTHALS FROM EL SIDRÓN CAVE (ASTURIAS, NORTHERN SPAIN)*. *Archaeometry* **55**, 148-158 (2013).
61. D. Serre *et al.*, No evidence of Neandertal mtDNA contribution to early modern humans. *PLoS biology* **2**, E57 (2004).
62. C. The Genomes Project, A global reference for human genetic variation. *Nature* **526**, 68-74 (2015).
63. K. Prüfer *et al.*, FUNC: a package for detecting significant associations between gene sets and ontological annotations. *BMC bioinformatics* **8**, 41 (2007).
64. S. Sankararaman *et al.*, The genomic landscape of Neanderthal ancestry in present-day humans. *Nature* **507**, 354-357 (2014).
65. G. McVicker, D. Gordon, C. Davis, P. Green, Widespread genomic signatures of natural selection in hominid evolution. *PLoS genetics* **5**, e1000471 (2009).
66. M. D. Rasmussen, M. J. Hubisz, I. Gronau, A. Siepel, Genome-wide inference of ancestral recombination graphs. *PLoS genetics* **10**, e1004342 (2014).
67. R. E. Green *et al.*, A draft sequence of the Neandertal genome. *Science* **328**, 710-722 (2010).